FUNDAMENTAL ASPECTS OF CONVECTIVE EVAPORATION AND DRYING

by

P.E. DOE B.Sc., B.E., M.I.E. Aust.

submitted in partial fulfilment of the requirements for the Degree of Doctor of Philosophy in the Faculty of Engineering of the University of Tasmania.

UNIVERSITY OF TASMANIA

HOBART

February, 1970

Acknowledgement

Thanks are due to a number of persons who were of assistance to the author in the course of this project. As always, it is not possible to mention everyone by name, so would those whose names do not appear below accept the appreciation and graditude of the author?

Mr. M. MacPherson and Mr. A. Robinson assisted in constructing the apparatus; Dr. A.C. Jason of the Torry Research Station, Aberdeen, Dr. R.G. Wylie of the C.S.I.R.O. Division of Physics, Sydney, Mr. J. Boothroyd, Mr. G.J. Burrell, Professor D. Elliott, Mr. R.F. Rish, Mr. G.J. Walker and Mr. P.A. Watt of the University of Tasmania were all generous with their assistance. Miss A. Clark and Miss S. Reynolds typed the various papers and the thesis.

The encouragement, guidance and criticism from the author's mentor and supervisor, Professor A.R. Oliver of the University of Tasmania is acknowledged with gratitude.

CONTENTS

PREFACE

Historical and Logical Development

This project began early in 1965 with the aim of developing a method of measuring concentration gradients in a mass transfer boundary layer. It was thought that the measurement of the detail within a boundary layer would lead to an increased understanding of the mass transfer process, in the same way that measurement of velocity and temperature within boundary layers has led to advances in the fields of fluid mechanics and heat transfer.

In situations involving convective mass transfer, a widely used method of analysis and design is to use measured values of heat transfer coefficients to predict mass transfer coefficients by applying an analogy between heat and mass transfer. This approach presupposes that the pressence of mass transfer does not effect the flow pattern. It may be that the presence of mass transfer effects the transition from laminar to turbulent flow. If this were the case, the use of data pertinent to heat transfer situations could lead to serious error when applied to the analogous mass transfer situation.

The scope of this study has not been extended into the transitional and turbulent flow regimes because even without the complications of heat and mass transfer, these flows are not well understood. In laminar flow there are certain situations (e.g. flow over a flat plate) in which a theoretical model is in close agreement with observations. In such situations, the validity of the various models of the mass transfer process can be assessed. A way of doing this, and consequently one of the aims of this project is to compare measured velocity, temperature and humidity profiles within a laminar boundary layer in which heat and mass transfer are taking place. The measurement of velocity and temperature poses no problems as the techniques of hot wire anemometry and fine wire resistance thermometry are established practices in boundary layer work. Measurement of humidity within

the boundary layer is another matter. A number of possible devices for measuring humidity within a boundary layer were investigated : fine hair hygrometers, high frequency measurement of dielectric properties, change of electrical resistance with absorption in hygroscopic media, and sampling through a fine tube. All were rejected because of the size limitation or because of the inherent property of absorbent type hygrometers to exhibit hysteresis at high humidities. The regions of high humidity close to evaporating surfaces were of particular interest.

The development of a device with sufficiently small spatial discrimination was continued until, in mid 1967, successful measurements were made of the humidity variation in the laminar boundary layer above a flat wet plate.

The device that did not suffer from hysteresis and had the potential to be made very small was a wet thermocouple psychrometer. A further attractive feature was that the reverse thermocouple or Peltier effect could be used to cool and thus wet the junction.

The first development was of the device described in Chapter 2 and published in Ref. 1. The basis of operation was the measurement (indirectly) of the surface heat transfer coefficient of the thermocouple; thus the device was quite sensitive to the air velocity, resulting in the abandonment of a calibration of the device in a moving air stream.

The next development was towards a dewpoint instrument. It was hoped to cool a thermocouple gradually and uniformly using the Peltier effect and, by some electrical means, identify the dewpoint. A theoretical and experimental investigation showed that this too was impracticable.

There remained a third method, that of using the thermocouple as a psychrometer. This method, described in Chapter 3 and in Ref. 2, proved successful. Measurements of humidity profiles along with temperature and velocity profiles were made in the laminar mass transfer boundary layer above a flat, wet plate. (Chapter 4).

A theoretical model based on finite difference approximations to the laminar boundary layer equations was set up, solved, and the results compared with the measured profiles. (Chapters 5 and 6). The model includes the effects of variation of air properties (viscosity, density, thermal conductivity, mass diffusivity and specific heat) with both temperature and humidity. An approximate method of analysis is also proposed, based on the momentum, temperature and concentration integral equations.

For six months from August, 1967, the author spent study leave as a visiting research fellow at the Torry Research Station in Aberdeen, Scotland. Part of the work undertaken was the theoretical study of the Torry fish drying kiln described in Appendix I. This work complemented the work on mass transfer boundary layers as it served as a practical application for the knowledge gained in the more academic field of boundary layer research. The work at Torry also led to the closely related study of the drying of asbestos sheeting, described in Appendix II.

Chapter 7 is an attempt to collate and rationalise the vast literature on the subject of evaporation. Out of this rationalisation emerges a picture of the evaporation process in which the controlling features are identified.

Regions of originality.

Parts of this work can be claimed to be original, but several sections mentioned here and acknowledged in the body of the text resulted from collaboration with others. In Chapter 1 the analogy model (section 1.4.1), models based on equations of convection (section 1.4.2), and section 1.5 are paraphrased from the references quoted. Chapters 2 and 3 with the exception of section 2.14 are original. Chapter 4 describes measurements made by the author. Sections 5.1 and 5.2 are summaries of the widely known and used mathematical models of the laminar boundary layer. The method of providing for the variation of fluid properties with humidity (section 5.1.3) is original.

The reduction of the partial differential equations to ordinary form (section 5.1.4) has been performed by various authors (Refs. 3, 4), but to the best of this author's knowledge has not before been carried out for the mass transfer boundary layer with varying fluid properties. The rest of Chapter 5 is original except where specific references are quoted. Chapter 6 reports the comparison between measured and computed boundary layers.

The mathematical models developed in Appendices I and III are the work of this author. The experimental part of the investigation reported in Appendix II was carried out by another worker.

CHAPTER 1

In this chapter it is proposed to outline the subject of convective mass transfer. A few concepts basic to the subject are discussed and some of the technical terms are explained.

Much of this chapter is repeated in greater detail in succeeding chapters. It is given here partly as an introduction to the subject and so that the detail which is to follow can be presented against the background of the broader field of convective mass transfer.

1.1 Mass transfer and boundary layers.

The term mass transfer applies to a large number of commercial industrial processes. Any process in which matter is removed from one position to another, with or without a change of state or phase can be described as mass transfer. Ablation, condensation, transpiration cooling, perspiration, erosion and drying are a few examples. The narrower term "evaporation" describes the situation in which a liquid changes phase and the gaseous phase is removed. A common process is that in which the gaseous phase is removed by a moving stream of gas. It is in this situation that the concept of a boundary layer arises.

For about half a century it has been recognised that when a stream of fluid flows past a solid boundary, the influence of that boundary is often confined to a region close to the boundary. This boundary layer can be roughly defined as the region in which the velocity of the fluid is different from that of the bulk of the fluid remote from the boundary. Much of modern fluid dynamics derives from this boundary layer concept.

Likewise, when a liquid evaporates into a gas, a mass transfer boundary close to the liquid surface can be identified. (Ref. 3). It is within this mass transfer boundary layer that the various processes controlling the evaporation are to be found. Because of this, mass transfer boundary layers are the main concern of this investigation into the evaporation process.

1.2 Convective evaporation.

The most convenient mass transfer boundary layer to investigate experimentally is that for the evaporation of water vapour into air. The evaporation can be pictured as molecules of water leaving the liquid surface as free gaseous water vapour molecules and diffusing into the near stationary air stream adjacent to the liquid surface. Then by the supplementary processes of diffusion and convection, molecules are transferred through the boundary layer.

1.3 Mass transfer boundary layer measurement.

One of the reasons for undertaking this investigation was the almost total lack of measurement of concentrations within mass transfer boundary layers. This situation arose from the difficulty of measuring mass concentration in a small space. There have been many measurements of mass transfer rates on an overall basis, (Ref. 4), but very little attention has been given to the detail within the boundary layer. Powell and Griffiths (Refs. 5 and 6), in perhaps the most comprehensive set of experiments on evaporation from bodies of different shapes and sizes, measured velocities and vapour pressures (humidities) above a wet surface using a quartz fibre anemometer and a thermocouple psychrometer. (No other details given). More recently El-Wakil et al. (Ref. 7) used an interferometric technique to study the mass transfer from a vertical plate at low Reynolds numbers.

1.4 Models of the evaporation process.

The use of the word model, here and in other parts of this thesis, requires some explanation. It is convenient to identify two models of a real situation. The first is termed the physical model. The physical model is an abstraction approximating the real situation. For example, if the real situation was the solar system, a physical model could be a number of points corresponding to the planets, each moving in an ellipse with the sun at the focus.

There could of course be any number of physical models, each giving a closer approximation to the real situation.

The second model is terms the mathematical model, and is a mathematical statement of the physical model. In our illustration, the mathematical model would be Kepler's "Laws of planetary motion".

This process of the identification of models serves as a constant reminder of the artificial nature of the calculation. There are approximations and hence errors in both the physical and mathematical models.

1.4.1 The analogy model.

The viscosity of a fluid is defined (Ref. 3) by the expression:

$$\tau = -\mu \frac{\partial u}{\partial y} \quad , \tag{1.1}$$

where τ is the shear stress,

u is the velocity in the direction parallel to the direction of shear,

and y is the distance perpendicular to the direction of shear.

Likewise the thermal conductivity k of a fluid is defined by the expression:

$$\frac{q}{A} = -k \frac{\partial T}{\partial y} \quad , \tag{1.2}$$

where q is the heat flux per unit time,

A is the area,

T is the temperature,

and y is the distance parallel to the heat flux.

In addition, mass diffusivity D is defined by the expression:

$$\frac{w}{A} = -D \frac{\partial c_w}{\partial y} \quad , \tag{1.3}$$

where w is the mass flux per unit time,

A is the area,

c_w is the concentration,

and y is the distance parallel to the mass flux.

It can be seen that there is a marked similarity between the definitions of viscosity, thermal conductivity and mass diffusivity. It is this similarity which gives rise to the Reynolds analogy of heat and mass transfer. The basis of the analogy is that heat and mass are diffused in a precisely similar way to the diffusion of momentum by viscosity, except that the scale is determined by thermal conductivity and mass diffusivity.

As heat, mass and momentum are transferred in a similar manner according to equations (1.1), (1.2) and (1.3), the boundary layers will be similar. If certain non-dimensional parameters, namely the Prandtl and Schmidt numbers, are equal to unity, then the three boundary layers are identical. In general, if, in the heat transfer relations, the Nusselt number is replaced by the Sherwood number, and the Prandtl number is replaced by the Schmidt number, then an expression for the mass transfer results.

This approach is widely applied with a reasonable degree of success. There are, however, certain basic differences between the transfer of heat and mass which can lead to significant errors in the analogy. The manner in which variations in temperature and humidity vary the properties of moist air is one cause of dissimilarity. Another dissimilarity arises from an inherent difference between the processes. This is perhaps best illustrated by an example of seemingly "similar" situations of heat and mass transfer.

Consider the heat and mass transfer from two cylinders in an air stream. One cylinder is provided with a heating element and the other has porous walls and a supply of water. Thus we have a case of heat transfer which should be similar by analogy to the case of mass transfer from the wet cylinder. A difference arises from the inability of the surface concentration in the case of the wet cylinder to adjust itself in the same way as does the analogous property, temperature, in the case of the hot cylinder. As the heat input to the hot cylinder is increased, so also does the surface temperature of the cylinder, and hence the heat transfer.

However, when the water supply to the wet cylinder is increased, evaporation can increase only up to the stage when the surface of the cylinder is uniformly wet; thereafter, no increase in evaporation is possible. The only result of increasing the water supply rate would be to run the excess water down the side of the cylinder.

Thus is illustrated a very real difference between the processes of heat and mass transfer. There is nothing in mass transfer analogous to the quantity "surface temperature" in heat transfer. Because there must be a phase change at the surface of the wet cylinder, there is an upper limit to the amount of water which can be evaporated into an air stream of a given humidity and velocity.

1.4.2 Models based on convection equations.

The general Navier Stokes equations describing convective fluid flow can be reduced to four simultaneous non-linear partial differential equations which describe the flow in a laminar two-dimensional boundary layer. (Ref. 9). Hartnett and Eckert (Ref. 10) proposed a model of the mass transfer boundary layer based on the simplified boundary layer equations which result when the fluid properties are considered constant.

The equations are as follows:

Continuity; $$\frac{\partial u}{\partial x} + \frac{\partial v}{\partial y} = 0 \quad , \tag{1.4}$$

Momentum; $$\rho u \frac{\partial u}{\partial x} + \rho v \frac{\partial u}{\partial y} = \mu \frac{\partial^2 u}{\partial y^2} - \frac{dp}{dx} \quad , \tag{1.5}$$

Diffusion; $$u \frac{\partial w}{\partial x} + v \frac{\partial w}{\partial y} = D \frac{\partial^2 w}{\partial y^2} \quad , \tag{1.6}$$

Energy; $$u \frac{\partial T}{\partial x} + v \frac{\partial T}{\partial y} = \alpha \frac{\partial^2 T}{\partial y^2} \tag{1.7}$$

These equations apply to a laminar two-dimensional boundary layer in an incompressible fluid where the viscous heating is negligible.

The boundary conditions chosen by Hartnett and Eckert are as follows:

Momentum; $u = 0$ at $y = 0$, $u = U_\infty$ as $y \to \infty$, $v = v_w$ at $y = 0$, (1.8)

Diffusion; $w = w_w$ at $y = 0$, $w = w_\infty$ as $y \to \infty$, $v_{air} = 0$ at $y = 0$, (1.9)

Energy; $T = T_w$ at $y = 0$, $T = T_\infty$ as $y \to \infty$. (1.10)

Hartnett and Eckert went on to solve the equations for various values of the "blowing velocity" v_w. The value of v_w is shown to be uniquely determined by w_w and w_∞ according to the equation

$$v_w = -\frac{D}{1 - w_w}\left(\frac{\partial w}{\partial y}\right)_{y=0} . \qquad (1.11)$$

Thus if the wall and bulk flow humidities are known, the "blowing velocity" and hence the evaporation rate can be found.

However there is no indication as to how either w_w or w_∞ is to be found. That the evaporation is uniquely determined by the air speed and humidity is apparent from experiment. The evaporation rate automatically adjusts itself to suit the prevailing velocity distribution and ambient humidity.

It seems that the Hartnett-Eckert approach applies more nearly to cases of boundary layer suction or transpiration cooling where there is a significant forced flow of fluid through the boundary. In the case of evaporation of water vapour into air, the mass flux across the liquid boundary is quite small compared with the flux of air further out in the boundary layer.

For these reasons, in the model of evaporation proposed in Chapter 5, the boundary condition $v = v_w$ at $y = 0$ is replaced by $v = 0$ at $y = 0$.

1.5 Factors affecting the evaporation rate.

So far, the various theories of evaporation have not given a means of predicting the evaporation rate. Berman (Ref. 11) goes some of the way towards this. From considerations of molecular

kinetics, Berman proposes that the evaporation rate be linearly related to the difference between the partial pressure p'_{wv} of the water vapour in the air immediately adjacent to the liquid surface and the saturation partial pressure of water vapour at the temperature of the surface p''.

Thus $$g_{ev} = K(p'' - p'_{wv}), \qquad (1.12)$$

where g_{ev} is the evaporation rate.

Berman shows that the factor of proportionality K is related to the accommodation coefficient f by the expression,

$$K = 3{\cdot}6 \times 10^{7}\, a\, f \sqrt{\frac{g M_{wv}}{2\pi R T}}\ , \qquad (1.13)$$

where a is a correction factor "to allow for a difference in the actual properties of the vapour from those of an ideal gas and for the effect of the directional motion of the vapour on the velocity distribution of its molecules,"

g is the gravitational acceleration,

M_{wv} is the molecular weight of the vapour,

R is the universal gas constant,

and T is the absolute temperature of the liquid surface.

The accommodation coefficient f, also called the "condensation", or "evaporation" coefficient, is the proportion of vapour molecules which on striking the liquid surface are absorbed into it.

Here, however, certain conflicts arise. There is a considerable scatter of measured values of the accommodation coefficient of water. (Refs. 12, 13). Theoretical estimates are larger than measured values by factors of 200. The difference has been partly explained by the peculiar structure of liquid water. Lype (Ref. 14) refers to water as a pseudocrystalline substance. Water is characterised by strongly polar, asymetrical molecules which behave as though bound in a crystal lattice.

Notwithstanding these difficulties, Berman's approach gives an insight into the detailed nature of evaporation. Firstly there is a driving force ($p'' - p^*_{ws}$) acting in the region close to the interface. This driving force determines the evaporation rate, provided the external conditions are such that the water vapour can be removed from near the water surface with sufficient rapidity to maintain the value of p^*_{ws} near the surface. The driving force which controls the movement of water vapour away from the surface is the partial pressure difference ($p^*_{ws} - p_{\infty}$), where p_{∞} is the partial pressure in the air remote from the evaporating surface. There is also a dependence on the velocity and temperature distributions in the boundary layer.

It appears that in most cases of evaporation of water vapour into air, the controlling factor is the convection from the surface. The value of the partial pressure close to the surface is near the saturation partial pressure at the surface. The upper limit to the partial pressure at the surface, that is the saturation partial pressure, gives rise to the difference between the heat and mass transfer processes mentioned above. The partial pressure near the surface cannot rise past the saturation pressure, thus the driving force tending to remove the water vapour by convection is limited.

Berman states that the partial pressure near the surface is indistinguishable from the saturation partial pressure at the surface temperature. This is one of the statements that it is proposed to investigate by direct measurement with the miniature thermocouple psychrometer developed to measure humidities within the boundary layer.

1.6 The 'bootlace' philosophy.

It should become apparent in the work to follow, that some of the existing models have been used, particularly in establishing the behaviour of the thermocouple psychrometer. Thus the measuring instrument has as its basis, the process it is to be used to investigate.

In justification of this, first there is the need to get started somewhere, and secondly, any modifications to the existing models which may arise from the investigation can be applied to the measuring instrument. This in turn could lead to a modification of the model.

CHAPTER 2

The thermocouple psychrometer used for measuring humidity gradients within a mass transfer boundary layer evolved from two devices, both of which proved unsatisfactory and were abandoned. The development of these two devices is set out in this chapter.

2.1 Introduction.

Measurement of humidity is characterised by the large number and variety of the methods used. This is illustrated by a list of measuring techniques taken from a recent transducer compendium. (Ref. 15).

PSYCHROMETERS	ABSORPTION HYGROMETERS
MECHANICAL HYGROMETERS	CONDENSING HYGROMETERS
DEWPOINT HYGROMETERS	THERMAL HYGROMETERS
ELECTRIC HYGROMETERS	REFRACTIVE HYGROMETERS
GRAVIMETRIC HYGROMETERS	ELECTROLYTIC HYGROMETERS
THERMAL CONDUCTIVITY HYGROMETERS	DEWCEL HYGROMETERS
SPECTROSCOPIC HYGROMETERS	

A recent symposium on humidity and moisture (Washington 1963) published a 686 page volume on the principles and methods of measuring humidity. (Ref. 16).

The overriding consideration in the choice of a technique for measuring humidity within a boundary layer is the need for spatial discrimination. The wind tunnel available for measurements of mass transfer boundary layers had a working section one metre long. This produced boundary layers about 2 cm. thick with air speeds in the laminar range similar to those encountered in natural draft cooling towers, drying kilns, etc. (in the range 1 to 4 m/s).

Spatial discrimination of around two orders of magnitude smaller than the boundary layer to be measured is the upper limit of size to give a meaningful traverse across the boundary layer.

This means a discrimination of around 2×10^{-4} m ; such a requirement rather narrows the field of suitable techniques.

There is a method of avoiding the spatial discrimination requirement by sampling to collect sufficient moist air to enable conventional humidity measuring methods to be used. However, there are drawbacks to sampling; in order not to disturb the boundary layer flow, the sampling must be at the local air velocity. This leads to unreasonably long sampling times and thus to difficulty in controlling the ambient conditions. There is always a risk of losing some of the water vapour in the sample by condensation or absorption. A further disadvantage is the unsuitability of the method for use in turbulent or rapidly changing flow.

Methods of humidity measurement which depend on the absorption of water vapour into a substance causing a change in some property of that substance, whether length, electrical resistivity, dielectric constant, etc., suffer from the disadvantage of increasing hysteresis at high humidities. These methods are unsuited to measurements in a boundary layer as there are regions of high humidity close to an evaporating surface.

2.2 The Peltier effect.

The method adopted is based on the Peltier effect (Refs. 17, 18, 19) which has of late found application in various thermo-electric cooling devices. In short, an electric current is passed through a junction between two thermo-electrically dissimilar metals. The effect of this current is to cool the junction. A thermocouple junction can function as a hygrometer by using the Peltier effect to cool the junction below the dewpoint temperature, whereupon the formation of moisture is detected, and the magnitude of the current at this point is a measure of the dewpoint temperature and hence the humidity.

The method is ideal for measurements in the boundary layer. The spacial discrimination is limited only by the size to which a single thermocouple junction can be made, and as the instrument is essentially a dewpoint hygrometer, it does not suffer from a loss of sensitivity at high humidities.

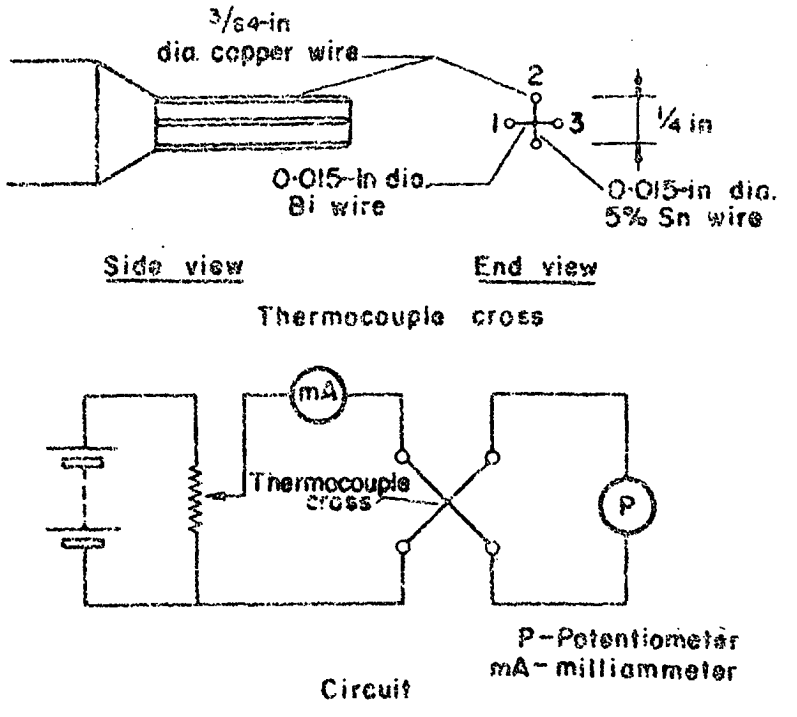

Fig. 2.1. Thermocouple cross and circuit. Bismuth and bismuth-tin alloy wires are soldered to copper supports and resistance welded together where they cross.

2.3 Early experiments.

The first attempts to measure humidity using Peltier effect cooling were made with a cross of two thermo-electrically different metals, bismuth and an alloy of bismuth and 5% tin. The cross was resistance welded and soldered to stout copper leads. The circuit (Fig. 2.1) enabled a current to be passed through one leg of the cross, while the other leg acted as a thermocouple junction. The current was slowly increased and the potential across the thermocouple junction recorded. Plots of cooling current vs. thermocouple potential were straight lines but with a kink, thought to correspond to the dewpoint as moisture accumulated on the junction with cooling

currents in excess of that required to give the kink. The method was slow and tedious, the kink ill-defined and did not always appear. Thus the method was abandoned in favour of a single junction.

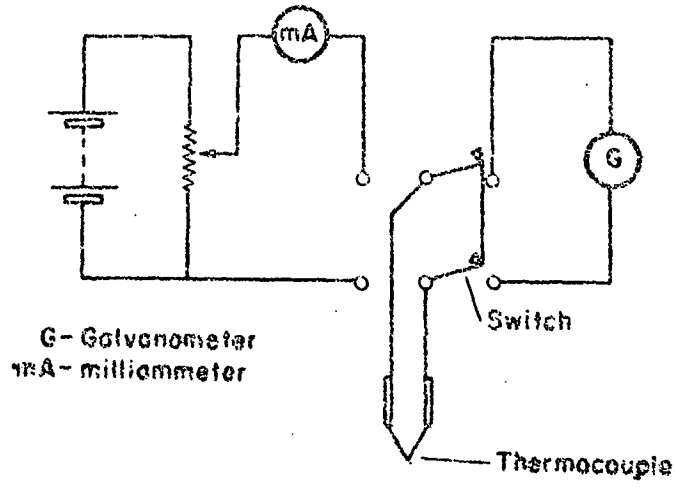

Fig. 2.2. Circuit using single thermocouple junction and double pole - double throw switch.

The first experiments with a single junction employed the technique described by Spanner (Ref. 20) as the "ballistic technique". The circuit (Fig. 2.2) used a double throw - double pole switch to switch the thermocouple from a battery circuit cooling the junction to a galvanometer circuit which measured the temperature of the junction. The method was to cool the junction for a fixed time at a current known to be greater than that required to cool the junction below the dewpoint and then to throw the switch, thus connecting the junction across the galvanometer and observing its maximum deflection. The method of Montieth and Owen (Ref. 21) was also attempted. This is similar to the Spanner method except that a measure of the wet-bulb temperature is obtained by recording the galvanometer deflection at a fixed time after switching.

An attempt was made to calibrate this apparatus in moving air, and after a number of modifications to the original circuit, including the use of rapid action switches and attempts to observe transient changes in the junction potential using an oscilloscope,

a calibration was obtained. The calibration, however, exhibited a considerable scatter of results and provoked some thought as to how it could be improved.

The most serious limitations to the "ballistic method" seem to lie in the switching delay and the switching resistances which are difficult if not impossible to keep constant over long periods. Furthermore, the method depends on the ballistic throw of a galvanometer with a response time for full scale deflection of about two seconds giving a measure of the much more rapid evaporation from the junction.

These limitations were overcome by suitable electronic circuitry which alternately cooled and heated the junction. The junction was pulsed with the square wave form shown in Fig. 2.3.

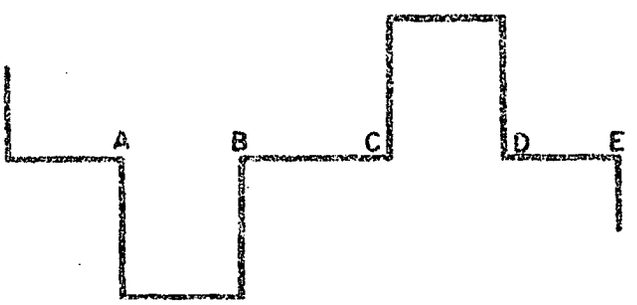

Fig. 2.3. Alternating square-wave current form.

The circuitry enables the thermocouple potential to be observed continuously and the fast rise time of the square waves (about 20μS) is several orders of magnitude faster than mechanical switching and is thought to be somewhat faster than the condensation of moisture onto a cold surface.

2.4 The method adopted.

Wave-form generator: The wave form generator is shown in Fig. 2.4. It comprises four monostable multivibrators in cascade, each with independently variable period provided by inserting shunts into a bank of capacitances, thus altering the period of the multivibrators. The period of the current waveform is 320 milliseconds.

Fig. 2.4. Wave-form generator.

Two of the multivibrators drive a current reversing switch to produce the wave form of Fig. 2.3.

During A to B the junction is cooled.

B to C there is no applied current and the junction functions as a thermocouple.

C to D the junction is heated, evaporating condensation which may have occurred during A to B.

D to E is as for B to C.

At E the cycle repeats.

By balancing the amplitudes and durations of the heating and cooling currents it is possible to avoid long-term heating or cooling of the junction. That is, the heat extracted from the junction during cooling is equal to the heat input to the junction during heating.

Bridge circuit: The junction is set up in a balanced bridge circuit (see Fig. 2.5). A sensitive differential amplifier and oscilloscope combination is used as the detecting instrument to observe the bridge unbalance.

2.5 Construction of thermocouple junction.

Preparation of wires: The thermocouple wires are produced by the Strong (Ref. 22) method. Briefly the method is to suck the molten metal into a glass tube, then draw out the tubing. The glass is etched from the wire with hydrofluoric acid solution. The author produced satisfactory wires (if rather brittle) by hand-drawing the glass over a Bunsen burner.

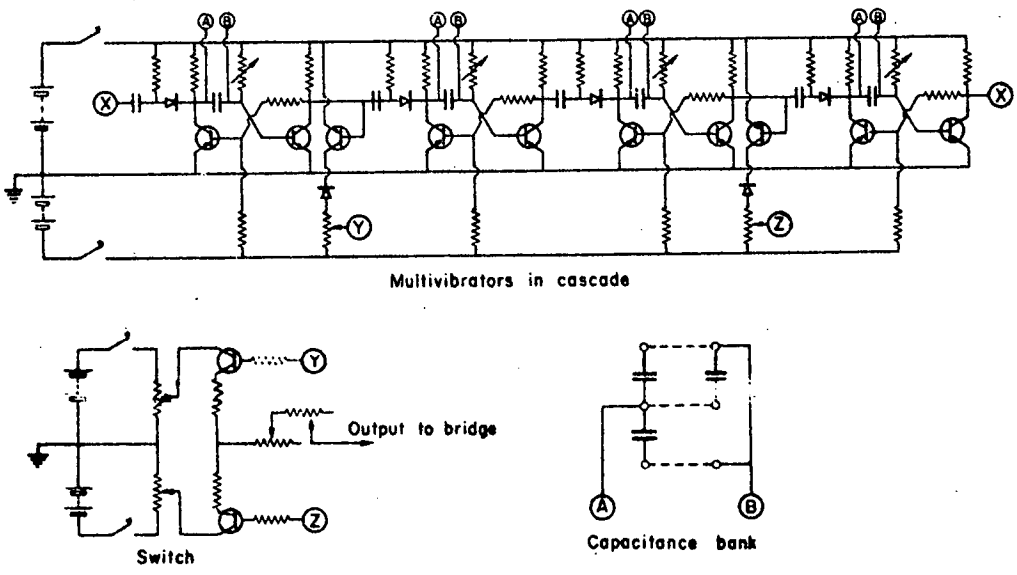

Fig.2.4. Wave-form generator circuit.

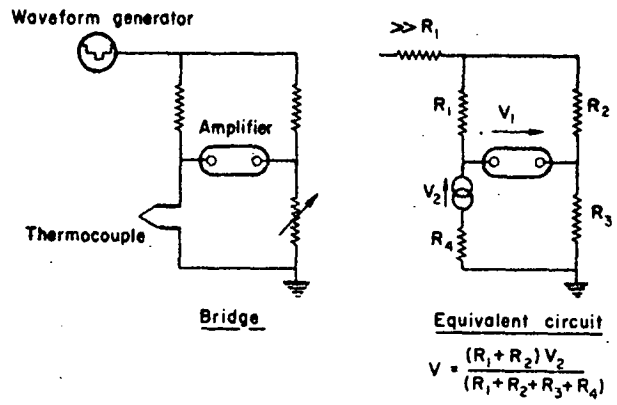

Fig. 2.5. Balanced bridge circuit.

Manufacture of the junction: The wires are first soldered onto copper supports with Wood's metal and a flux of 40% $ZnCl_2$, 20% NH_4Cl, 40% H_2O. A soldering iron made from a fine needle with a Nichrome wire heating element was used. The work was carried out under a binocular microscope approximately 30 x magnification. The wires were crossed over and resistance welded together. Welding voltage needed to be carefully adjusted so as to fuse the wires without causing them to disintegrate. The junction was then carefully washed in a very mild caustic solution to neutralize the acidic flux. The author has produced temperatures as low as 12 degF below ambient with Bismuth, Bismuth-tin thermocouple wires about 0.0009-0.0012 in. diameter arranged as shown in Fig. 2.6.

2.6 Method of operation.

The method of operation is to increase the amplitude of the pulsing waveform until the signal detected by the amplifier and oscilloscope is of the identifiable form shown in Fig. 2.7. Also shown in Fig. 2.7 are the signals corresponding to a slight increase and a slight decrease in the amplitude of the pulsing waveform about the identifiable amplitude. The potential V_o shown in Fig. 2.7. corresponding to a cooling current i_o which produces the identifiable signal, is recorded.

The effect of unbalancing the bridge is that the signal from the thermocouple is superimposed on an attenuated pulsing waveform. This causes discontinuities in the observed signal as shown in Fig. 2.8. By adjusting the variable bridge resistance to eliminate the discontinuities the bridge may be balanced.

2.7 Principle of operation.

In order to establish the principle of operation of the hygrometer and in particular to determine the cause of the observed change in the waveform, a mathematical model of the thermocouple junction was set up and an expression obtained for the temperature distribution in one of the thermocouple wires resulting from a cooling current in the thermocouple (see Appendix to Ref. 1). The "humps" in the observed waveform (Fig. 2.7) are caused by the addition of exponential error function terms arising from the Peltier effect cooling and an exponential term arising from the Joule heating in the thermocouple wires.

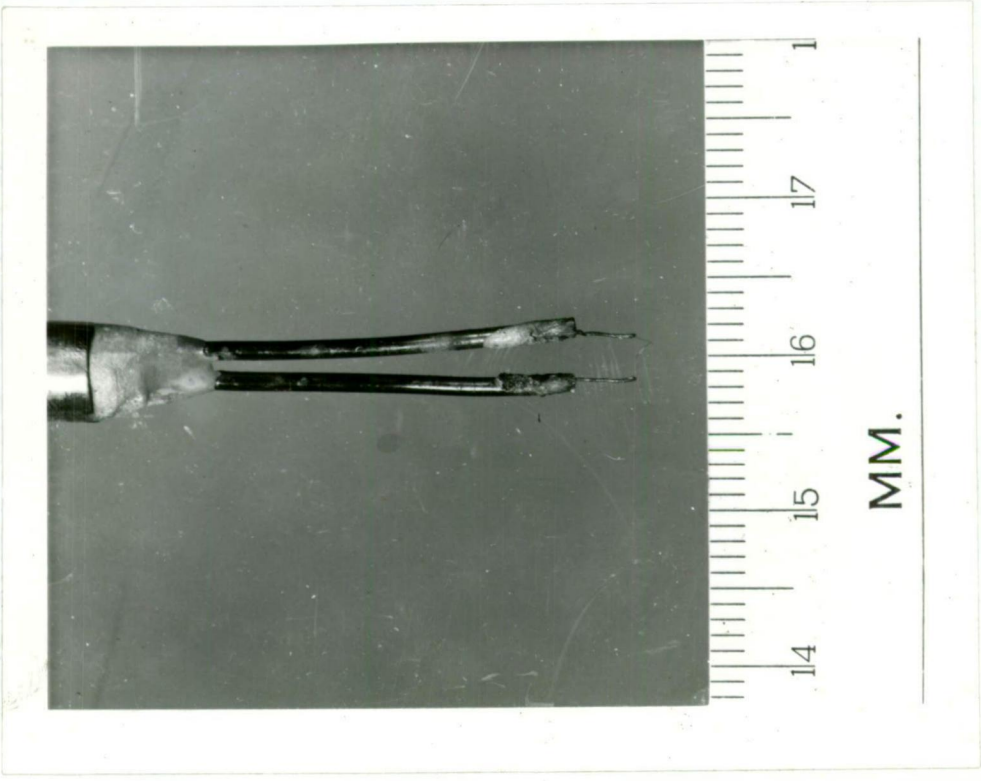

Fig. 2.6. Thermocouple junction used in calibration.

A digital computer was used to calculate the behaviour of a thermocouple junction undergoing the steady pulsing current of Fig. 2.3. During the part of the cycle when there is no applied current, there is still a current flowing in the thermocouple due to the thermoelectric potential of the junction if the temperature of the junction is different from that of the rest of the circuit. This current is about one thousandth of the driving current used to cool the thermocouple, thus the Thompson effect (Ref. 17) can be

neglected as insignificant. In this case, the thermo-electric potential of the junction is directly proportional to the junction temperature and is independent of the temperature distribution along the wires. Thus by computing the temperature of the junction around the cycle it was possible to compute the junction potential observed by the amplifier and oscilloscope.

The computed signal closely resembled the observed potential change shown in Fig. 2.7 except in regions close to a change in current.

The same characteristic change in shape of the signal with a change in current as shown in Fig. 2.7 was produced by the calculation.

By varying the current, i , and the surface heat-transfer coefficient, it was possible to show that for a particular value of the surface heat-transfer coefficient there is only one value of the driving current i_o , which will give the easily identifiable horizontal signal. The surface heat-transfer coefficient depends on whether or not the junction and wires are dry or wet, and if wet, depends on the amount of moisture condensed on the junction. By pulsing the junction long enough for steady-state conditions to establish, the quantity of water condensed each cycle will be constant and will depend on the humidity of the air surrounding the junction. Thus the potential V_o (Fig. 2.7) recorded which is proportional to the driving current and hence to the surface heat-transfer coefficient serves as a measure of the humidity of the air at the junction. The identifiable horizontal signal does not correspond to the dewpoint or wet-bulb temperature since it indicates that there is enough moisture condensed on the junction to produce the effect.

2.8 Calibration.

The thermocouple junction hygrometer was calibrated against the equilibrium humidity of still air above saturated salt solutions (Ref. 23). The apparatus is shown in Fig. 2.9. The Perspex box is hermatically sealed with petroleum jelly. The microscope is used for visual observations of condensation at low pulsing frequencies.

The calibration (Fig. 2.10) of potential corresponding to the identifiable horizontal signal against the depression of the dewpoint below ambient temperature is approximately linear. Above about 5 degF dewpoint depression, the hygrometer fails to register any further increase in dewpoint depression. This is because the maximum temperature drop obtainable with the bismuth, bismuth-tin thermocouple used is about 5 degF so that beyond this point, no moisture is condensed on the junction. It may be possible to increase the range of the instrument by using semiconductor materials, which have a much larger thermo-electric effect. (The Peltier coefficient of a n- and p-type bismuth-telluride couple at 0 degC is 100-120 mV whereas that of a bismuth, bismuth-tin thermocouple at 0 degC is 20 mV). Due to the long times necessary to ensure that the air above the saturated salt solution had reached equilibrium humidity, the calibration took place over a period of 28 days. This gives some idea of the long-term stability of the method.

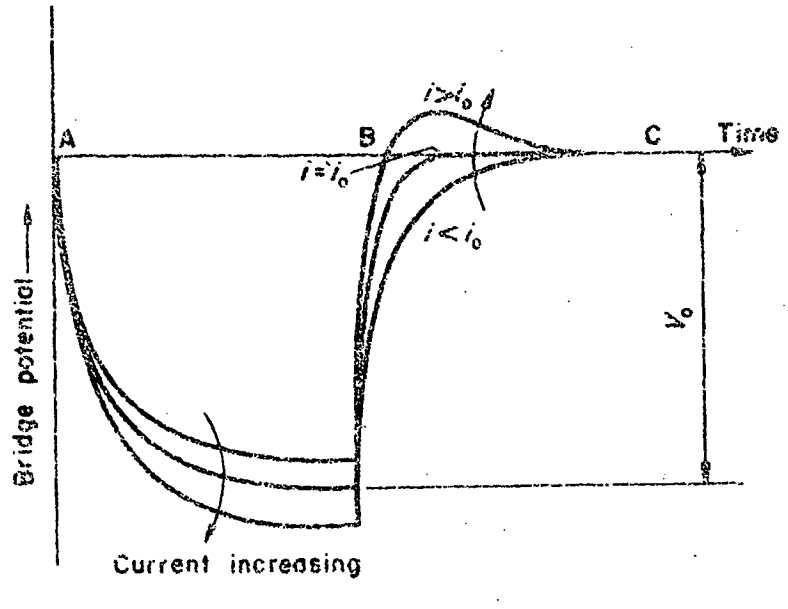

Fig. 2.7. Potential observed across bridge.

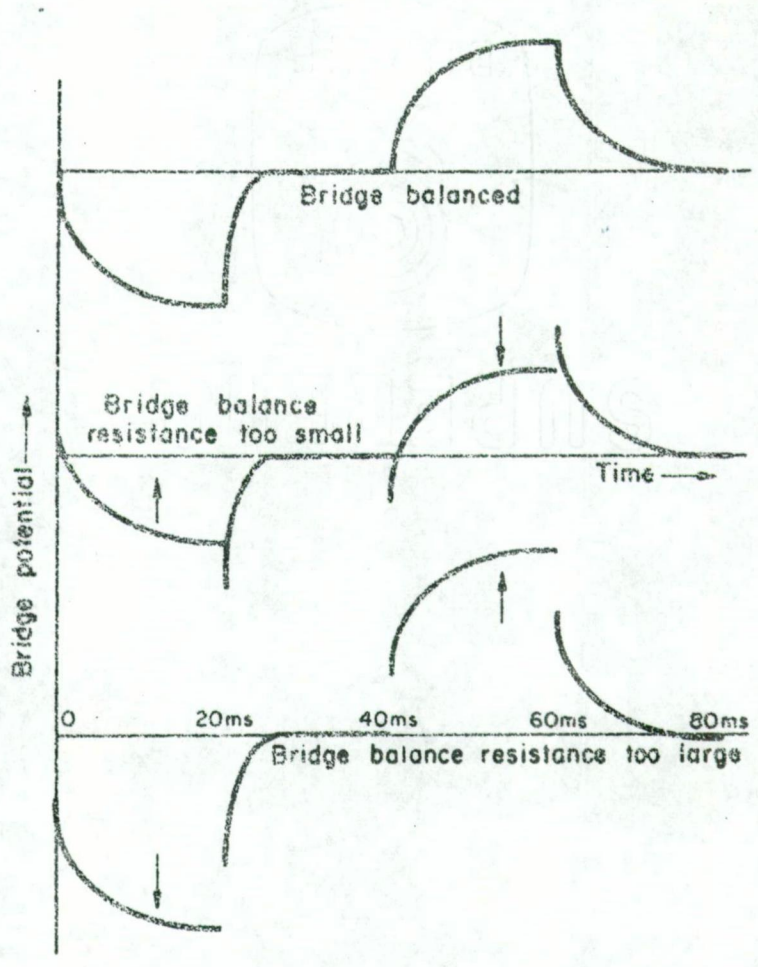

Fig. 2.8. Effect on observed potential of bridge unbalance.

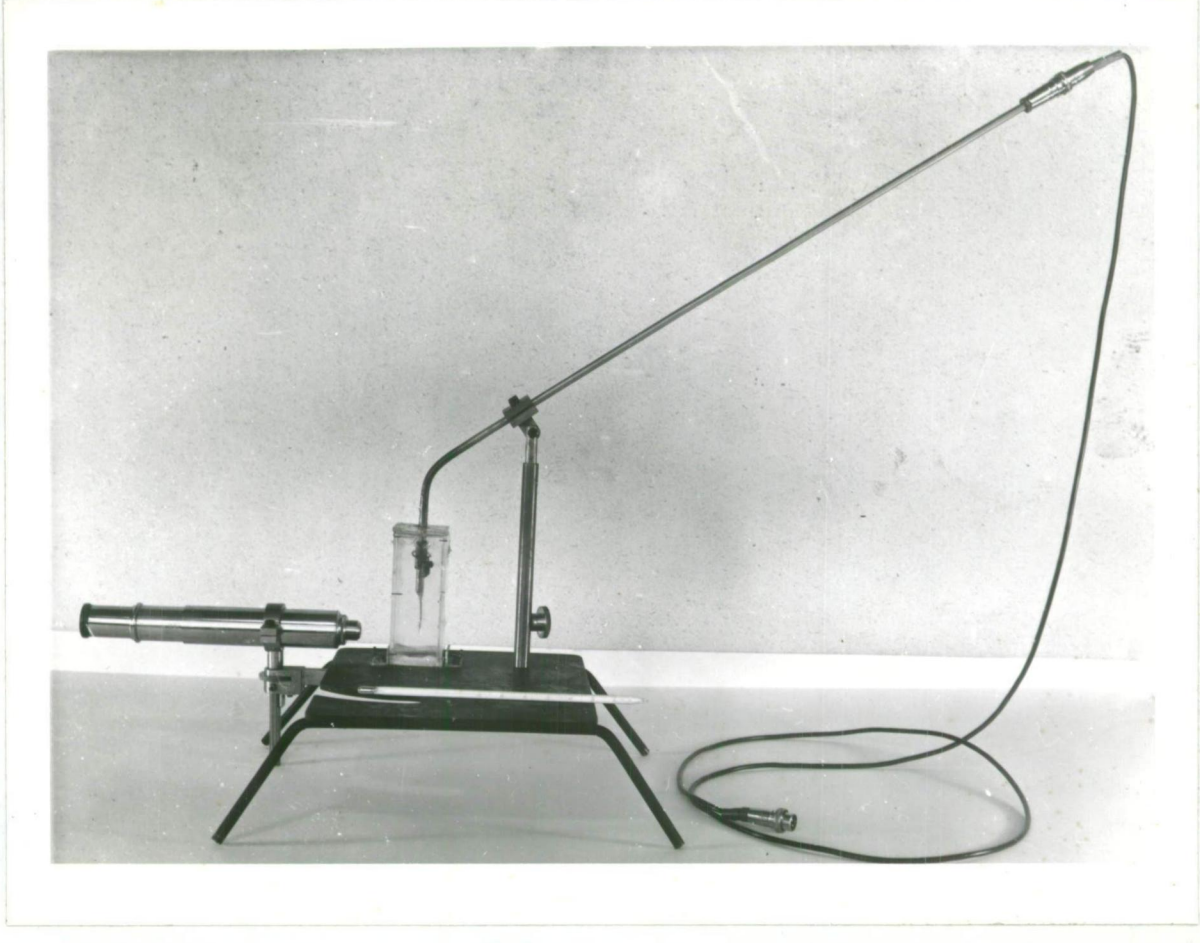

Fig. 2.9. Apparatus used in calibration in still air above saturated salt solutions.

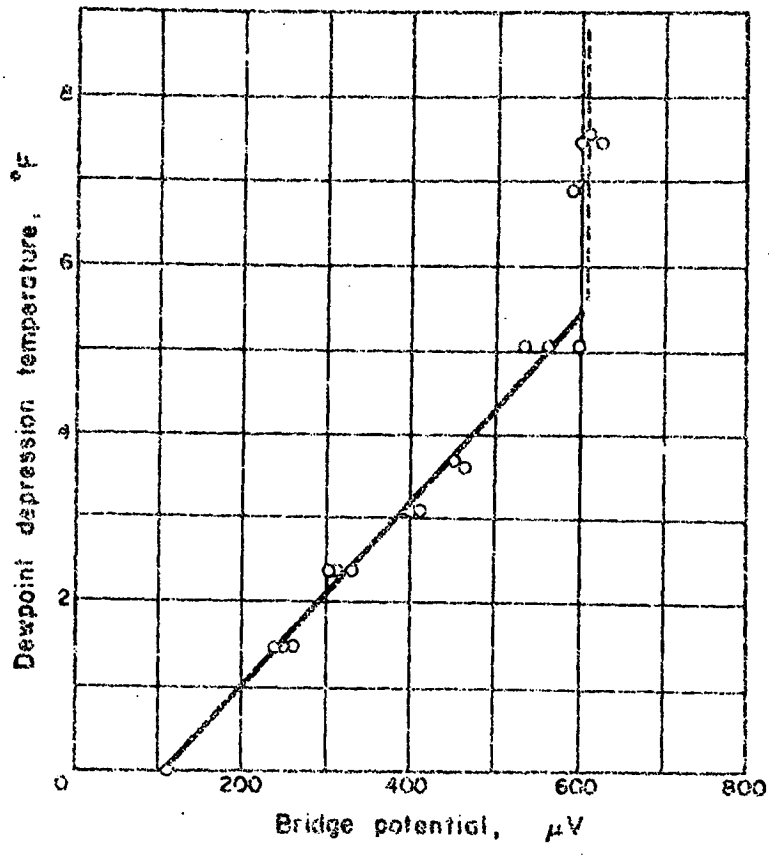

Fig. 2.10. Calibration of hygrometer in still air above saturated salt solutions.

2.9 Limitations and reason for abandoning the method.

This investigation demonstrated that it is possible to measure humidity with the required spatial discrimination. The intention at the conclusion of this work was to attempt a calibration in moving air and for this purpose a small closed circuit wind tunnel was constructed. (Fig. 2.16, 2.17). The tunnel had provision for adjusting the humidity by bubbling the air through various saturated salt solutions.

It became apparent both from the attempt at calibration in moving air and from consideration that the basis of the measuring process is the assessment of the surface heat transfer coefficient of the wet wire, that the method is very sensitive to changes in air velocity; so much so as to preclude calibration in moving air.

However this investigation showed that it is possible to cool a thermocouple junction to below the dewpoint of the surrounding air (provided that the dewpoint is not more than about 5 degF below ambient temperature) and that it is possible, by means of the alternating current bridge technique developed, to observe continuously the junction temperature.

2.10 The sawtooth cooling approach.

The limited success of the method described above led to the investigation of a technique which involved a progressive cooling of the thermocouple junction by means of Peltier cooling with a sawtooth wave form current. The new method sought to identify the onset of condensation and hence the dewpoint temperature. It is possible to observe the onset of condensation under a microscope, but the eventual requirement that the method should be suitable for turbulent flow and the difficulty of microscopic observation without disturbing the air flow, necessitated some sort of electrical indication of the onset of condensation. It was hoped that the wetting of the junction would cause a sharp change in the surface heat transfer coefficient and hence a sharp change in junction temperature.

In order to find what the effect would be on the observable junction temperature of the junction becoming wet through condensation, a detailed mathematical and experimental study was made of the Peltier cooling of a thermocouple with a saw-tooth wave-form current. An analytical solution has been found for the case of a linearly increasing current, and a more general numerical solution has been developed to predict the behaviour of a thermocouple with an arbitrarily varying applied current. It is possible to cool a thermocouple about 20 times a second - a considerable increase in the time response over that of the Spanner method (Ref. 20) which required about 12 seconds for each reading.

2.11 Model of Peltier cooled thermocouple.

Spanner developed the following equation for the transient behaviour of a Peltier cooled thermocouple from the Fourier equation of heat conduction.

$$\frac{\partial\theta}{\partial t} = \alpha \frac{\partial^2\theta}{\partial x^2} - b^2\left(\theta + \frac{i^2 r}{h a A}\right) \quad , \qquad (2.1)$$

where $\alpha = k/\rho c$,

$b^2 = ha/A\rho c$,

θ is wire temperature,

t is time,

x is distance,

k is the thermal conductivity of the wire material,

a is the wire perimeter,

A is the cross sectional area of the wire,

h is the surface heat transfer coefficient of the wire,

r is the resistivity of the wire material,

ρ is the density of the wire material,

c is the specific heat of the wire material,

and i is the current flowing in the wire.

The boundary conditions are:-

(1) The heat conducted from the junction along the wires must have the value $-Pi$, (where P is the Peltier coefficient of the thermocouple junction).
A fraction $-\lambda Pi$ is conducted along one of the wires and $-(1-\lambda)Pi$ along the other.
Thus

$$kA\left(\frac{\partial\theta}{\partial x}\right)_{x=0} = -\lambda Pi \quad . \qquad (2.2)$$

The model can be extended to include the case of a thermocouple made of wires of different sizes. This has been done in the similar situation of Appendix III.

(2) Initially, the temperature is everywhere constant and equal to the ambient air temperature.

That is at $t = 0, \theta = 0$ for all x. (2.3)

(3) The influence of the Peltier effect is insignificant, sufficiently far away from the junction.

That is as $x \to \infty, \theta \to \theta(t)$ for all t, or substituting in equation (2.1),

$$\frac{\partial \theta}{\partial t} + b^2\left(\theta + \frac{i^2 r}{haA}\right) \to 0 \text{ as } x \to \infty. \quad (2.4)$$

The physical model of the thermocouple is one-dimensional in that it assumes that the temperature and Joule heating are uniform across the wire cross-section and heat convected at the surface reaches the whole of the cross-section uniformly and simultaneously.

2.12 Solution of the Equations.

A current increasing linearly with time may be described by the exprassion

$$i = \frac{I}{T} t \quad , \quad (2.5)$$

which on substitution into equation (2.1) gives

$$\frac{\partial \theta}{\partial t} = \alpha \frac{\partial^2 \theta}{\partial x^2} - b^2\left(\theta + \frac{I^2 r t^2}{T^2 haA}\right) ,$$

or more conveniently

$$\frac{\partial \theta}{\partial t} = \alpha \frac{\partial^2 \theta}{\partial x^2} - b^2\theta - \ell t^2 \quad , \quad (2.6)$$

where

$$\ell = \frac{b^2 I^2 r}{T^2 haA} = \frac{r I^2}{A^2 \rho c T^2} .$$

On substitution of equation (2.5), the condition at the boundary (equation 2.2) becomes

$$\left(\frac{\partial \theta}{\partial x}\right)_{x=0} = -\frac{\lambda P I}{k A T} t ,$$

or more conveniently

$$\left(\frac{\partial \theta}{\partial x}\right)_{x=0} = -\vartheta t , \quad (2.7)$$

where

$$\vartheta = \frac{\lambda P I}{k A T} .$$

Equation (2.4) becomes

$$\frac{\partial\theta}{\partial t} + b^2\theta + \ell t^2 \to 0 \quad \text{as} \quad x \to \infty . \tag{2.8}$$

Equations (2.7) and (2.8), with the initial condition (2.3) are sufficient to solve the partial differential equation (2.6). It can be seen that (2.6) is linear in θ . Thus we can put $\theta = \theta_P + \theta_J$ where $\theta_P = \theta_P(x, t)$ and $\theta_J = \theta_J(t)$ independent of x so that (2.6) may be written as two equations

$$\frac{\partial\theta_P}{\partial t} = \alpha \frac{\partial^2\theta_P}{\partial x^2} - b^2\theta_P \ , \tag{2.9}$$

and

$$\frac{\partial\theta_J}{\partial t} = - b^2\theta_J - \ell t^2 \ . \tag{2.10}$$

The conditions (2.3), (2.7) and (2.8) become; for θ_P,

$$\left.\begin{aligned} &\frac{\partial\theta_P}{\partial x} = -Jt \quad \text{at} \quad x = 0 , \\ &\theta_P \to 0 \quad \text{as} \quad x \to \infty , \\ &\text{at } t = 0, \ \theta_P = 0 \text{ for all } x \quad ; \end{aligned}\right\} \tag{2.11}$$

and for θ_J; $\theta_J = 0$ at $t = 0$. (2.12)

Equation (2.9) describes a thermocouple of zero resistance (no Joule heating) undergoing Peltier cooling, while equation (2.10) describes an infinite wire with uniform Joule heating exchanging heat with the surroundings. It can be seen that equation (2.10) is an ordinary differential equation of the first order and degree. The following solution has been found which satisfies equation (2.10) and the initial equation (2.12);

$$\theta_J = \frac{\ell}{b^6}\left[2e^{-b^2t} - b^4t^2 + 2b^2t - 2\right] . \tag{2.13}$$

Equation (2.9) may be solved explicitly for the case of a linearly increasing current. The equation is also amenable to a finite difference solution which has the advantage that it may be applied to an arbitrary variation of current.

2.13 Finite difference solution.

The method follows normal practice (Ref. 24).

A grid is set up with the origin at the junction, the abscissa corresponding to distance along the wire and the ordinate corresponding to time. The method used is described as explicit or marching as the values of temperature at the grid points are calculated directly from other points on the grid.

2.13.1 Partial differential equation in finite difference form.

There are various ways, based on Taylor Series expansions of the derivatives, of expressing equation (2.6) in finite difference form. The solution by a marching process involves the selection of suitable differences so that the calculation can proceed.

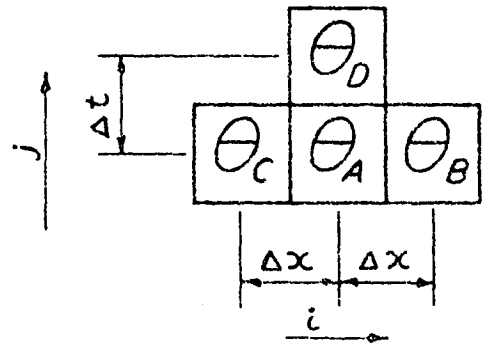

Fig. 2.11.

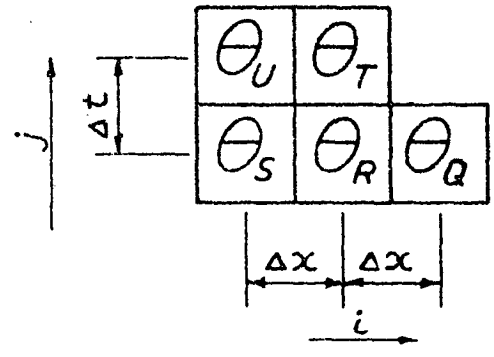

Fig. 2.12.

Away from the boundary, points on the grid involved in satisfying the finite difference equation are arranged as shown in Fig. 2.11. With a central difference for $\frac{\partial^2\theta}{\partial x^2}$ and forward difference for $\frac{\partial\theta}{\partial t}$ we have;

$$\frac{\partial^2\theta}{\partial x^2} = \frac{\theta_B - 2\theta_A + \theta_C}{\Delta x^2} \quad ; \quad \frac{\partial\theta}{\partial t} = \frac{\theta_D - \theta_A}{\Delta t} \; .$$

So that, for equation (2.6) to be satisfied at point A (corresponding to θ_A),

$$\frac{\theta_D - \theta_A}{\Delta t} = \frac{a}{\Delta x^2}(\theta_B - 2\theta_A + \theta_C) - b^2\theta_A \; ,$$

or rearranging

$$\theta_D = (1 - 2\beta - b^2\Delta t)\theta_A + (\theta_B + \theta_C)\beta ,$$

$$\text{with} \quad \beta = \frac{\alpha \Delta t}{\Delta x^2} .$$

More generally, if $\theta_{i,j}$ is a temperature at grid point i, j,

$$\theta_{i,j+1} = (1 - 2\beta - b^2\Delta t)\theta_{i,j} + (\theta_{i-1,j} + \theta_{i+1,j})\beta . \qquad (2.14)$$

Thus, once the values of temperature in the j^{th} row have been calculated the values in the $(j + 1)^{th}$ row may be obtained. However, at the end of each row, the value in the $(j + 1)^{th}$ row uses the $(i + 1)^{th}$ term in the previous row, so that the rows become shorter and the calculation proceeds in a triangular fashion.

2.13.2 Boundary condition in finite difference form.

Points involved are as shown in Fig. 2.12. It is presumed that θ_S, θ_R and θ_Q have been calculated previously.

By applying the finite difference equation (2.14) to points T, S, R and Q, θ_T may be found; thus

$$\theta_T = (1 - 2\beta - b^2\Delta t)\theta_R + (\theta_S + \theta_Q)\beta .$$

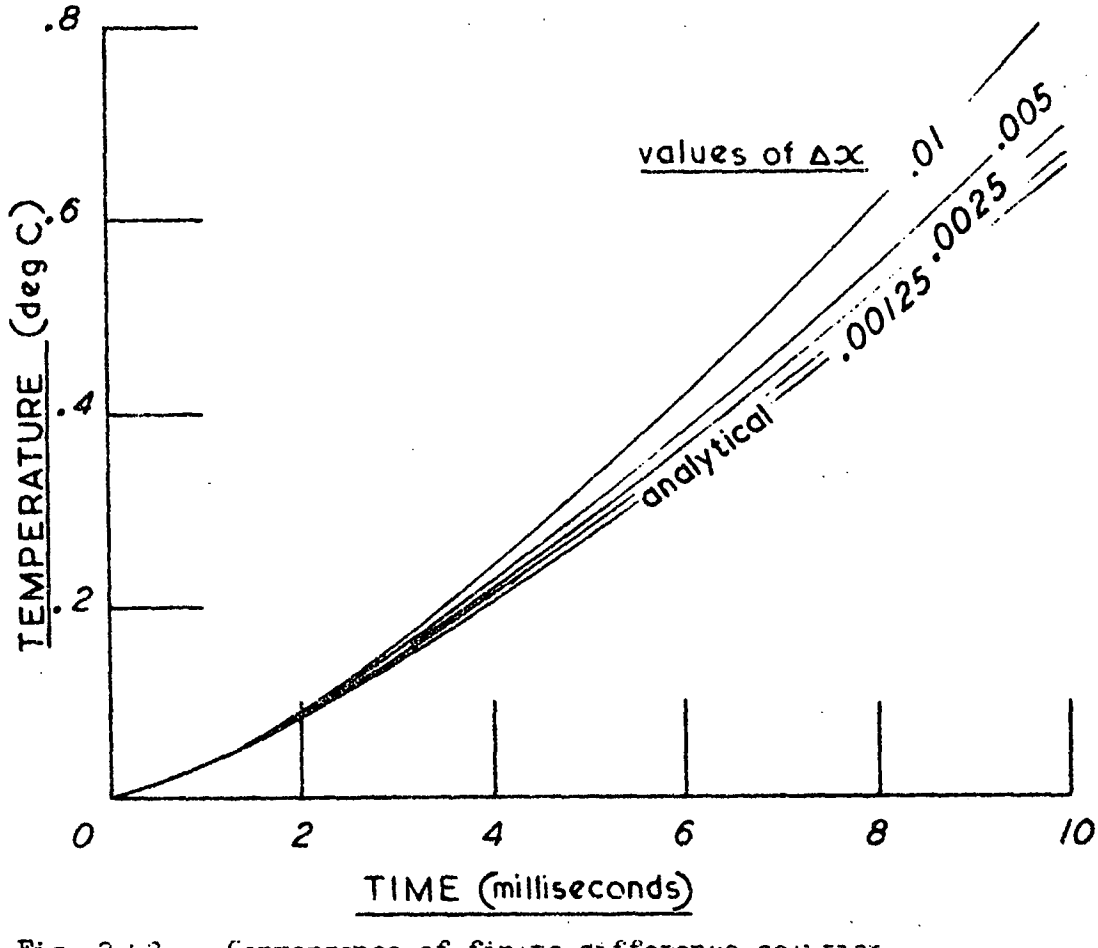

Fig. 2.13. Convergence of finite difference solution.

θ_U is then computed by applying the boundary condition with a forward difference for $\frac{\partial\theta}{\partial x}$;

via. $$\frac{\partial\theta}{\partial x} = \frac{\theta_T - \theta_U}{\Delta x} \quad ,$$

and from (2.7),

$$\frac{\theta_T - \theta_U}{\Delta x} = -\vartheta t \quad ,$$

thus

$$\theta_U = \theta_T + \vartheta \Delta x t \quad ,$$

or more generally, for the j^{th} row,

$$\theta_{o,j} = \theta_{1,j} + \vartheta \Delta x \Delta t j \quad . \qquad (2.15)$$

2.13.3 Start of calculation.

The initial condition is represented by the first (j = 0) row. Thus the temperature at grid points in the first row are set to zero. The first non-zero temperature is at the grid point i = 0, j = 1 and can be computed by substituting these values of i and j in equation (2.15)

$$\theta_{o,1} = \vartheta \Delta t \Delta x \quad .$$

2.13.4 Stability and convergence of calculation.

A marching type of solution is deemed "conditionally" stable. The condition for a stable solution is that

$$\beta = 0.5 \qquad \text{where} \quad \beta = \alpha \frac{\Delta t}{\Delta x^2} \quad . \qquad (2.16)$$

If this is satisfied, small errors introduced either at the boundaries or elsewhere are "washed out" as the solution progresses. The convergence of the solution is illustrated in Fig. 2.13 which shows numerical solutions with the same value of β , but with

different grid spacings. They converge towards the analytical solution. It is possible to extrapolate the numerical solutions to give the analytical solution using an extrapolation based on the square of the grid spacing.

2.14 The analytical solution.

The following solution was contributed by Prof. D. Elliott, Professor of Applied Mathematics at the University of Tasmania. It is given here for the sake of completeness and for comparison with the finite difference solution.

The equations for θ_p, dropping the subscript, are

$$\frac{\partial\theta}{\partial t} = \alpha \frac{\partial^2\theta}{\partial x^2} - b^2\theta \,, \tag{2.17}$$

$$\left.\begin{aligned} &\text{and } \frac{\partial\theta}{\partial x} = -\vartheta t \quad \text{at} \quad x = 0 \,, \\ &\theta \to 0 \quad \text{as} \quad x \to 0 \,, \\ &\text{at } t = 0, \ \theta = 0 \text{ for all } x. \end{aligned}\right\} \tag{2.18}$$

The Laplace transform $\bar{\theta}(x, p)$ of $\theta(x, t)$, with respect to t may be written as follows

$$\mathcal{L}[\theta(x,t)] = \bar{\theta}(x,p) = \int_0^\infty e^{-pt}\theta(x,t)\,dt \,.$$

It follows from this definition that

$$\mathcal{L}\left[\frac{\partial\theta}{\partial t}\right] = p\,\bar{\theta}(x,p) \,,$$

and

$$\mathcal{L}\left[\frac{\partial^2\theta}{\partial x^2}\right] = \frac{\partial^2}{\partial x^2}\bar{\theta}(x,p) \,,$$

which, when substituted into equation (2.17) give

$$p\,\bar{\theta}(x,p) = \alpha \frac{\partial^2}{\partial x^2}\bar{\theta}(x,p) - b^2\bar{\theta}(x,p) \,,$$

or rearranging;

$$\frac{\partial^2\bar{\theta}}{\partial x^2} = \frac{b^2 + p}{\alpha}\,\bar{\theta} \,.$$

which is an ordinary differential equation of the second order first degree and has the solution

$$\bar{\theta} = A(p)\, e^{\sqrt{\frac{b^2+p}{\alpha}}\, x} + B(p)\, e^{-\sqrt{\frac{b^2+p}{\alpha}}\, x} \quad .$$

Now, one of the conditions in (2.18) is that

$$\theta \to 0 \quad \text{as} \quad x \to \infty \quad ,$$

thus $A(p) = 0$,

and
$$\bar{\theta} = B(p)\, e^{-\sqrt{\frac{b^2+p}{\alpha}}\, x} \quad . \tag{2.19}$$

Another condition in (2.18) is

$$\text{at } x = 0 \quad , \quad \frac{\partial \theta}{\partial x} = -\mathcal{J} t \quad ,$$

or more generally

$$\frac{\partial \theta}{\partial x} = -\mathcal{J} f(t) \quad , \tag{2.20}$$

which on transforming becomes

$$\frac{\partial \bar{\theta}}{\partial x} = -\mathcal{J} \mathcal{L}[f(t)] \quad . \tag{2.21}$$

From (2.19) above we have

$$\frac{\partial \bar{\theta}}{\partial x} = -B(p)\, e^{-\sqrt{\frac{b^2+p}{\alpha}}\, x} \sqrt{\frac{b^2+p}{\alpha}} \quad ,$$

which, at $x = 0$ becomes

$$\frac{\partial \bar{\theta}}{\partial x} = -B(p) \sqrt{\frac{b^2+p}{\alpha}} \quad ;$$

so that, with equation (2.21) we have

$$B(p) = \mathcal{J} \sqrt{\frac{\alpha}{b^2+p}}\, \mathcal{L}[f(t)] \quad ,$$

and on substitution into equation (2.19);

$$\bar{\theta} = \mathcal{J} \sqrt{\frac{\alpha}{b^2+p}}\, \mathcal{L}[f(t)]\, e^{-\sqrt{\frac{b^2+p}{\alpha}}\, x} \quad ,$$

which may be written

$$\bar{\theta} = \mathcal{J} \sqrt{\alpha}\, \mathcal{L}[f(t)]\, \mathcal{L}[g(t)] \quad , \tag{2.22}$$

where
$$g(t) = \frac{e^{-b^2 t}\; e^{-\frac{x^2}{4\alpha t}}}{\sqrt{\pi t}} \quad .$$

By applying the convolution theorem to equation (2.22) namely

$$\mathcal{L}[f(t)]\mathcal{L}[g(t)] = \mathcal{L}\left[\int_0^t g(u)\, f(t-u)\, du\right],$$

and taking the inverse transforms of both sides, we have

$$\theta(x,t) = \vartheta\sqrt{\alpha}\int_0^t \frac{e^{-(b^2u + x^2/4\alpha u)}}{\sqrt{\pi u}} f(t-u)\, du;$$

which, with $f(t-u) = t-u$ for a linearly increasing current becomes

$$\theta(x,t) = \vartheta\sqrt{\alpha}\int_0^t \frac{e^{-(b^2u + x^2/4\alpha u)}}{\sqrt{\pi u}} (t-u)\, du.$$

This expression is integrable by parts to give

$$\theta(0,t) = \frac{\vartheta\sqrt{\alpha}}{b}\left(\frac{1}{2b^2} - t\right)\mathrm{erf}(b\sqrt{t}) - \frac{\vartheta\sqrt{\alpha}}{b^2}\sqrt{\frac{t}{\pi}}\, e^{-b^2t}, \qquad (2.23)$$

where $\theta(0,t)$ is the temperature at the junction ($x=0$) and

$$\mathrm{erf}(b\sqrt{t}) = \frac{2}{\sqrt{\pi}}\int_0^{b\sqrt{t}} e^{-s^2}\, ds.$$

2.15 Predicted characteristics.

It can be seen from the form of the equation (2.17) and its solution, equation (2.23), that the temperature $\theta(0, t)$ at the junction is dependent on the parameters α, ϑ and b as well as time t.

However by slightly modifying the equations, it is possible to reduce the number of parameters so as to display the solution in graphical form with one parameter.

By making the substitution

$$\phi = \frac{\theta_p}{\vartheta}, \qquad (2.24)$$

the boundary condition becomes

$$\frac{\partial\phi}{\partial x} = t,$$

and the partial differential equation is

$$\frac{\partial\phi}{\partial t} = \alpha\frac{\partial^2\phi}{\partial x^2} - b^2\phi.$$

The parameter $\alpha = \frac{k}{\rho c}$ is seen to be dependent only on the properties of the thermocouple material. Thus for a particular thermocouple the variation of θ_p with time may be plotted as a graph of $\phi = \frac{\theta_p}{v}$ against t with b^2 as a parameter (Fig. 2.14). Likewise on substituting $\psi = \frac{\theta_J}{\ell}$ into equation (2.10), we obtain

$$\frac{\partial \psi}{\partial t} = -b^2\psi - t^2 \quad , \tag{2.25}$$

and thus the variation of θ_J can be shown as a plot of against t with b^2 as a parameter (Fig.2.15). The response of a particular thermocouple to a linearly increasing current may readily be found by computing b^2, finding the corresponding curves for ϕ and ψ against t in figures 2.14 and 2.15 and then combining $v\phi + \ell\psi$ to give the temperature of the thermocouple junction at any time t.

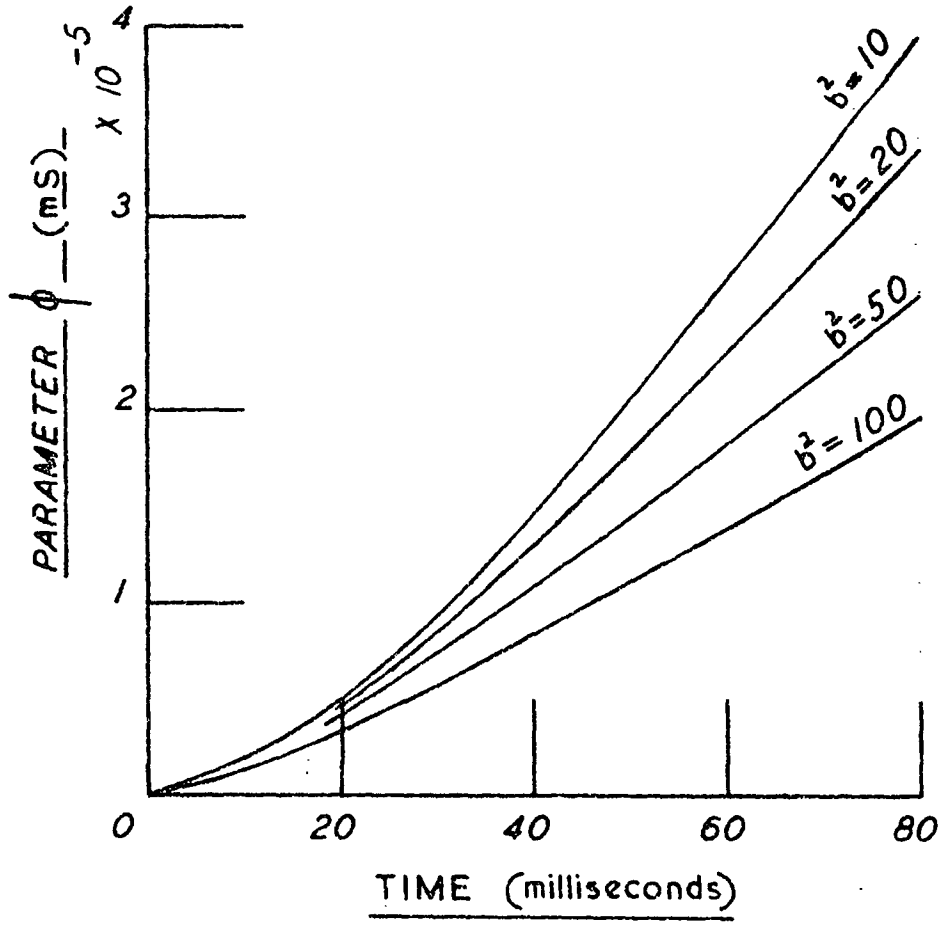

Fig. 2.14. Variation of parameter ϕ with time and parameter b.

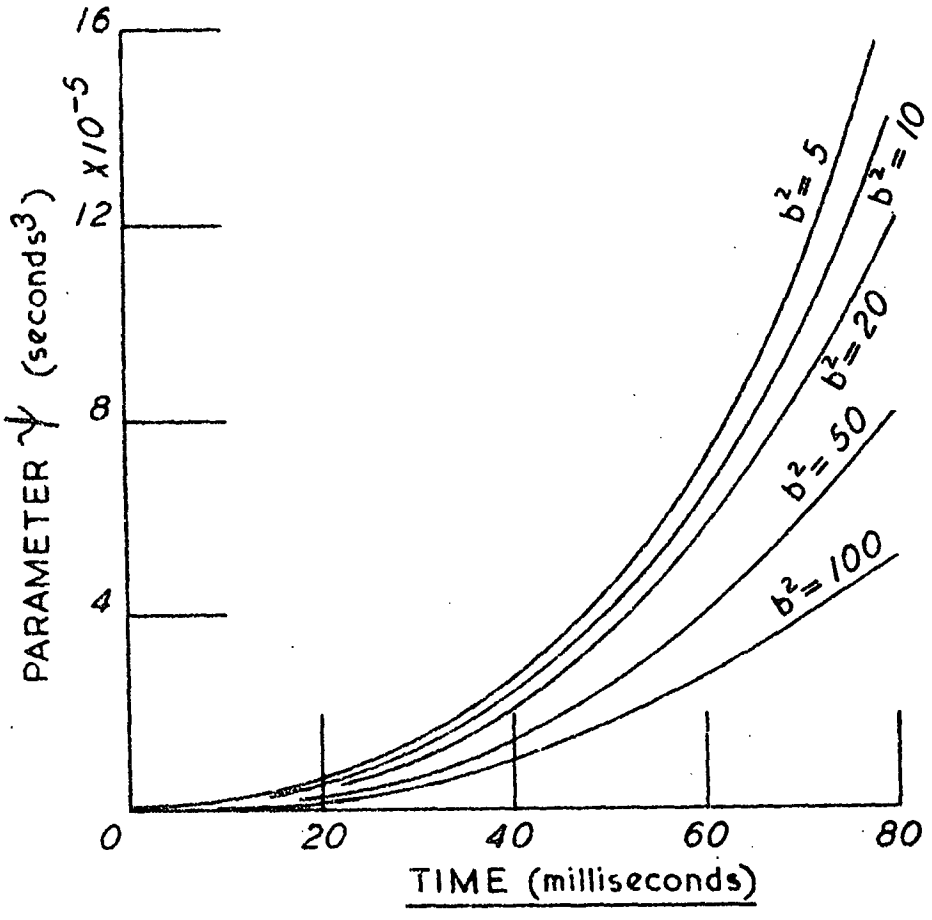

Fig. 2.15. Variation of parameter ψ with time and parameter b.

Thus once ϕ, ψ and b have been determined for a particular thermocouple, the mathematical model, or curves 2.14 and 2.15 in the case of a linearly increasing current may be used to predict the behaviour of the thermocouple for any particular cooling current.

2.16 Real Thermocouple behaviour.

In order to determine how close the theory approximated the real situation, a comparison was made between the behaviour predicted by the above model, and the observed behaviour of a real thermocouple. The experiment involved the use of a bridge circuit comprising three resistors and the thermocouple. (Fig. 2.5). A current wave form was passed through the bridge while a sensitive amplifier placed across the bridge detected the out-of-balance potential resulting from the change in thermocouple temperature.

A disadvantage of this system was the difficulty encountered in balancing the bridge. Small D.C. currents used to balance the bridge either introduced a potential due to the Peltier effect in the thermocouple or produced out-of-balance potentials across the bridge too small to be detected by the amplifier. Potential across the bridge during balancing also tended to be lost in thermocouple potentials resulting from air temperature fluctuations. The effect of a very small bridge unbalance is significant; with a typical cooling current of 10 mA., the expected change in thermocouple temperature is about 4 degC giving rise to a potential across the amplifier of around 0.12 mV. This potential could as well be caused by a bridge unbalance of 0.01 ohm, which is only 0.02% of the resistance of a typical thermocouple. Thus it was necessary, in the presentation of the experimental results to assume that the potential across the amplifier includes a potential directly proportional to the current, resulting from the bridge unbalance, in addition to that resulting from the cooling of the thermocouple. The magnitude of the bridge unbalance is inferred from the experimental results, there being only one value of the bridge unbalance which gives reasonable fit of the experiment to the theory.

2.17 Manufacture of thermocouples.

The method used is basically that described in section 2.5 above. Wires were produced by drawing glass containing the metal, then etching away the glass with hydrofluoric acid. Wires of bismuth and a bismuth with 5% tin alloy with diameters from .0005 to .003 inches were produced. Rather than soldering and resistance welding the wires to form thermocouples as described above, it was found that a silver conducting paint (DAG 915 Acheson Colloids Ltd.) produced a neater junction and was easier to use. Several thermocouples with different wire diameters and different lengths

were made. All responded in a similar manner when cooled as is described below. Two were subjected to an extensive examination and their behaviour compared with that predicted by the theory.

2.18 The Experiment.

A thermocouple was set up in a miniature closed circuit wind tunnel (Figs. 2.16, 2.17) in air with a velocity of 0.61m/s. A linearly increasing or ramp current, supplied from a "Servomex Waveform Generator" was applied to the bridge circuit. A sensitive A.C. differential amplifier (Tektronix 2A61) coupled to an oscilloscope and camera was used to record the potential appearing across the bridge. Typical currents used were zero to between 3mA and 15mA in about 100 milli-seconds.

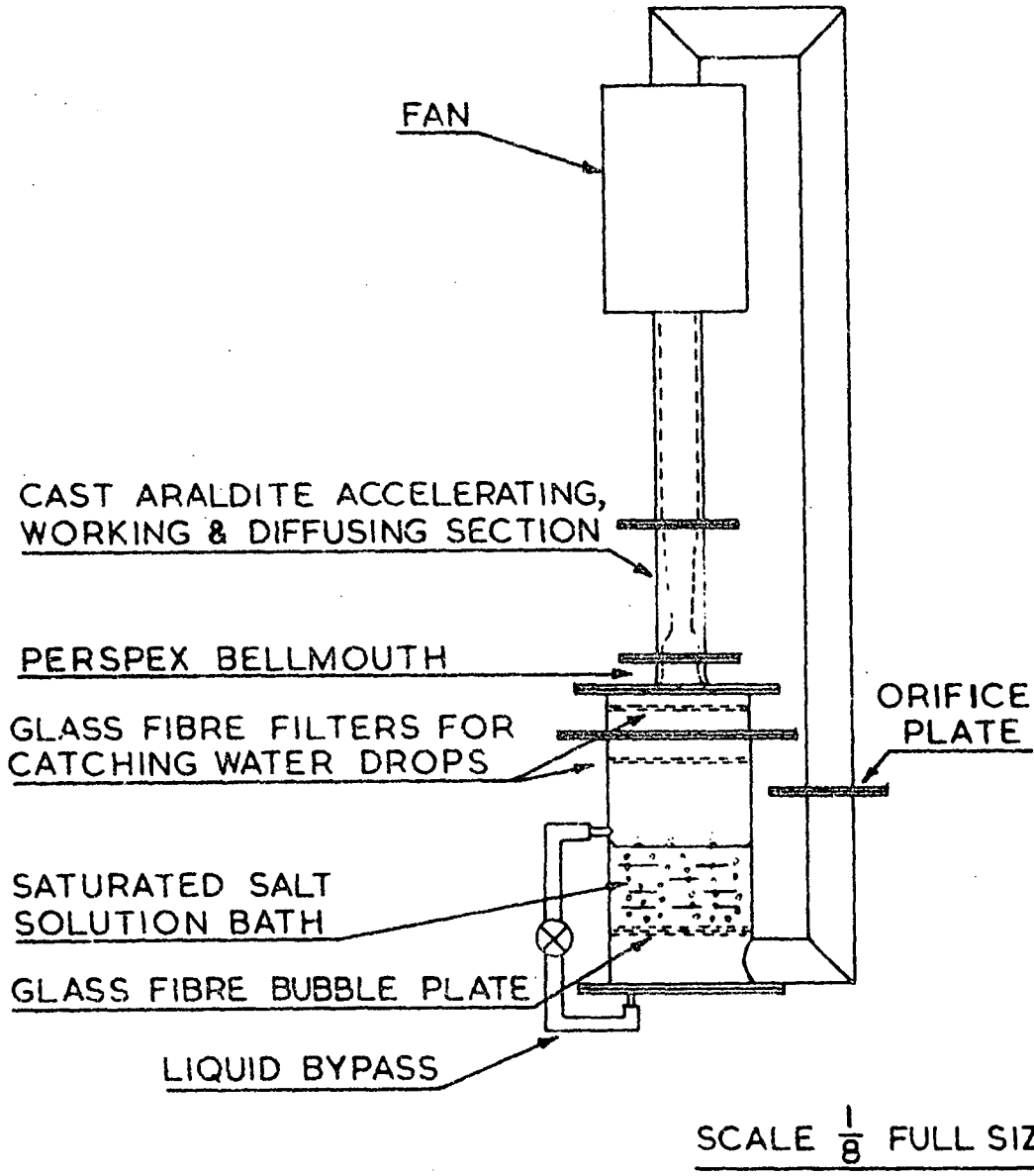

Fig. 2.16. Miniature closed circuit wind tunnel.

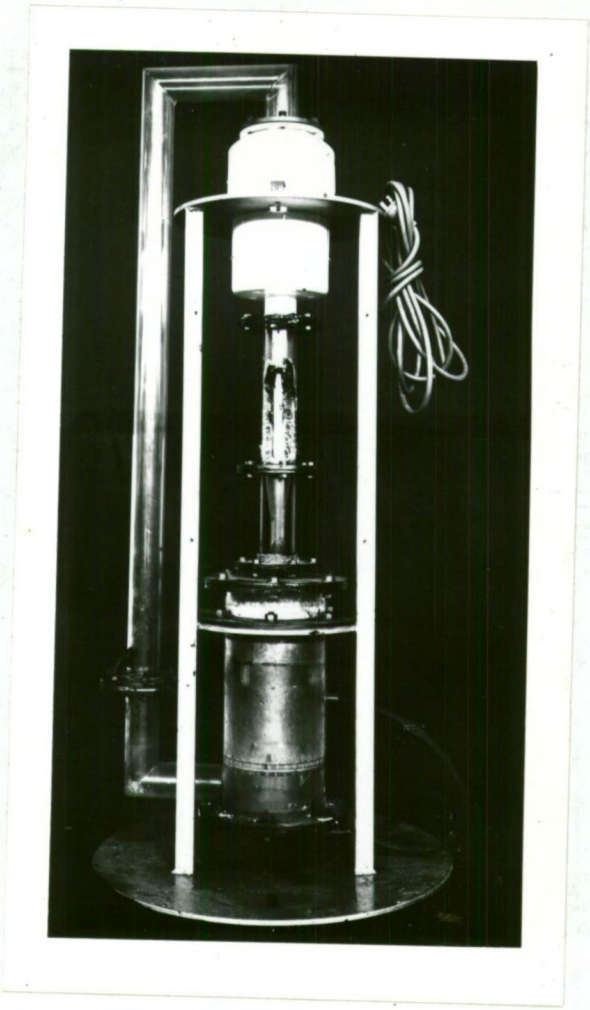

Fig. 2.17. Miniature closed circuit wind tunnel (photo).

2.19 Comparison with theory.

A comparison of the theory with the experimental results is given in Fig. 2.18. This shows potential - time curves for various ramp currents as recorded by the oscilloscope camera as well as a set of potential - time curves for the same currents, calculated from the expressions for the time variation of junction temperature derived in section 2.14 above. The results are presented as potential-time curves rather than temperature - time curves as the latter involves the difference of two relatively large quantities, the recorded potential and the potential arising from the bridge unbalance.

The equations describing the behaviour of a Peltier cooled thermocouple (equations (2.13) and (2.23)) contain four parameters α, b, ℓ, and ϑ expressed as follows;

$$\alpha = \frac{k}{\rho c}, \qquad b^2 = \frac{ha}{A\rho c},$$

$$\ell = \frac{I^2 r}{T^2 A^2 \rho c} \quad \text{and} \quad \vartheta = \frac{\lambda P I}{k A T}.$$

These parameters were computed from the data given in Reference 20, viz.

$k = 8.4$ W/m deg , $P = 2.96 \times 10^{-2}$ V at 0°C ,

$\rho = 9.8 \times 10^{3}$ kg/m^3 , $r = 1.065 \times 10^{-6}$ Ω-m ,

$c = 1.23 \times 10^{2}$ J/kg deg , $\lambda = 0.45$.

The value of h , the surface heat transfer coefficient was calculated from data in the International Critical Tables (Ref. 25).

Data pertinent to the thermocouples tested is as follows

	Thermocouple 1.	Thermocouple 2.
d	1.7×10^{-5} m	3.93×10^{-5} m
A	2.27×10^{-8} m	1.21×10^{-7} m
a	5.35×10^{-5} m	1.23×10^{-4} m
V	0.61 m/s	0.23 m/s
h	3.82×10^{2} W/m^2 deg	1.06×10^{2} W/m^2 deg

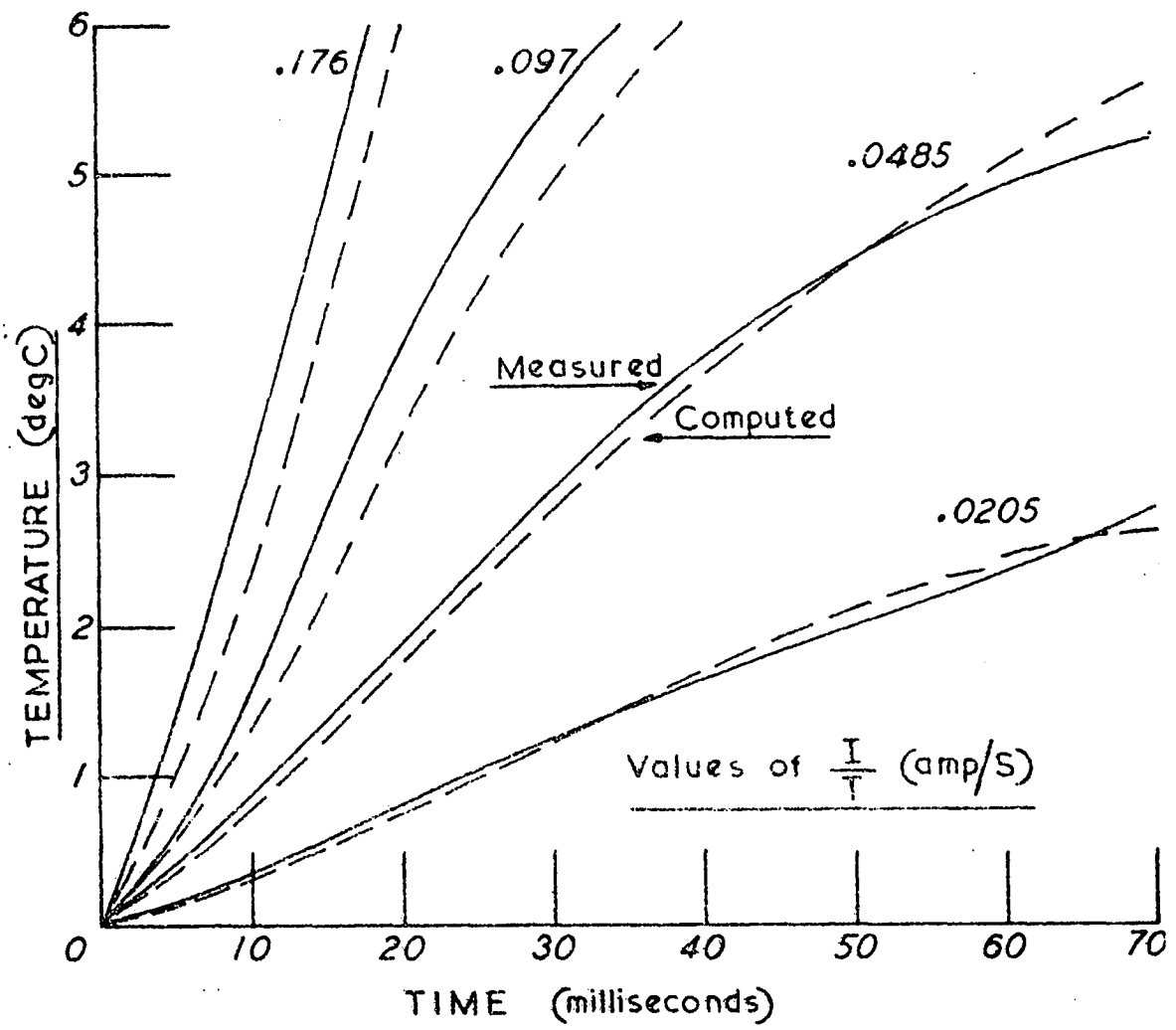

Fig. 2.18. Variation of thermocouple temperature with time for various values of cooling current ramp slope.

There are several possible reasons for the discrepancies between the theory and the experiment. The effect of the additional heat capacity at the junction due to the blob of metal and wire ends resulting from the weld is not included. One of the thermocouple metals may diffuse into the other resulting in a region of finite length over which the Peltier effect is manifested. There may also be significant two-dimensional effects in the simple geometry of two butting cylinders due to the presence of radial as well as longitudinal heat flux. It is also quite probable that the surface heat transfer coefficient, h, varies both over the surface of the wire and with temperature and time.

2.20 Behaviour of moist air.

The presence or absence of moisture on the wire is readily taken into account by the appropriate choice of the parameter b. There is some hope that values of the surface heat transfer coefficient may be inferred from psychrometric data. Work by Wylie (Ref. 26) and Powell (Ref. 27) shows that, as the diameter of an ordinary wet bulb is decreased, the threshold above which the effect of air velocity is negligible is reduced and the wet-bulb depression approaches the temperature of adiabatic saturation, or the "ideal" wet-bulb temperature. Likewise as the thickness of the muslin covering the junction is reduced, the wet-bulb depression approaches the ideal. Thus it is reasonable to assume that data from a standard hydrometer can be applied to the thermocouple psychrometer. The empirical data of Powell (Ref. 6) would seem to be the best estimate of the surface heat transfer coefficient.

i.e. Heat transfer by convection,

$$h = \left[\frac{2.7 + 5.7\,(Vd)^{0.56}}{d}\right] \times 10^{-1} \quad W/m^2 deg \ , \qquad (2.26)$$

and Heat transfer by evaporation;

$$f_d = 1.72 \times 10^{-3} (V_d)^{0.6} L (p_w - p_a) , \qquad (2.27)$$

where L is latent heat of vaporisation,

and $(p_w - p_a)$ is the difference between the water vapour pressure of the ambient air and the saturated vapour pressure at the temperature of the wet bulb.

The effect of condensation on the variation of the junction temperature is illustrated in Figure 2.19. Two curves are shown. One has a constant value of the surface heat coefficient (corresponding to a dry wire). The other has two values of h. The first is applied at temperatures above an arbitrarily chosen dewpoint, the second is applied to temperatures below this dewpoint and corresponds to a wet thermocouple.

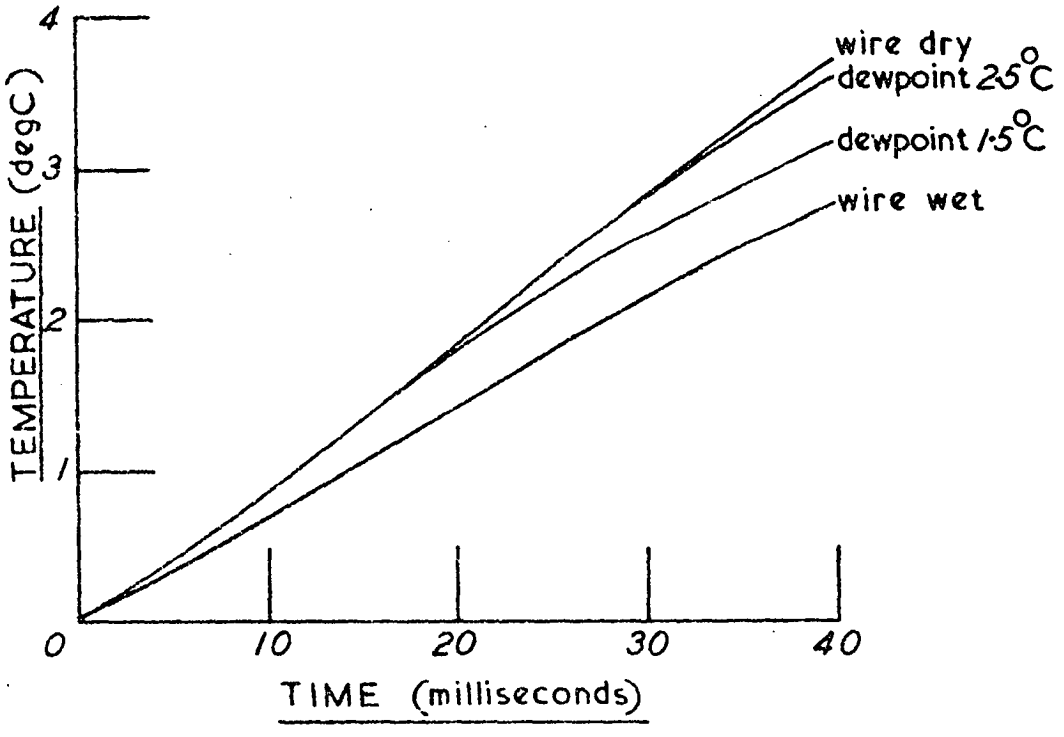

Fig.2.19. Effect of condensation on thermocouple output.

2.21 Reason for abandoning the progressive cooling method.

The reason for not pursuing the method of progressive cooling is best illustrated by Figure 2.19. It can be seen that,

due to the incipient nature of the onset of condensation, there is no marked change in the thermocouple temperature at the dewpoint. It was thought that suitable differentiating circuitry would accentuate the change, but in view of the limitation of the method to use in high humidities imposed by the relatively small cooling obtainable with conventional thermocouple materials, this approach was not followed up. It may be, that with semiconductor thermoelectric materials, at least the last mentioned objection could be overcome, but in view of the success with the rather simpler method described in the following chapter, the methods using a thermocouple as a dewpoint instrument were abandoned.

CHAPTER 3

In this chapter, the method used to measure humidity within a boundary layer is described. The efficacy of the successful method - the "thermocouple psychrometer" - is discussed with reference to various published works on thermocouples and psychrometers. The mathematical models of the thermocouple psychrometer, included as Appendix III, are outlined. Two methods of calibrating the thermocouple psychrometer, firstly by the measurement of the Seebeck coefficient of the junction, and secondly an in situ calibration as a psychrometer, are described. Part of this chapter has been published as reference 2.

3.1 The thermocouple psychrometer.

The limited success of the dewpoint methods led to a revaluation of the whole technique. The desirable features of thermocouple psychrometry, namely the small size and the lack of hysteresis at high humidities, supported the original choice of a thermocouple psychrometer. The difficulties which proved insurmountable with the pulsed cooling methods were the small degree of cooling obtainable and the dependence of the method on the identification of the dewpoint. This latter objection is overcome if, instead of the dewpoint temperature, the wet bulb depression is measured. This necessitates working with a constantly wet thermocouple. The requirement of a wet thermocouple then enables the first objection to be overcome as, in boundary layer work, there is always a region of high humidity close to the evaporation surface in which the degree of Peltier cooling obtainable enables the junction to be wet.

This, then, is the basis of the successful method of humidity measurement within a mass transfer boundary layer. The thermocouple used is as described in section 2.17. The thermocouple junction is brought into the region of high humidity close to the evaporating surface. The junction is cooled by passing a current (about 3 mA.) through the thermocouple in order to condense water on the junction.

The cooling current is discontinued, the thermocouple is switched into a potential measuring circuit, and then traversed through the boundary layer. Time available for the traverse before the junction dries is about 10 seconds.

A complication arises in that the temperature indicated by the thermocouple is relative to the so-called "cold-junction" temperature of the thermoelectric circuit. The "cold-junction" or better, the "other-junction", as in this case it is at a higher temperature than the wet thermocouple junction, is effectively at the junctions of the thermocouple wires with the copper supports. Because these points move through temperature gradients in the boundary layer, potentials additional to that from the wet junction appear in the thermoelectric circuit. These additional potentials are measured by repeating the thermocouple traverse through the boundary layer with the thermocouple junction dry. The difference between the potential generated in the thermoelectric circuit during the traverses with the junction wet and the potential generated during the traverse with the junction dry gives the wet bulb depression temperature through the boundary layer. Figure 3.1 shows a typical photograph of the thermocouple output with the junction wet; figure 3.2 is the photograph taken immediately after with the junction dry.

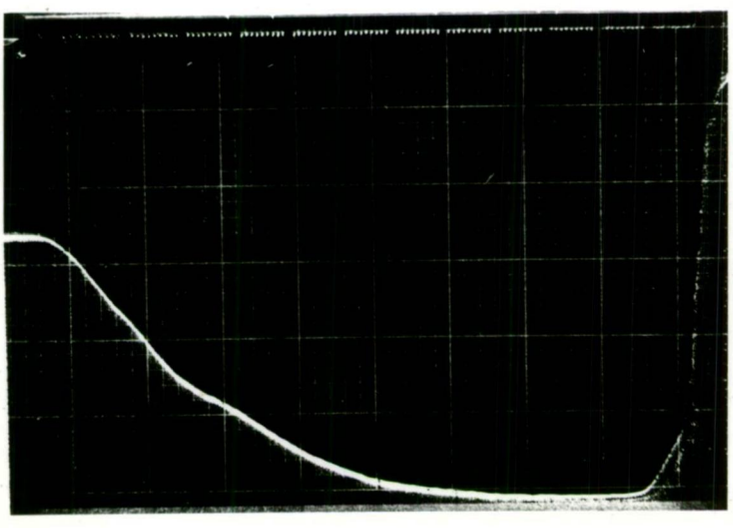

Fig. 3.1. Response of thermocouple psychrometer with wet junction.

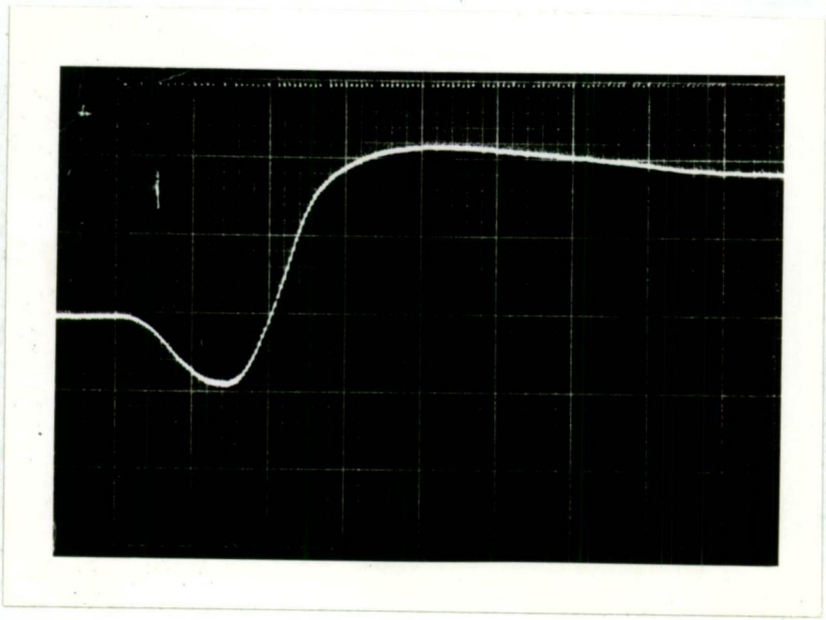

Fig. 3.2. Response of thermocouple psychrometer with dry junction.

The thermocouple is traversed through the boundary layer with the motor driven device sketched in figure 3.3. Incorporated in the device is a transducer which outputs electrical pulses as the probe passes levels above the plate at intervals of 127 microns (.005 inches). This makes possible the location of the probe even when accelerating at the start of a traverse. The output potentials from the thermocouple and displacement transducer are displayed and photographed on an oscilloscope. (Tektronix type 564 storage C.R.O.) A D.C. operational amplifier (Philbrick type P65A) with a gain of 1000 is used to match the output of the thermocouple to the oscilloscope.

The length of time that the thermocouple junction is cooled determines the amount of water condensed on the junction and thus the time available for a traverse before the junction dries. Figure 3.4 shows the effect on the thermocouple output of various cooling durations.

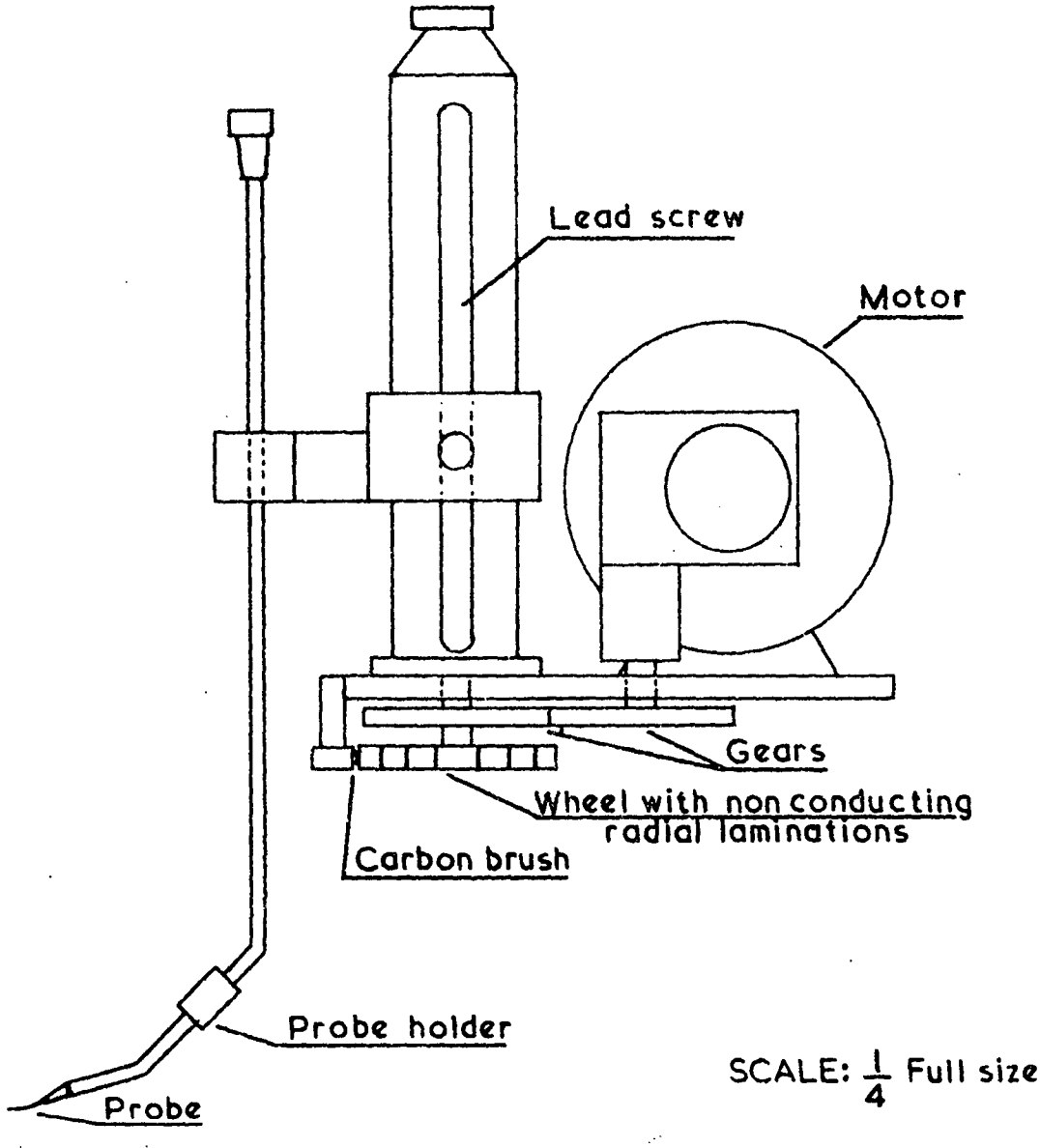

Fig. 3.3. Motor driven traverse.

3.2 The efficacy of the thermocouple psychrometer.

There is perhaps a need to establish that the output of the thermocouple psychrometer gives a true measure of the wet bulb depression. The term "wet bulb depression" needs some clarification. A distinction is made between the temperature of the wet bulb of a properly constructed psychrometer (whether sling, aspirated, etc.) and the so called "thermodynamic wet bulb temperature" or more strictly the temperature of adiabatic saturation. (Ref. 28). A theoretical psychrometer constant A_o can be defined in terms of the temperature of adiabatic

saturation by the expression

$$A_o = \frac{1}{P}\left(\frac{e^*_s - e}{T - T^*_s}\right) \quad , \qquad (3.1)$$

where P is the total pressure of the air-water vapour mixture,

e^*_s is the partial pressure of the water vapour at the temperature of adiabatic saturation,

e is the partial pressure of the water vapour at the "dry bulb" temperature,

T^*_s is the temperature of adiabatic saturation,

and T is the "dry bulb" temperature.

The psychrometer constant A_o has the value $A_o = 0.0006465$ $(degC^{-1})$.

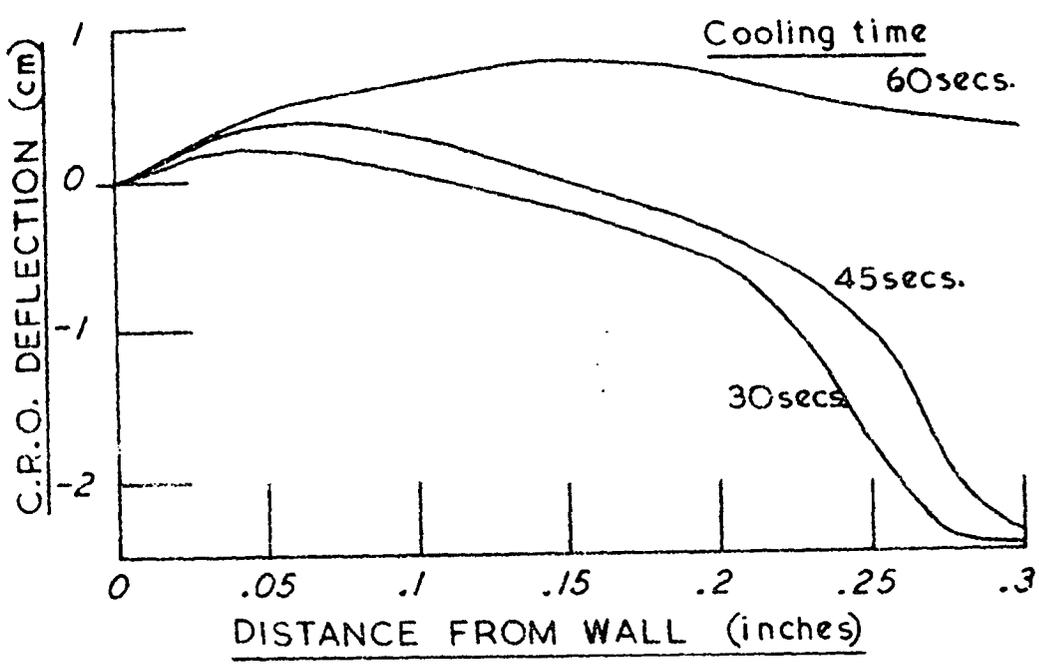

Fig. 3.4. Effect of cooling time on response of a thermocouple psychrometer.

It appears that, with well ventilated psychrometers giving turbulent flow over the wick, the measured wet bulb temperature is very close to the temperature of adiabatic saturation. Work of Montieth and Owen (Ref. 21) on wet thermocouples gave psychrometer constants ranging from 0.000615 $degC^{-1}$ to 0.000624 $degC^{-1}$ over the

range of air speeds 0.1 to 3.0 mS^{-1} and wet bulb element dia. 0.01 to 0.5 cm. Wylie (Ref. 26), using thermocouple bulbs of various diameters covered with wicks, presented a figure showing the variation with air speed of a ratio α, the ratio of the wet bulb depression of a particular thermocouple to the depression of a "standard" thermometer psychrometer with a bulb 3.0 mm. in diameter, ventilated at 3.0 mS^{-1}. Wylie's results show that for a wet thermocouple element less than 1.0 mm in diameter, the least value of α was 0.94 in still air, while in the range of air speeds 1 to 3 mS^{-1}, α was in the range 0.997 to 1.005. The smaller the diameter of the wet bulb element, the closer the values of α approached unity.

Powell published similar conclusions in Reference 27. Powell found that as the diameter of the wet bulb element is decreased, so also does the threshold below which the ventilation rate is significant. The wet bulb depression in still air of a 0.012 mm. dia. thermocouple was 98.4% of the depression when fully ventilated. The ratio of wet bulb depression in still air to that when fully ventilated tended to unity linearly with the square root of the thermocouple diameter. The output of a fully ventilated thermocouple psychrometer 0.012 mm. in diameter was found by Powell to be within 1% of that of a fully ventilated thermometer psychrometer.

A rather different approach is that of Fuchs (Ref. 29) who, in measuring evaporation rates of water droplets, used thermocouples to measure temperature within the droplets. Fuchs maintains that heat conduction along the thermocouple wires has an important effect on the thermocouple junction temperature; however, the thickness of the film of water on the junction in Fuchs' case is rather greater than for thermocouple psychrometers.

The steady state heat transfer processes associated with the evaporation of water from a wet thermocouple can be described as follows:- The heat flux associated with the phase change of the evaporating water is balanced by heat convected to the junction from the surrounding air stream and conducted along the thermocouple wires. The temperature of the thermocouple varies so as to maintain the balance between these heat fluxes. The real situation is complicated by the transient effect of the water being evaporated from the thermocouple and not replaced. An attempt was made to compute a psychrometer constant for the thermocouple psychrometer using various empirical data. Rather than try to incorporate the rather complicated geometry of the junction, two models chosen for simplicity of analysis and having simpler geometries which approximate the real situation were used as the basis for the calculation. The first model assumes that the wet junction can be described as a sphere of water approximately the same size as the junction supported on the two thermocouple wires, and that the wires outside the water droplet are dry. There is no temperature gradient within the sphere and across the wires; the supports are at the dry bulb temperature, and heat is convected to the wires and droplet as well as being conducted along the wires.

The second model assums that the wires are butt jointed and covered uniformly with water to a distance from the junction corresponding to the length of the thermocouple wires which reached the dewpoint temperature of the surrounding air during the Peltier cooling of the junction.

No attempt is made in either model to take into account the transient effect of the net flux of water from the junction. It is assumed that the mass of water evaporated is insignificant compared with the mass of water on the junction. In other words, the calculation is only applicable for a short time after the cooling current is cut off.

The calculations are given in detail as Appendix III. The psychrometer constants of the two models are .00059 $degC^{-1}$ for the water droplet case and .00045 $degC^{-1}$ for the wet wire case.

3.3 Calibration.

Provided there is no current flowing in the thermocouple, that is, provided a potentiometric method of measuring the thermoelectric potential is used, the potential appearing between the thermocouple support wires is given by;

$$V = T_a \alpha_{ab} + T_j \alpha_{bc} + T_b \alpha_{ca} \quad , \qquad (3.2)$$

where T_a is the temperature of the Cu-Bi connection,

T_b is the temperature of the Cu-BiSn connection,

T_j is the temperature of the Bi-BiSn junction,

α_{ab} is the thermoelectric potential of Cu w.r. to Bi,

α_{bc} is the thermoelectric potential of Bi w.r. to BiSn,

and α_{ca} is the thermoelectric potential of BiSn w.r. to Cu.

Which provided $T_a = T_b$ and substituting $\alpha_{ca} + \alpha_{ab} = -\alpha_{bc}$ becomes

$$V = \alpha_{bc} (T_j - T_a) \quad . \qquad (3.3)$$

That is, the potential appearing across the thermocouple is directly proportional to the difference between the temperatures of the junction and the ambient air, and the Seebeck coefficient of the junction. The thermocouple or Seebeck coefficient α_{bc} is usually defined in terms of the potential developed in a closed circuit of two different metals when the junctions of those metals are held at different temperatures.

In order to measure this coefficient, it is necessary to have two junctions at different measurable temperatures. This is rather difficult when short lengths of wire are involved as is the case with the bismuth and bismuth-tin alloy wires used in the thermocouple psychrometer. The method of manufacture and brittleness of the wires precludes lengths over about two centimetres.

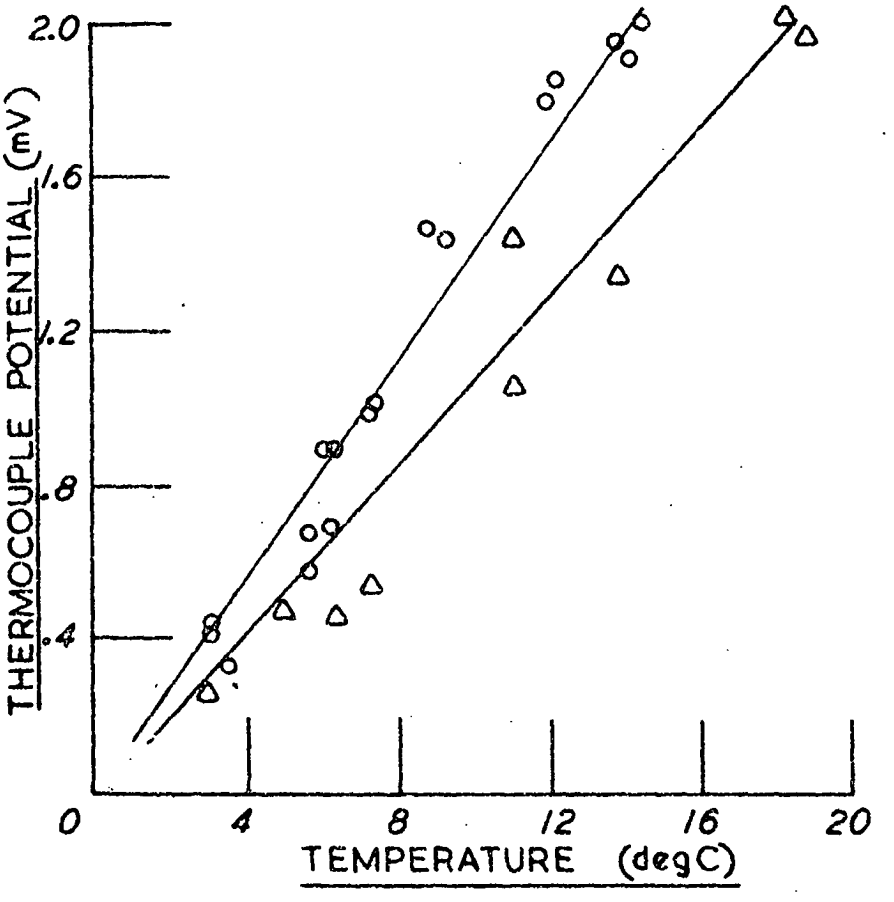

Fig. 3.5. Calibrations of two thermocouples.

Thus it is necessary to adopt a transient method of measuring the Seebeck coefficient. A single junction of bismuth and the bismuth-tin alloy was prepared and mounted as for the thermocouple psychrometer on relatively stout copper wires. The calibration was made by rapidly dipping the junction (but not the supports) into a stirred water bath at various temperatures. The output of the thermocouple under this conditions rose rapidly to the recorded value then fell slowly as the temperature of the supports approached the bath temperature. Two calibrations made in this manner are shown as figure 3.5. Figure 3.6 shows a typical thermocouple output when dipped into the water bath. The horizontal time scale is 10 milliseconds/div.

There are two possible sources of error in measuring humidity with a thermocouple psychrometer. The first is the uncertainty that the junction temperature is close to the temperature of adiabatic saturation; the second arises from the difficulty in measuring the thermoelectric potential of short lengths of wire.

Perhaps the most satisfactory way of taking these uncertainties into account is to use the wet bulb depression of the air outside the boundary layer to give a one point in situ calibration. The alternative, that of measuring the thermoelectric potential of longer thermocouple wires from the same batch and assuming that the temperature of the junction is at the temperature of adiabatic saturation when wet, gives rather less consistent results than the in situ calibration.

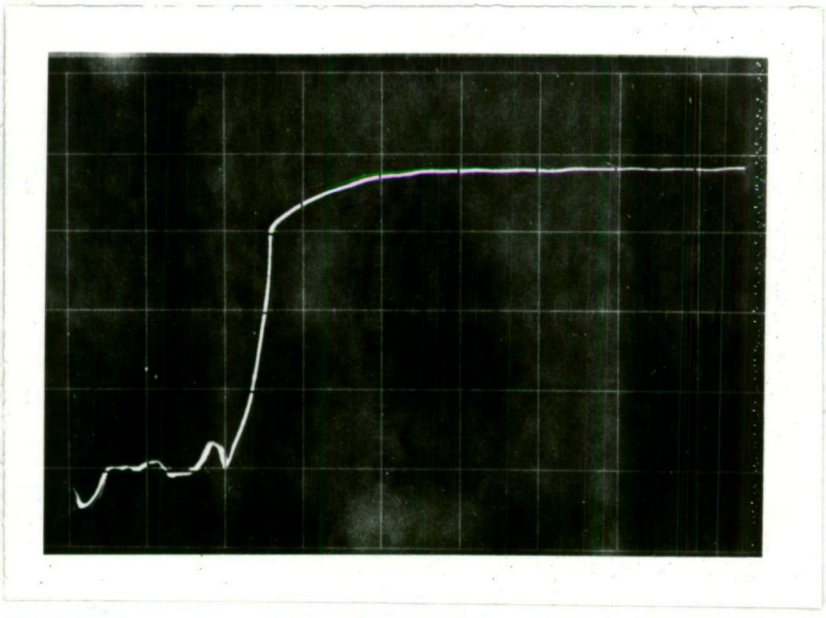

Fig. 3.6. Variation of thermocouple output when junction is dipped rapidly in water.

3.4 Conclusion.

With the development of a method of measuring humidity within a boundary layer, one of the aims of the project is realised.

The development was reported in reference 2, together with a single measurement of the concentration profile above a flat wet plate in a laminar air stream. This was followed by the detailed experimental and theoretical study of the laminar flat plate boundary layer described in the following three chapters.

CHAPTER 4

This chapter describes the measurement of velocity, temperature and humidity profiles in the laminar boundary layer above a flat wet plate. The results are presented non-dimensionally so as to correlate measurements made under differing conditions.

4.1 Generation of a mass transfer boundary layer.

A mass transfer boundary layer was set up by evaporating water through a 50% porosity sintered bronze plate. The plate (15 cm wide and 61 cm long) was set flush with the bottom of the working section of an open ended wind tunnel with a working cross section 23 cm. square and 1 m. long (Figs. 4.1, 4.2). Water supply to the porous plate was by gravity feed to a reservoir below the plate. During a run, additional water was supplied to a feeder reservoir, connecting with and at the same level as the reservoir below the plate. The water level in the feeder reservoir was held to within 1 mm. of a hook gauge set at the same height as the plate surface.

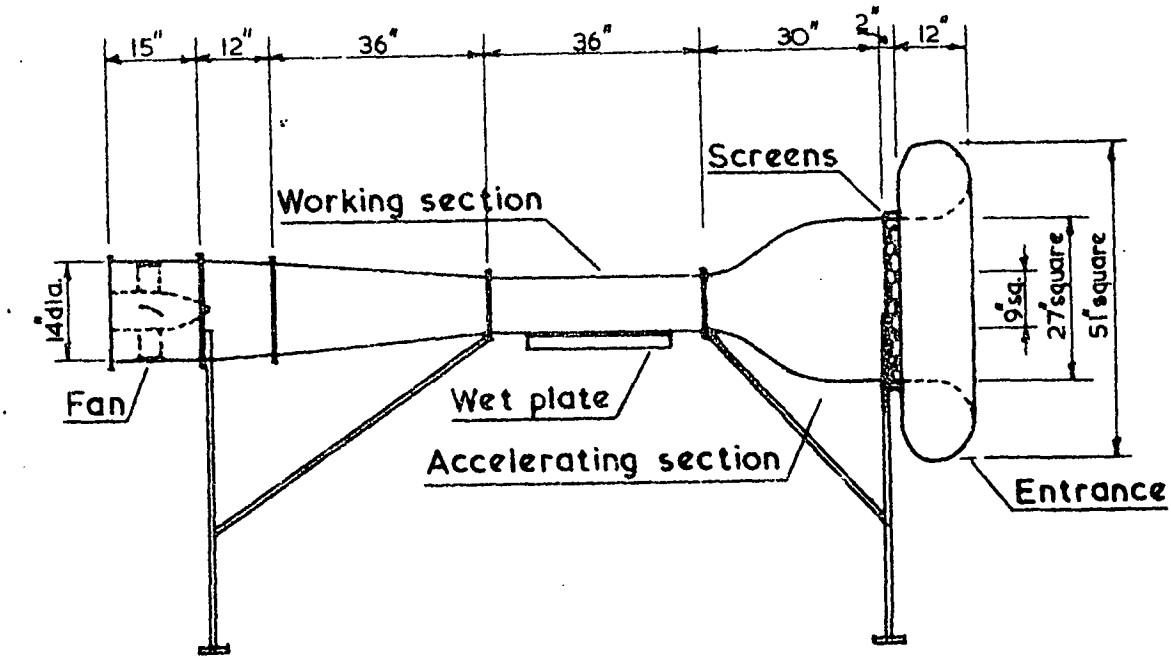

Fig. 4.1. Open-ended wind tunnel (diagram).

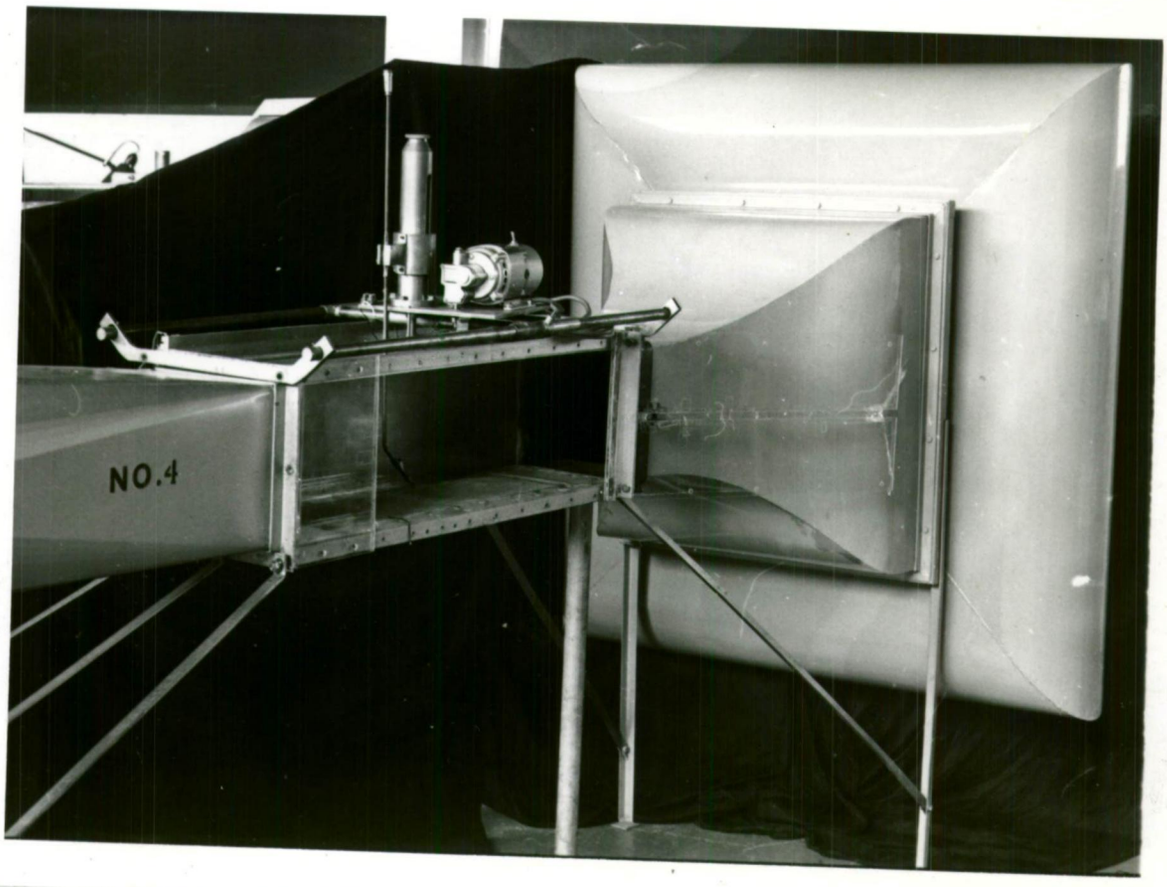

Fig. 4.2. Open-ended wind tunnel (photo).

Humidity and temperature of the air outside the boundary layer were measured with wet and dry bulb thermometers in the working section and a sling psychrometer at the tunnel entrance. The temperature of the wet plate was found from a copper-constantan thermocouple peened into the plate. Velocities of the bulk air flow in the tunnel were measured with a vane anemometer which was calibrated against the hot wire anemometer used for boundary layer velocity measurements.

When examined under a microscope the sintered bronze plate has the appearance of loosely packed spheres, each about 200 microns in diameter. When wet, the water surface is held by surface tension close to the tops of the spheres and presents to the air stream a flat, slightly undulating surface.

4.2 Measurement of velocity within the boundary layer.

Air velocities within the boundary layer above the wet plate were measured using the well known technique of hot wire anemometry (Ref. 30). The wire used was of tungsten, 8 microns in diameter and about 0.5 cm. long. A "DISA" anemometer type 55A01 provided constant wire temperature operation. The hot wire probe was moved through the boundary layer by a hand operated micrometer screw traverse. The hot wire anemometer was calibrated against a standard pitot-static tube with a Betz micro anemometer at velocities between 1.5 and 10 mS^{-1}. King's Law (Ref. 31) was used to extrapolate the calibration to the low velocities within the boundary layer.

4.3 Measurement of temperature within the boundary layer.

The temperature within the boundary layer was measured with the same traverse and tungsten wire probe used for the velocity measurement, but with a small current (2 mA.) through the wire so that the wire functioned as a resistance thermometer. A simple resistance bridge with nulling galvanometer was used to measure the wire resistance. The temperature resistance coefficient of the tungsten wire was found by calibrating the probe against the thermometer in an oil bath. Individual wires were calibrated at one temperature in the air outside the boundary layer in the wind tunnel immediately before use, using the value of the temperature resistance coefficient determined from the full calibration.

4.4 Sequence of measurements.

Associated with each measurement there was a calibration. It was usual to calibrate a hot wire probe for velocity in another small recirculating wind tunnel, move the probe to the humidity tunnel and measure velocity profiles at various stations along the plate and various air velocities. The same probe was then used for temperature measurement being calibrated in situ by the method described in section 4.3. Finally the thermocouple

psychrometer and associated circuitry was set up and used to measure the wet bulb temperature distribution across the boundary layer.

In each case the wall position was located relative to the probe by carefully bringing the probe up to the wall until electrical contact was made between the probe and the wall.

To obtain steady conditions in the boundary layer, it was necessary to run the wind tunnel for several hours at the same speed before each measurement. Thus the traverses of velocity, temperature and humidity at each station were made on different days and consequently with different ambient air and wet plate temperatures. These differences were taken into account by expressing the velocity, temperature and humidity in non-dimensional form, described in section 4.5.

In order to obtain at least one set of mutually consistent traverses, a series of measurements at the same station and air speed comprising a velocity traverse, a temperature traverse, a wet bulb depression traverse and a further velocity traverse was carried out in under three hours with nearly constant ambient conditions.

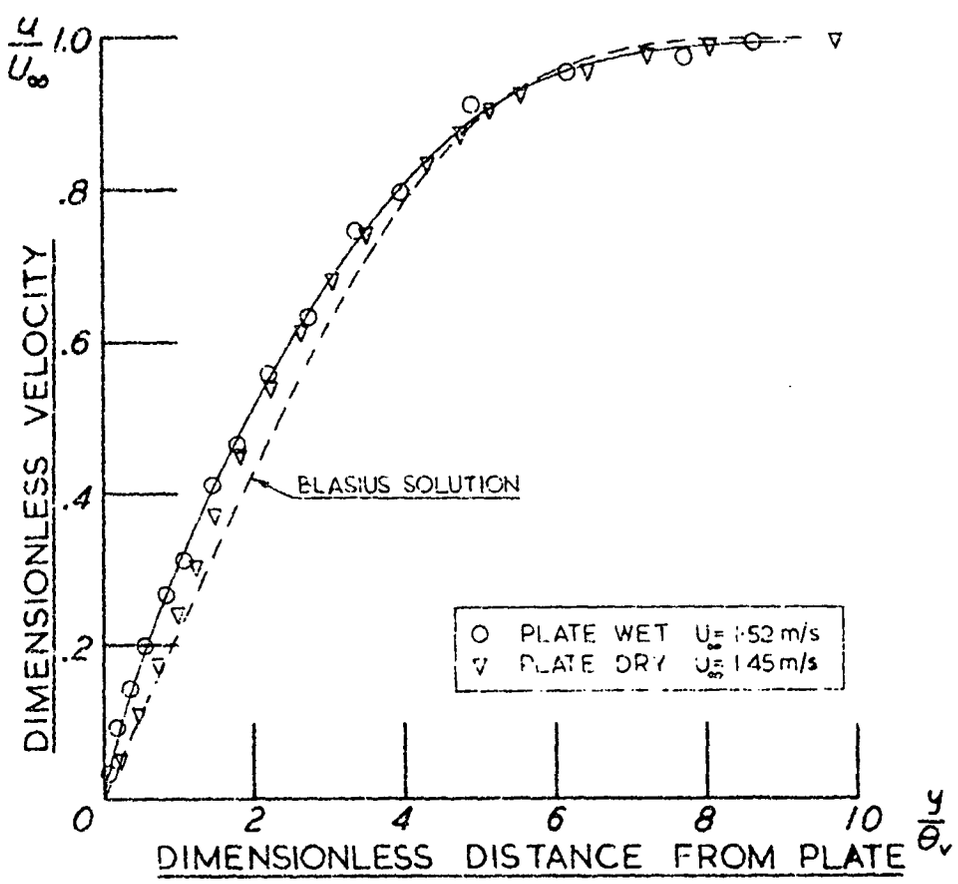

Fig. 4.3. Velocity profiles .147 m. downstream from leading edge of wet plate.

4.5 Experimental Results.

4.5.1 Velocity Profiles.

The measurements of velocity in the mass transfer boundary layer are shown in figures 4.3, 4.4, 4.5. The profiles presented have been corrected for the proximity to a solid boundary using the method of Wills (Ref. 32). Velocities in the boundary layer are presented as the non-dimensional ratio $\frac{u}{U_\infty}$ where u is the local velocity and U_∞ is the velocity of the bulk flow outside the boundary layer. Non-dimensional velocity is plotted against the non-dimensional distance parameter

$$\eta_w = \frac{y}{\theta_w} \quad , \tag{4.1}$$

where y is the distance from the wet plate,

and θ_w is the momentum thickness of the profile, defined by the expression;

$$\theta_w = \int_0^\infty \frac{u}{U_\infty}\left(1 - \frac{u}{U_\infty}\right) dy \quad . \tag{4.2}$$

A comparison is made in figure 4.3 between a velocity profile measured with the plate wet, a velocity profile measured at the same station and same (laminar) velocity with the plate dry, and the well known solution attributed to Blasius (Ref. 33) for the laminar velocity profile over a flat plate with zero pressure gradient.

4.5.2 Temperature Profiles.

The measurements of temperature in the mass transfer boundary layer are shown in figures 4.6, 4.7, 4.8. Temperature is expressed as the non-dimensional ratio

$$\theta = \frac{T - T_w}{T_\infty - T_w} \tag{4.3}$$

where T_w is the plate temperature,

T is the temperature within the boundary layer,

and T_∞ is the temperature outside the boundary layer.

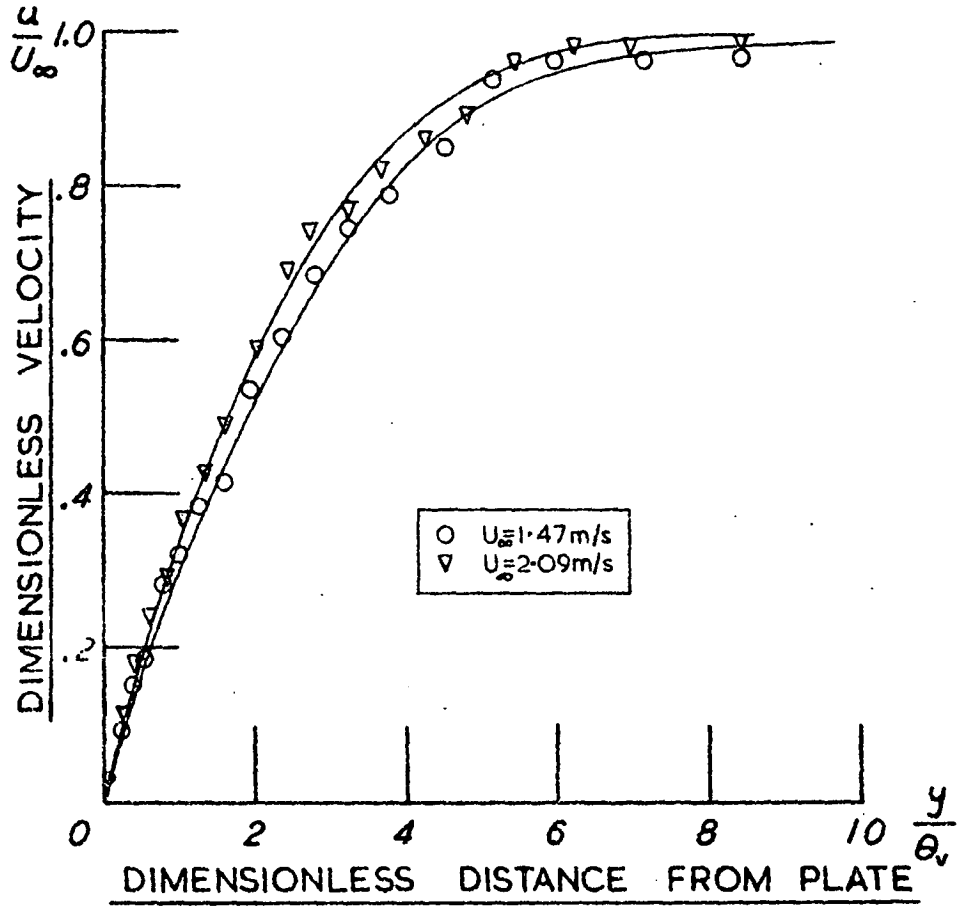

Fig. 4.4. Velocity profiles 0.203 m downstream from leading edge of wet plate.

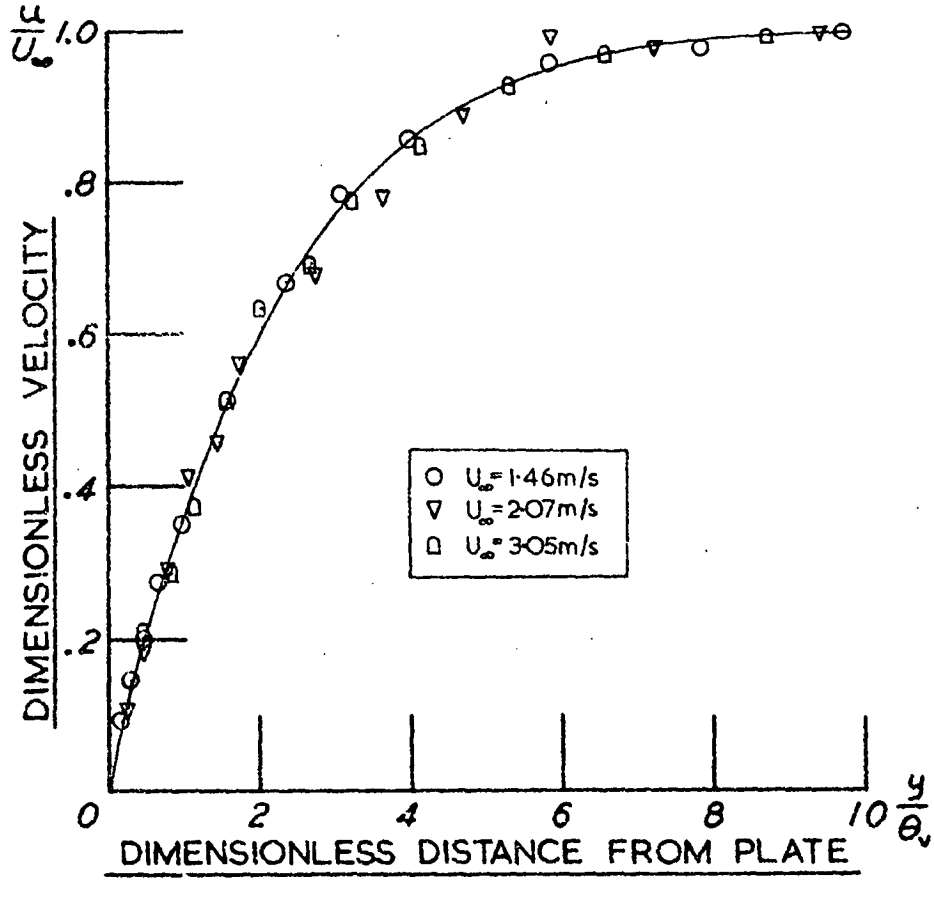

Fig. 4.5. Velocity profiles 0.267 m downstream from leading edge of wet plate.

Non-dimensional temperature is plotted against the non-dimensional distance parameter

$$\eta_t = \frac{y}{\theta_t} \quad , \tag{4.4}$$

with θ_t defined by the expression

$$\theta_t = \int_0^\infty \theta(1-\theta)\,dy \quad , \tag{4.5}$$

where y is the distance from the wet plate.

The non-dimensional distance parameter θ_t can be thought of as the analogue of the momentum thickness θ_x used in section 4.5.1 to represent the distance in the boundary layer. The reason for choosing these second order integrals in preference to the simpler displacement thickness

$$\delta = \int_0^\infty \left(1 - \frac{u}{U_\infty}\right) dy \quad , \tag{4.6}$$

and the temperature displacement thickness

$$\delta_T = \int_0^\infty (1-\theta)\,dy \quad , \tag{4.7}$$

is that the "momentum type" parameters θ_t and θ_x place less emphasis on measurements close to the wall and at the edge of the boundary layer, and so lead to a better correlation.

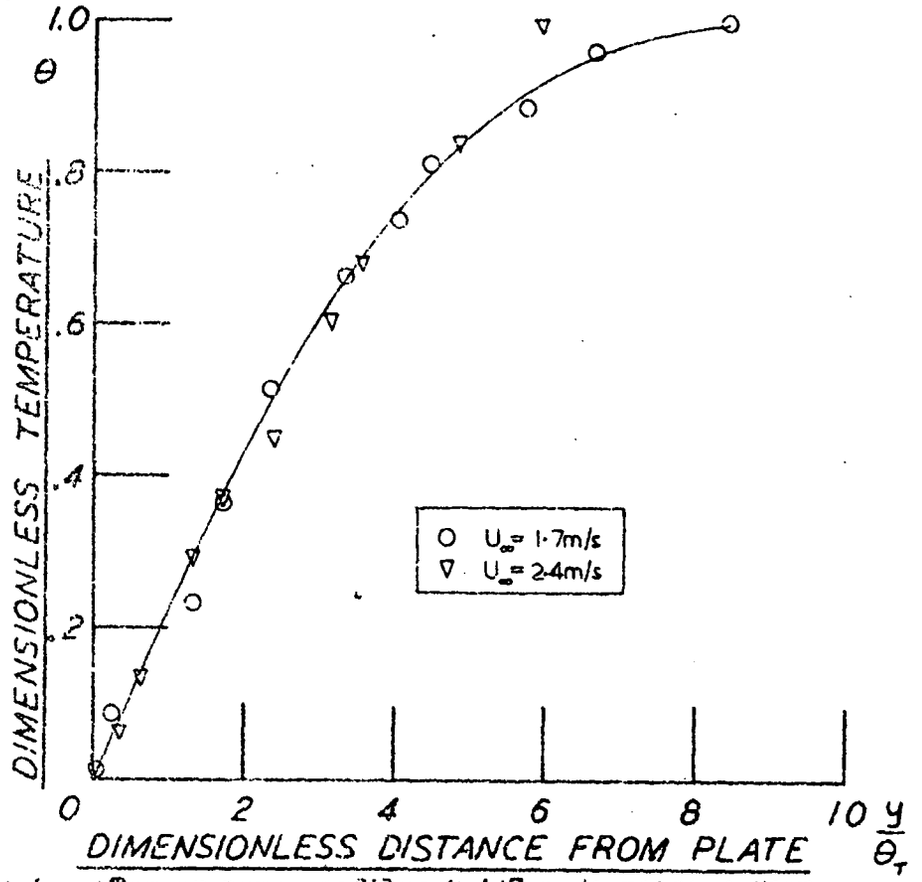

Fig. 4.6. Temperature profiles 0.147 m downstream from leading edge of wet plate.

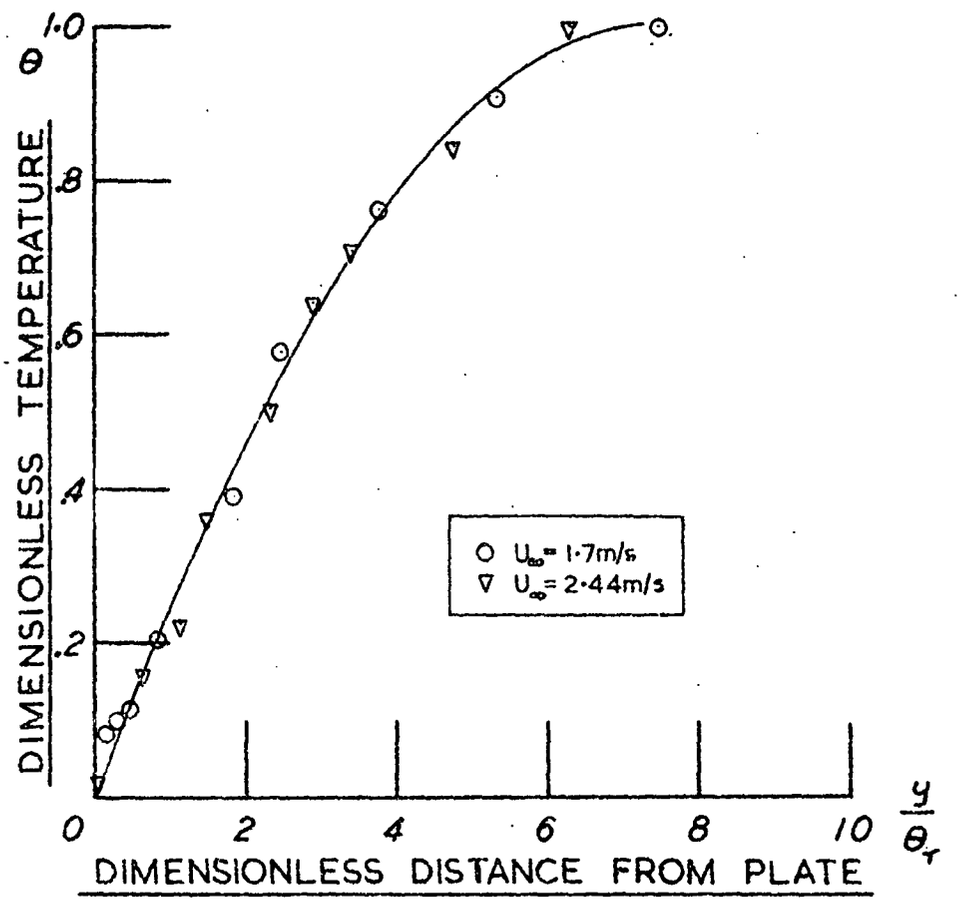

Fig. 4.7. Temperature profiles 0.203 m downstream from leading edge of wet plate.

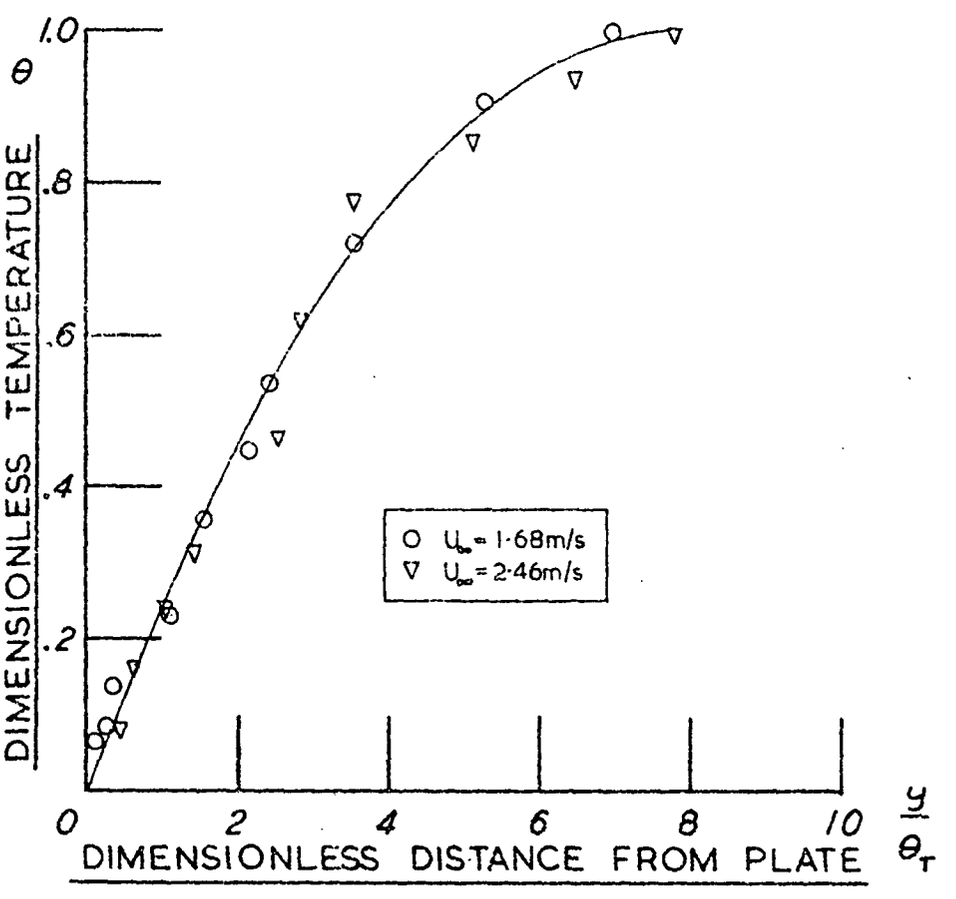

Fig. 4.8. Temperature profiles 0.267 m downstream from leading edge of wet plate.

4.5.3 Humidity Profiles.

Humidity profiles were measured by the method described in Chapter 3.

The variation of humidity through the boundary layer is shown in figures 4.9 and 4.10 as a plot of non-dimensional wet bulb depression ratio ϕ against the parameter

$$y\sqrt{U_\infty}$$

where y is the distance from the wet plate,

and U_∞ is the velocity of the bulk flow.

The non-dimensional wet bulb temperature ratio ϕ is defined as the ratio of the wet bulb depression within the boundary layer to the wet bulb depression of the bulk flow outside the boundary layer. The reason for using the rather inconvenient dimensional quantity $y\sqrt{U_\infty}$ as the absissa is because of the scatter of the profiles near to the wall. The use of a dimensionless distance parameter as for the velocity and temperature profiles would place unwarranted emphasis on the measurements close to the wet plate.

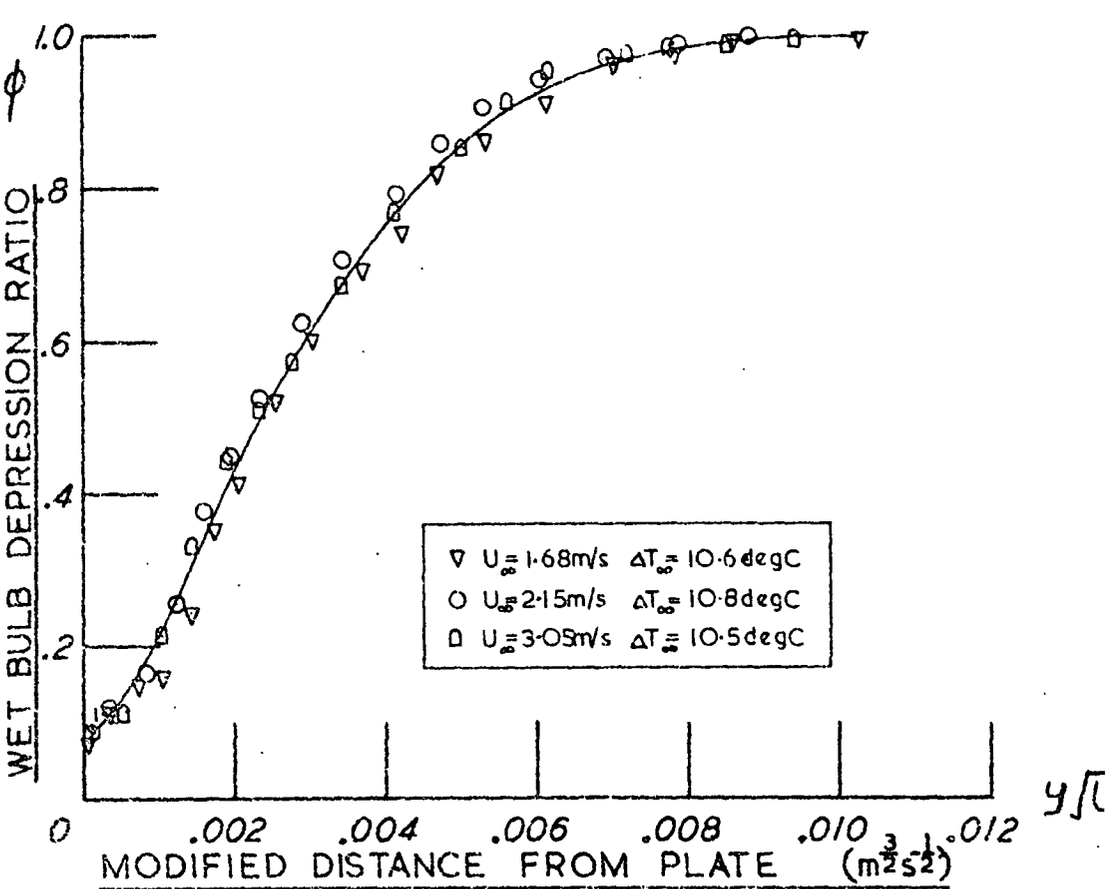

Fig. 4.9. Wet bulb depression ratio profile .147 m downstream from leading edge of wet plate.

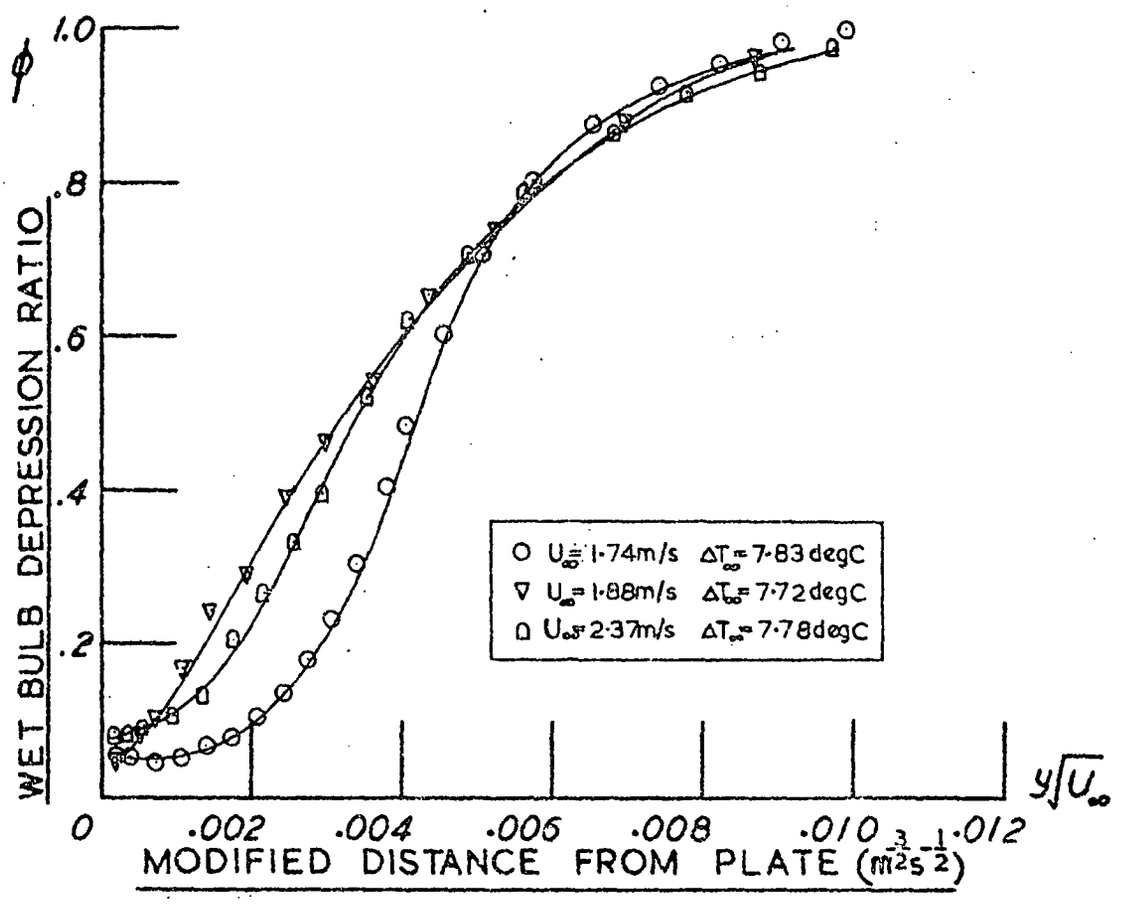

Fig. 4.10. Wet bulb depression ratio 0.267 m downstream from leading edge of wet plate.

Wet bulb temperature ratio was used rather than, say, absolute humidity because of the uncertainty of the temperature distribution within the boundary layer at the time of the humidity traverse. Temperature distributions were measured on different days with consequently different plate and ambient temperatures. However one set of velocity, temperature and humidity measurements was made on the same day with reasonably constant conditions and for this case the specific humidity profile, calculated from the wet bulb depression and temperature profiles is shown in Figure 4.11. The corresponding velocity and temperature profiles are shown in Figures 4.12 and 4.13. The non-dimensional

parameter used to express specific humidity in Figure 4.11 is given by

$$\Gamma = \frac{q - q_w}{q_\infty - q_w} \quad , \tag{4.8}$$

where q is the specific humidity within the boundary layer,

q_w is the specific humidity adjacent to the wet plate,

and q_∞ is the specific humidity of the bulk flow.

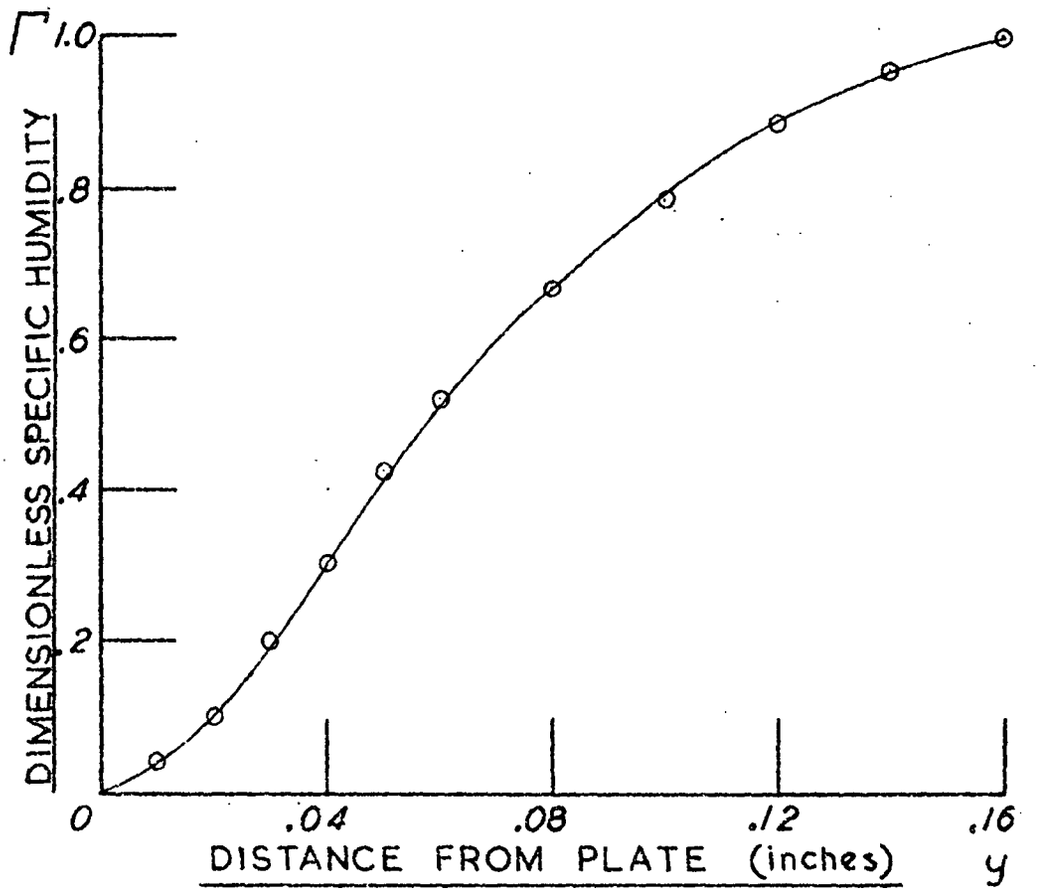

Fig. 4.11. Humidity profile 0.147 m downstream from leading edge of wet plate.

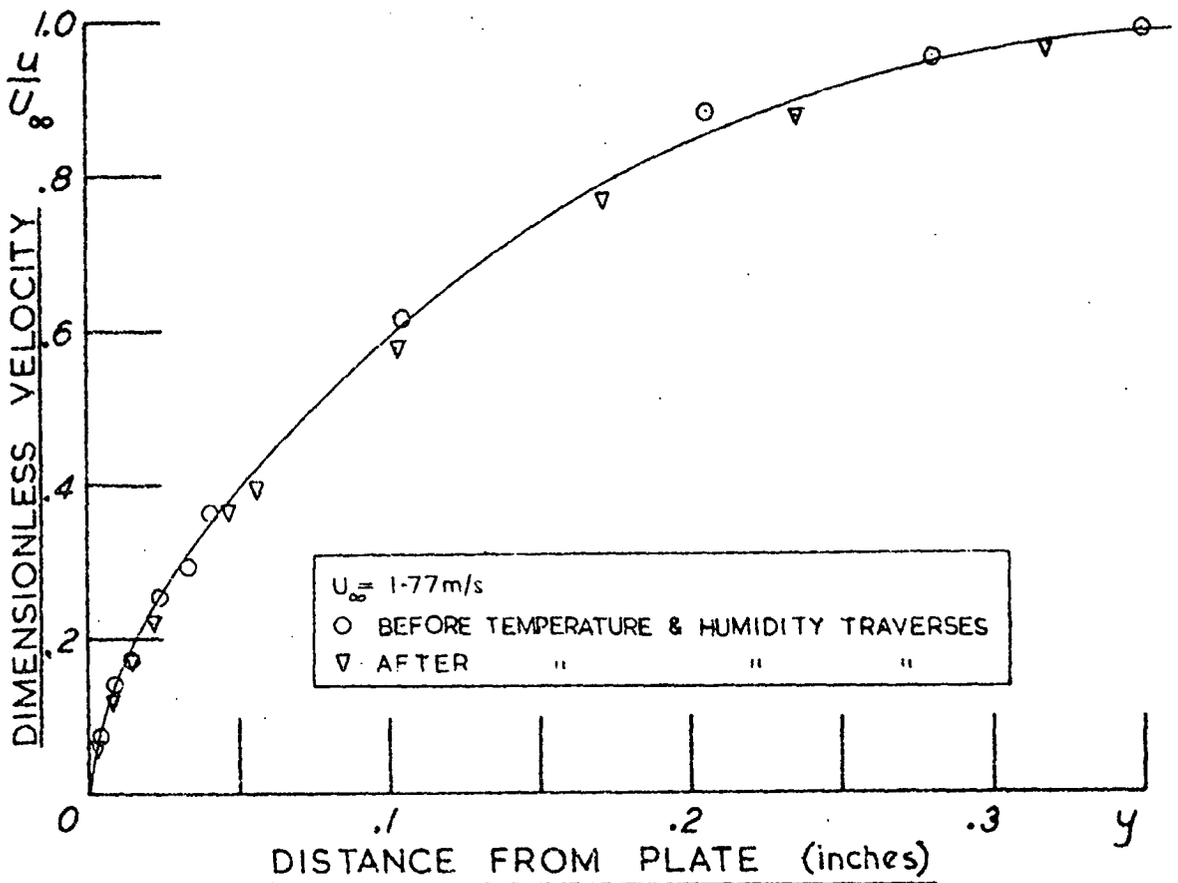

Fig. 4.12. Velocity profile 0.147 m downstream from leading edge of wet plate.

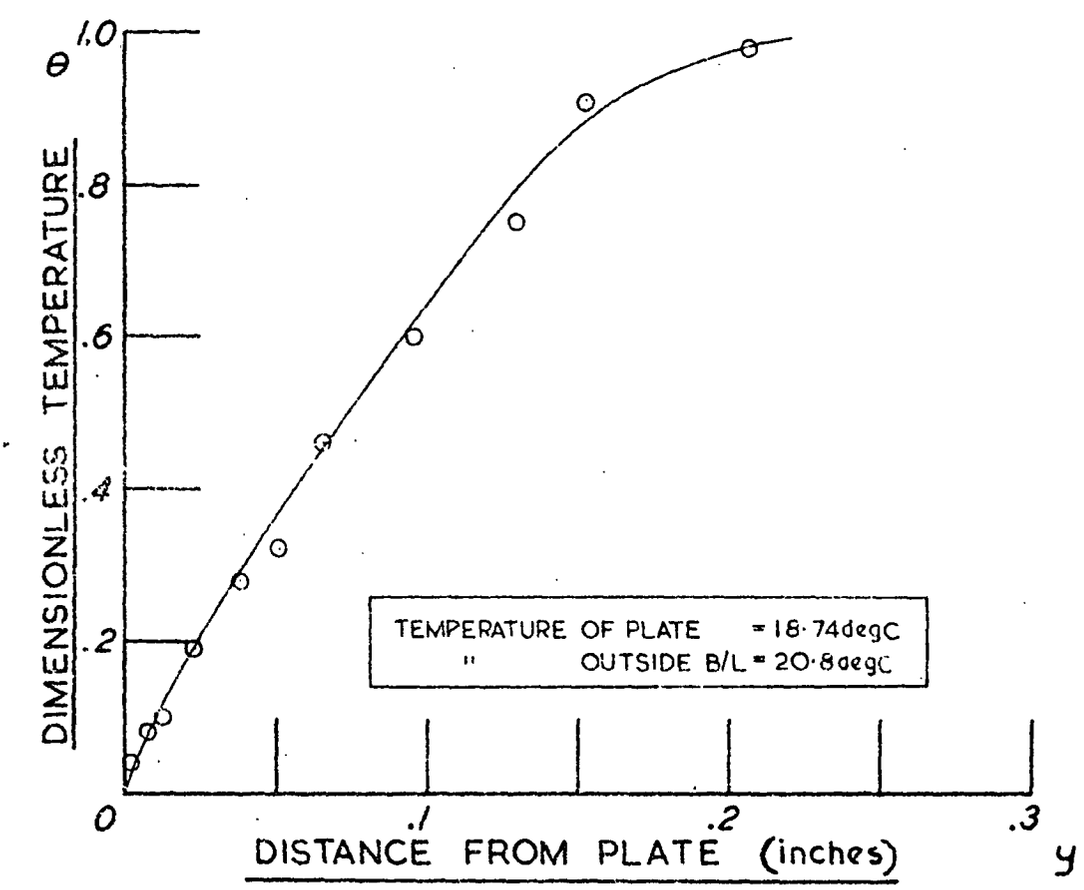

Fig. 4.13. Temperature profile 0.147 m downstream from leading edge of wet plate.

4.6 Conclusion.

The points plotted in the figures of the velocity and temperature profiles are as measured without "smoothing", except that wall corrections (section 4.5.1) have been made to the velocity profiles. The points plotted on the humidity profiles have been scaled from photographs such as Figures 3.1 and 3.2 and are thus arbitrary in that they represent a continuous curve.

Comment on the measurements and a comparison with the profiles predicted by various models appears in Chapter 6.

CHAPTER 5

Two mathematical models of the laminar boundary layer above a flat wet plate are presented in this chapter. The first model is based on the familiar two-dimensional partial differential boundary layer equations and is solved for the boundary conditions appropriate to a flat wet plate by reducing the equations to ordinary differential form and then computing boundary layer profiles by finite difference techniques. The second model is an approximate integral method based on fitting an approximate expression to the measured velocity profile.

The reduction to ordinary differential form of the partial differential boundary layer equations follows the general method used by Oliver (Ref. 34) and also by Brown (Ref. 35) for thermal boundary layers. What can be claimed to be original is the extension of the reduction to mass transfer boundary layers and the inclusion of fluid property variation. The form of the finite difference solution and the computer program are due to the author, although the technique of using finite differences to solve differential equations is well established.

5.1 Theoretical calculation of heat, mass and momentum boundary layers over a flat wet plate.

The partial differential equations describing two dimensional steady state convective heat mass and momentum transfer in laminar flow are deduced from the general three-dimensional (Navier-Stokes) equations of momentum conservation together with energy and diffusive mass transfer balances. The equations have been presented by various authors (Refs. 36, 10) and are here quoted in full. All the moist air properties ρ , c_p , k & μ vary in both directions x and y . No body forces or mass and heat sources are included. Boundary layer analysis neglects changes in u in

the x direction as being negligible compared with the changes in u in the y direction. In addition the second derivative $\frac{\partial^2 u}{\partial x^2}$ is negligible compared with $\frac{\partial^2 u}{\partial y^2}$. The required equations are:-

Continuity Equation:

$$\frac{\partial \rho u}{\partial x} + \frac{\partial \rho v}{\partial y} = 0 , \qquad (5.1)$$

Momentum Equation:

$$u \frac{\partial u}{\partial x} + v \frac{\partial u}{\partial y} = -\frac{1}{\rho} \frac{\partial p}{\partial x} + \frac{1}{\rho} \frac{\partial}{\partial y}\left(\mu \frac{\partial u}{\partial y}\right) , \qquad (5.2)$$

Energy Equation:

$$\rho u \frac{\partial c_p T}{\partial x} + \rho v \frac{\partial c_p T}{\partial y} = \frac{\partial}{\partial y}\left(k \frac{\partial T}{\partial y}\right) + \mu\left(\frac{\partial u}{\partial y}\right)^2 + u \frac{\partial p}{\partial x} , \qquad (5.3)$$

Diffusion Equation:

$$u \frac{\partial \rho q}{\partial x} + v \frac{\partial \rho q}{\partial y} = \frac{\partial}{\partial y}\left(D \frac{\partial \rho q}{\partial y}\right) + \frac{\partial}{\partial x}\left(D \frac{\partial \rho q}{\partial x}\right) . \qquad (5.4)$$

All symbols have their usual meaning except q which represents the specific humidity of water vapour in air.

Several terms in these equations are neglibible in the case of evaporation of water into air from a flat surface at near transitional air velocities. The viscous friction term in equation (5.3), $\mu\left(\frac{\partial u}{\partial y}\right)^2$, is only significant in viscosity dominated situations such as flow in oil bearings. The along-the-plate diffusion term, $\frac{\partial}{\partial x}\left(D \frac{\partial \rho q}{\partial x}\right)$, in equation (5.4) is negligible when compared with the perpendicular-to-the-plate term $\frac{\partial}{\partial y}\left(D \frac{\partial \rho q}{\partial y}\right)$.

5.1.1 Simplified zero pressure gradient equations.

For the purposes of obtaining a solution to equations (5.1) to (5.4) which most nearly represents the experimental conditions, pressure gradient terms $\frac{1}{\rho} \frac{\partial p}{\partial x}$ in equation (5.2) and $u \frac{\partial p}{\partial x}$ in equation (5.4) have been neglected. It is shown in sections 5.15 and 5.16 how the pressure terms and the other terms which have been discarded may be included in the analysis.

The density of moist air, ρ at temperature T is calculated from an expression given in reference 37, viz.;

$$\frac{P v' M_a}{RT} = C\left[\frac{1 + r M_a/M_v}{1 + r}\right] \quad , \qquad (5.14)$$

where r is the mixing ratio of the moist air,

P is the total pressure of the moist air,

R is the gas constant,

$v' = \frac{1}{\rho}$ is the specific volume of moist air at temperature T ,

M_v and M_a are the molecular weights of water vapour and dry air respectively,

and C is a factor tabulated in Ref. 37 which differs from unity by only about 5 parts in 10000 at normal temperatures and pressures.

By substituting the values $C = 1.0$ and $\frac{M_a}{M_v} = 1.607$ together with equation (5.12) into equation (5.14) there results

$$\rho = \rho_a\left(\frac{1 + r}{1 + 1.607r}\right) \quad ,$$

which, with equation (5.13), gives

$$\rho = \frac{\rho_w}{g}\left(\frac{1 + r}{1 + 1.607r}\right) \quad . \qquad (5.15)$$

Equation (5.15) can be expressed in terms of the specific humidity q by substituting the expression

$$r = \frac{q}{1 - q} \quad , \qquad (5.16)$$

giving

$$\rho = \frac{\rho_w}{g}\left(\frac{1}{1 + 0.607q}\right) \quad . \qquad (5.17)$$

Thus the density of moist air can conveniently be expressed as a function of the non-dimensional temperature g and humidity q by

$$\rho = \frac{\rho_w}{g} P(q) \quad , \tag{5.18}$$

where $$P(q) = \frac{1}{1 + 0.607\,q} \quad .$$

Viscosity.

A "semi-theoretical" tabulation of the viscosity of moist air (Ref. 38) gives the variation with temperature and mole fraction x. The mole fraction of water vapour in air is related to the mixing ratio r and the specific humidity q by

$$x = \frac{r}{0.622 + r} = \frac{q}{0.622 - 0.378q} \quad . \tag{5.19}$$

The tabulated data is fitted over the range of mole fractions at near normal temperatures by the logarithmic type expression

$$\mu = \mu_w\, g^{0.75}\left(1.0 - 0.473\, x^{1.697}\right) \quad , \tag{5.20}$$

where μ_w is the absolute viscosity of dry air at temperature T_w.

Equation (5.20) assumes a more convenient form on the substitution of equation (5.19);

$$\mu = \mu_w\, g^{0.75} M(q) \quad , \tag{5.21}$$

where $$M(q) = \left(1.0 - 0.473\left(\frac{q}{0.622 - 0.378q}\right)^{1.697}\right) .$$

Thermal Conductivity.

An expression for the thermal conductivity of moist air was obtained in a manner similar to that for viscosity by fitting a logarithmic expression to tabulated data.

Reference 39 gives a table of the thermal conductivities of moist air in terms of temperature and mole fraction. The expression applicable to near normal temperatures is -

$$k = k_w g^{0.85}(1.0 - 0.336 x^{1.865}) ,$$

which can be rewritten in terms of specific humidity as -

$$k = k_w g^{0.85} K(q) , \qquad (5.22)$$

where $K(q) = \left[1.0 - 0.336\left(\frac{q}{0.622 - 0.378q}\right)^{1.865}\right]$.

Mass Diffusivity of Water Vapour into Air.

The variation of mass diffusivity of water vapour into air, D, with temperature T is given by the expression (Ref. 40)

$$D \propto T^{3/2} .$$

Thus, if D_w is the mass diffusivity at the temperature of the wall T_w, D can be written in terms of g as -

$$D = D_w g^{1.5} . \qquad (5.23)$$

Specific Heat.

The variation of the specific heat of air with temperature may be neglected as insignificant over the range of temperatures used in the measurements.

Reference 41 gives the relation for the variation of specific heat of moist air with humidity as -

$$C_p = \frac{1}{r+1}\left(C_{pa} + r C_{ps}\right) ,$$

where C_{pa} is the specific heat of dry air (approx. 1.005kJ/kg deg),

and C_{ps} is the specific heat of water vapour (approx. 1.846 kJ/kg deg).

In terms of q,

$$c_p = c(q) = q c_{pw} + (1-q) c_{pa} \quad . \qquad (5.24)$$

Thus the variations in transport and thermodynamic properties with temperature and humidity may be summarised by the expressions

$$\left.\begin{aligned} \rho &= \frac{\rho_w}{g} P \quad , \quad \mu = \mu_w g^{0.75} M \quad , \\ k &= k_w g^{0.85} K \quad , \quad D = D_w g^{1.5} \quad , \\ \text{and} \quad c_p &= C \quad , \end{aligned}\right\} \qquad (5.25)$$

where P, M, K and C are all functions of the specific humidity given by equations (5.18), (5.21), (5.22) and (5.24).

5.1.4 Reduction of the partial differential boundary layer equations to ordinary form.

In order to satisfy the continuity equation (equation 5.1) a stream function is defined by the expressions -

$$u = \frac{1}{\rho} \frac{\partial \psi}{\partial y} \quad , \qquad (5.26)$$

and

$$v = -\frac{1}{\rho} \frac{\partial \psi}{\partial x} \quad . \qquad (5.27)$$

Equations (5.9 and (5.18) give values of ρ and u in terms of g, q and f, and on substitution into equations (5.26) and (5.27) give

$$f = \frac{g}{U_\infty \rho_w P(q)} \frac{\partial \psi}{\partial y} \quad , \qquad (5.28)$$

and

$$v = -\frac{g}{\rho_w P(q)} \frac{\partial \psi}{\partial x} \quad . \qquad (5.29)$$

Equation (5.10), viz.

$$\eta = \frac{y}{\sqrt{x}} \sqrt{\frac{U_\infty}{\nu_w}} \quad ,$$

when differentiated with respect to y gives

$$\frac{\partial \eta}{\partial y} = \frac{1}{\sqrt{x}} \sqrt{\frac{U_\infty}{\nu_w}} \quad , \qquad (5.30)$$

and when differentiated with respect to x gives

$$\frac{\partial \eta}{\partial x} = y\sqrt{\frac{U_\infty}{\nu_w}}\left(-\frac{1}{2x^{3/2}}\right) = -\frac{1}{2}\frac{\eta}{x} \quad . \tag{5.31}$$

When equations (5.28) and (5.30) are combined there results

$$f = \frac{g}{\rho_w P\sqrt{x U_\infty \nu_w}} \frac{\partial \psi}{\partial \eta} \quad , \tag{5.32}$$

where $P(q)$ is written more conveniently as P.

Equation (5.32) can be integrated while holding x constant to give

$$\psi = \rho_w \sqrt{x U_\infty \nu_w} \int \frac{f P}{g}\, d\eta \quad , \tag{5.33}$$

which can be written as

$$\psi = \rho_w \sqrt{x U_\infty \nu_w}\, I \tag{5.34}$$

so as to define the integral I as

$$I = \int \frac{f P}{g}\, d\eta \quad . \tag{5.35}$$

It is now possible to use equation (5.29) to give an expression for v in complete differential form. By differentiating equation (5.34) with respect to x there results

$$\frac{\partial \psi}{\partial x} = \rho_w \sqrt{U_\infty \nu_w}\, \frac{\partial (\sqrt{x}\, I)}{\partial x} \quad , \tag{5.36}$$

which when substituted into equation (5.29) gives

$$v = -\frac{g\sqrt{U_\infty \nu_w}}{P}\left[\frac{I}{2\sqrt{x}} + \sqrt{x}\,\frac{\partial I}{\partial \eta}\,\frac{\partial \eta}{\partial x}\right] , \tag{5.37}$$

and when the values of $\frac{\partial I}{\partial \eta}$ from equation (5.35) and $\frac{\partial \eta}{\partial x}$ from equation (5.31) are inserted there results, after some rearrangement,

$$v = \frac{\sqrt{U_\infty \nu_w}}{2\sqrt{x}}\left[\eta f - g\frac{I}{P}\right] \quad . \tag{5.38}$$

The partial derivatives $\frac{\partial u}{\partial x}$ and $\frac{\partial u}{\partial y}$ follow directly from the definition of f, (equation 5.8) together with the

values of $\frac{\partial \eta}{\partial y}$ and $\frac{\partial \eta}{\partial x}$ from equations (5.30) and (5.31);

thus

$$\frac{\partial u}{\partial x} = U_\infty \frac{\partial f}{\partial x} = U_\infty \frac{\partial \eta}{\partial x} \frac{df}{d\eta} = - \frac{U_\infty f' \eta}{2x}, \quad (5.39)$$

and

$$\frac{\partial u}{\partial y} = U_\infty \frac{\partial f}{\partial y} = U_\infty \frac{\partial \eta}{\partial y} \frac{df}{d\eta} = \frac{U_\infty f'}{\sqrt{x}} \sqrt{\frac{U_\infty}{\nu_w}}, \quad (5.40)$$

where f' is used to denote $\frac{df}{d\eta}$.

The second derivative $\frac{\partial}{\partial y} \mu \frac{\partial u}{\partial y}$ appearing in the momentum equation (equation 5.5) is expressed using equations (5.21) and (5.40) as

$$\frac{\partial}{\partial y} \mu \frac{\partial u}{\partial y} = \frac{\partial}{\partial y} \left(\mu_w g^{0.75} M \frac{U_\infty f'}{\sqrt{x}} \sqrt{\frac{U_\infty}{\nu_w}} \right)$$

$$= \frac{\mu_w U_\infty}{\sqrt{x}} \sqrt{\frac{U_\infty}{\nu_w}} \frac{d}{d\eta} \left(g^{0.75} M f' \right) \frac{\partial \eta}{\partial y},$$

which, with equation (5.30) for $\frac{\partial \eta}{\partial y}$ gives, after rearranging,

$$\frac{\partial}{\partial y} \mu \frac{\partial u}{\partial y} = \frac{\mu_w}{\nu_w} \frac{U_\infty^2}{x} \frac{d}{d\eta} \left(g^{0.75} M f' \right). \quad (5.41)$$

Substituting equations (5.8), (5.18), (5.38), (5.39), (5.40) and (5.41) into the momentum equation

$$u \frac{\partial u}{\partial x} + v \frac{\partial u}{\partial y} = \frac{1}{\rho} \frac{\partial}{\partial y} \mu \frac{\partial u}{\partial y},$$

gives

$$U_\infty f \left(- \frac{U_\infty f' \eta}{2x} \right) + \frac{\sqrt{\nu_w U_\infty}}{2\sqrt{x}} \left(\eta f - \frac{g I}{P} \right) \frac{U_\infty f'}{\sqrt{x}} \sqrt{\frac{U_\infty}{\nu_w}}$$

$$= \frac{g}{\rho_w P} \frac{\mu_w}{\nu_w} \frac{U_\infty^2}{x} \frac{d}{d\eta} \left(g^{0.75} M f' \right),$$

which, with $\nu_w = \frac{\mu_w}{\rho_w}$ reduces to

$$- I f' = 2 \frac{d}{d\eta} \left(g^{0.75} M f' \right), \quad (5.42)$$

that is, the momentum equation expressed in a complete differential form.

The energy equation, (equation 5.6), can be written

$$u\frac{\partial C_pT}{\partial x} + v\frac{\partial C_pT}{\partial y} = \frac{1}{\rho}\frac{\partial}{\partial y}k\frac{\partial T}{\partial y} \quad . \qquad (5.43)$$

The term on the right hand side of this equation can be expressed in terms of η by

$$\frac{1}{\rho}\frac{\partial}{\partial y}k\frac{\partial T}{\partial y} = \frac{1}{\rho}\frac{d}{d\eta}\left(k\frac{dT}{d\eta}\frac{\partial \eta}{\partial y}\right)\frac{\partial \eta}{\partial y} \quad .$$

Substituting values of ρ , k , T and $\frac{\partial \eta}{\partial y}$ from equations (5.18), (5.22), (5.9) and (5.30) gives

$$\frac{1}{\rho}\frac{\partial}{\partial y}k\frac{\partial T}{\partial y} = \frac{g}{\rho_w P}\frac{1}{\sqrt{x}}\sqrt{\frac{U_\infty}{\nu_w}}\frac{d}{d\eta}\left(k_w g^{0.85} K T_w \frac{dg}{d\eta}\frac{1}{\sqrt{x}}\sqrt{\frac{U_\infty}{\nu_w}}\right),$$

which simplifies to

$$\frac{1}{\rho}\frac{\partial}{\partial y}k\frac{\partial T}{\partial y} = \frac{g}{\rho_w P}\frac{k_w T_w}{x}\frac{U_\infty}{\nu_w}\frac{d}{d\eta}\left(K g^{0.85} g'\right), \qquad (5.44)$$

where $g' = \frac{dg}{d\eta}$.

The terms on the left hand side of equation (5.43) $\frac{\partial C_pT}{\partial x}$ and $\frac{\partial C_pT}{\partial y}$, are rewritten in terms of η and g by using equations (5.9), (5.30), (5.31) and (5.24).

Thus

$$\frac{\partial C_pT}{\partial x} = \frac{d(C_gT_w)}{d\eta}\frac{\partial \eta}{\partial x} = -\frac{T_w}{2}\frac{\eta}{x}\frac{d(Cg)}{d\eta}, \qquad (5.45)$$

and $$\frac{\partial C_pT}{\partial y} = \frac{d(C_gT_w)}{d\eta}\frac{\partial \eta}{\partial y} = \frac{T_w}{\sqrt{x}}\sqrt{\frac{U_\infty}{\nu_w}}\frac{d(Cg)}{d\eta} \quad . \qquad (5.46)$$

Thus the energy equation can be expressed in complete differential form by inserting equations (5.8), (5.38), (5.44), (5.45) and (5.46) into equation (5.43) to give

$$-U_0 f\frac{T_w}{2}\frac{1}{x}\frac{d(Cg)}{d\eta} + \sqrt{\frac{\nu_w U_\infty}{2x}}\left(\eta f - g\frac{I}{P}\right)\frac{d(Cg)}{d\eta}\frac{T_w}{\sqrt{x}}\sqrt{\frac{U_\infty}{\nu_w}}$$
$$= \frac{g}{\rho_w P}\frac{k_w T_w}{x}\frac{U_\infty}{\nu_w}\frac{d}{d\eta}\left(K g^{0.85} g'\right) ,$$

which simplifies to

$$-I\frac{d(Cg)}{d\eta} = 2\left(\frac{k_w}{\rho_w \nu_w}\right)\frac{d}{d\eta}\left(K g^{0.85} g'\right) . \qquad (5.47)$$

In a similar manner, the diffusion equation, (equation 5.8), reduces to the complete differential equation

$$-I \frac{d\, P q/g}{d\eta} = 2 \frac{D_W}{\partial_W} \frac{P}{g} \frac{d}{d\eta} \left(g^{1.5} \frac{d\, P q/g}{d\eta} \right) \quad . \qquad (5.48)$$

A significant feature of the three ordinary differential equations (5.42), (5.47) and (5.48) for the velocity, temperature and humidity profiles is that they have the same (parabolic) form as the ordinary differential equation for the laminar, two dimensional boundary layer over a flat plate (Ref. 42), without heat or mass transfer, viz.,

$$2f''' + I f'' = 0 \quad .$$

This parabolic form is preserved, even though heat and mass transfer and the variation of fluid properties with temperature and humidity is included in the analysis. This greatly simplifies the solution of the boundary layer equations as it makes possible "similar" type solutions. (Ref. 43).

5.1.5 Variation of free stream velocity and pressure.

Functional forms of free stream velocity, that is with U_∞ given by

$$U_\infty = U_\infty (x) \, ,$$

are related to the pressure in the boundary layer by Bernoulli's equation

$$p + \tfrac{1}{2} \rho_\infty U_\infty^2 = \text{constant} \, ,$$

or in differential form,

$$\frac{dp}{dx} = - \rho_\infty U_\infty \frac{dU_\infty}{dx} \quad , \qquad (5.49)$$

assuming that ρ_∞ remains constant.

The pressure term in the momentum equation, $\frac{1}{\rho} \frac{dp}{dx}$ is expressed in terms of g and U_∞ using equations (5.18) and (5.49) by

$$\frac{1}{\rho} \frac{dp}{dx} = - \frac{g}{\rho_W P} \rho_\infty U_\infty \frac{dU_\infty}{dx} \quad . \qquad (5.50)$$

In general, the term $U_\infty \frac{dU_\infty}{dx}$ in equation (5.50) is some function of the streamwise distance x; then the "similar" nature of the velocity profiles is lost. The velocity, temperature and humidity profiles are peculiar to the value of x, but it is still possible to use the step-wise computation process outlined below to find boundary layers at particular values of x.

There is, however, a particular functional form of the free stream velocity, the Falkner Skan flow (Ref. 44), which leads to similar solutions. The form of the distribution is

$$U_\infty = \text{const.}\ x^m \quad , \tag{5.51}$$

which, when substituted in equation (5.50) gives

$$\frac{1}{\rho}\frac{dp}{dx} = -\frac{g}{P}\frac{\rho_\infty}{\rho_w}\frac{m U_\infty^2}{x} \tag{5.52}$$

and when included with the other terms of equation (5.2) from equations (5.8), (5.18), (5.38), (5.39), (5.40) and (5.41) as was done to obtain equation (5.42) yields the momentum equation in complete differential form for Falkner Skan flow;

$$-I f' = 2\frac{d}{d\eta}(g^{0.75} M f') - 2m\frac{\rho_\infty}{\rho_w} \quad . \tag{5.53}$$

Similarly, the pressure term $u\frac{\partial p}{\partial x}$ in the energy equation (equation 5.3), on substituting values of u and $\frac{\partial p}{\partial x}$ from equations (5.8) and (5.52), becomes

$$u\frac{\partial p}{\partial x} = -U_\infty f \rho_\infty \frac{m U_\infty^2}{x} \quad ,$$

which, if included together with the other terms used in derive equation (5.47) results in the energy equation in complete differential form for Falkner Skan flow;

$$-I\frac{d(Cg)}{d\eta} = 2\frac{k_w}{\rho_w \bar{\nu}_w}\frac{d}{d\eta}(K g^{0.05} g') - 2\frac{\rho_\infty m}{\rho_w}\left(\frac{U_\infty^2 f}{T_w}\right). \tag{5.54}$$

5.1.6 Viscous friction heating term.

The viscous friction heating term $\mu\left(\frac{\partial u}{\partial y}\right)^2$ appearing in equation (5.3) is readily included by using the value of μ from equation (5.21) and the value of $\frac{\partial u}{\partial y}$ from equation (5.40).

Thus,

$$\mu\left(\frac{\partial u}{\partial y}\right)^2 = \rho_w\, g^{0.75}\, M\, \frac{U_\infty^3}{x}\, f'^2 \quad . \tag{5.55}$$

On the substitution of equation (5.55) into the energy equation, together with the other expressions used to derive equation (5.47), the streamwise distance variable x disappears leaving a complete differential form suitable for obtaining "similar" profiles.

5.2 Finite difference solution of boundary layer equations.

Equations (5.42), (5.47) and (5.48) are the complete differential equations governing convective momentum, heat and mass transfer in a laminar boundary layer with zero pressure gradient and fluid properties varying with temperature and humidity. These equations are applicable to various boundary geometries, by specifying initial and boundary conditions on the velocity, temperature and humidity in the boundary layer.

The initial conditions applicable to a flat plate can be stated in terms of the temperature, velocity and humidity of the air adjacent to the plate surface.

Thus at $\eta = 0$, $T = T_w$ and $g = 1.0$, (5.56)

$u = 0$ giving $f = 0$, (5.57)

and $q = q_w$, (5.58)

where q_w and T_w are the specific humidity and temperature of the air adjacent to the plate.

The boundary conditions are in terms of the state of the air in the free-stream remote from the plate.

Thus as $\eta \to \infty$, $T \to T_w$ and $g = \frac{T_\infty}{T_w}$, (5.59)

$u = U_\infty$, $f = 1.0$, (5.60)

and $q = q_\infty$, (5.61)

where T_∞, U_∞ and q_∞ are the values of the temperature, velocity and specific humidity in the air outside the boundary layer.

The boundary layer equations are solved numerically after being expressed in finite difference form so as to allow a progressive or "marching" solution. If $\xi(g,q)$ represents one of the three variables f, g or q in the boundary layer equations (5.42), (5.47) and (5.48), then the complete derivatives with respect to η are written in finite difference form as follows;

$$\frac{d\xi}{d\eta} = \frac{\xi[i+1] - \xi[i-1]}{2h} \quad , \qquad (5.62)$$

where $\xi[i+1]$ etc. are the values of ξ at the discrete points $\eta=(i+1)h$ etc. h is the incremental length of the parameter η. Nested derivates appearing in the boundary layer equations of the form $\frac{d}{d\eta} g^n \frac{d\xi}{d\eta}$ are represented by

$$\frac{d}{d\eta} g^n \frac{d\xi}{d\eta} = \frac{1}{h}\left\{g[i+1]^n(\xi[i+1]-\xi[i]) - g[i]^n(\xi[i]-\xi[i-1])\right\} \qquad (5.63)$$

The dimensionless integral function I is computed successively through the boundary layer by expressing equation (5.35) in finite difference form and integrating with the trapezoidal rule to give

$$I[i+1] = I[i] + \left\{f[i]P[i]/g[i] + f[i-1]P[i-1]/g[i-1]\right\}\frac{h}{2} \quad . \qquad (5.64)$$

The boundary layer equations (5.41), (5.47) and (5.48) are transformed into finite difference equations by substituting equations (5.62), (5.63) and (5.64). The equations are rearranged to give $\xi[i+1]$ in terms of previously computed values.

A complication arises from the variation of air properties with temperature and humidity. It transpires that values of $q[i+1]$ and $g[i+1]$ are required for the calculation of $f[i+1]$ before the former values have been computed. This necessitates two calculations at each finite difference step. The first to predict values of $q[i+1]$ and $g[i+1]$, and the second, using these values, to give corrected values of $f[i+1]$, $g[i+1]$ and $q[i+1]$.

The block diagram of the computer program is given as figure 5.1.

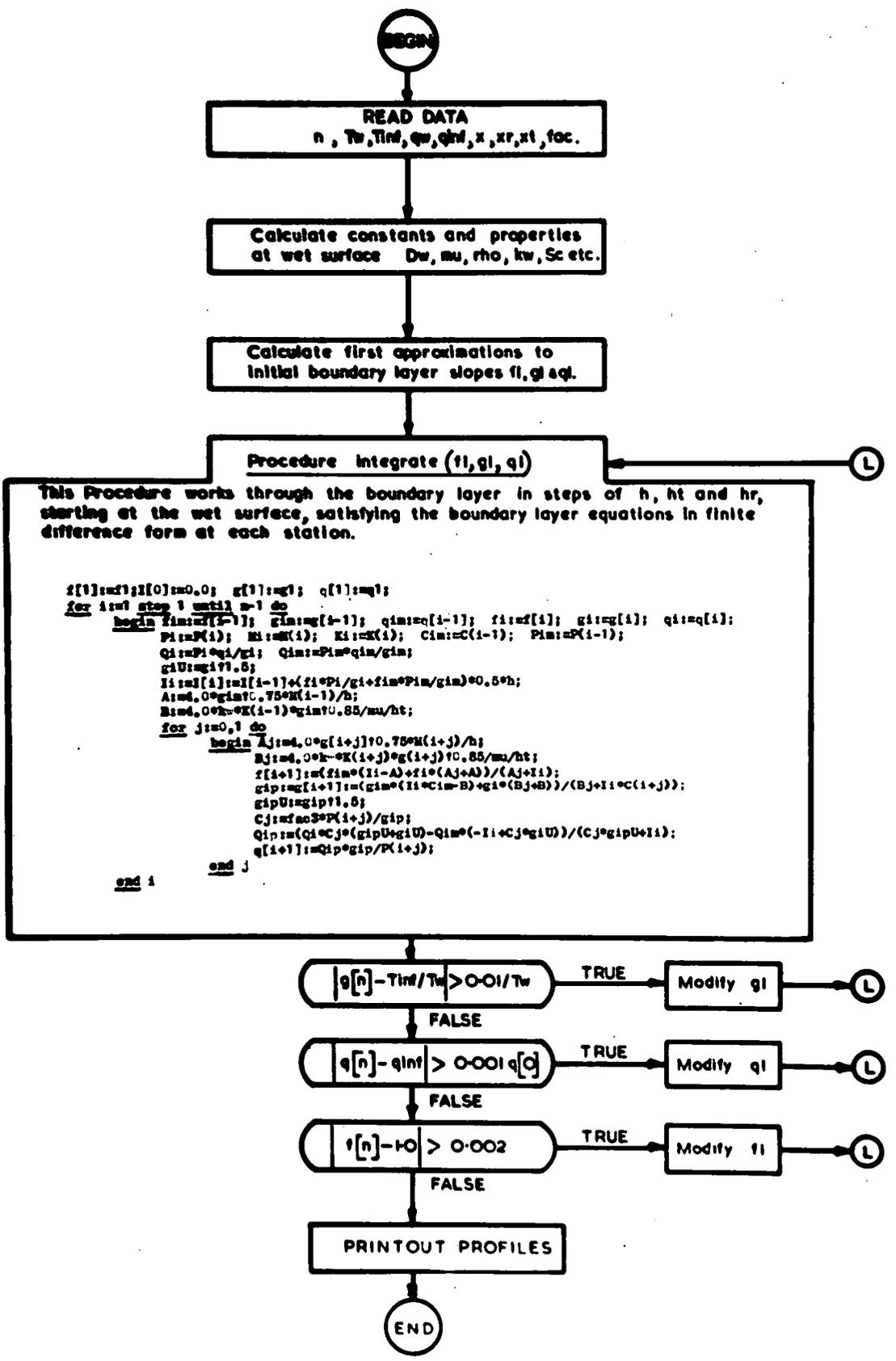

Fig. 5.1. Block diagram of computer program for finite difference solution of laminar boundary layer equation.

The boundary conditions (equations 5.59, 5.60 and 5.61) are met by a method of successive adjustment of initial gradients. Initially the three boundary layers are computed by assuming that the slope near the plate is equal to that of the classical solution of Blasius. The solution is terminated at a sufficiently large value of η and the computed values of f, g and q are compared with their respective values as specified by the boundary conditions. The initial slope of the temperature boundary layer is adjusted and the temperature, humidity and velocity profiles are again computed. This process of adjustment of initial gradients, calculation and comparison with boundary values continues until in turn the temperature, humidity and velocity boundary conditions are met.

5.3 Boundary layers with different origins.

In many cases of practical importance, the origins of the velocity, temperature and humidity boundary layers do not coincide. This is the case with the wet plate used for the experimental part of this project: the velocity boundary layer starts some distance upstream of the temperature and humidity layers which effectively start at the leading edge of the wet plate. Thus a situation arises in which the temperature and humidity boundary layers are growing within an already established velocity layer. In addition to the equations of mass, energy and momentum conservation, there is the requirement that the mass and energy entering or leaving the boundary layer must do so through the solid boundary. This requirement is expressed mathematically by the equations:-

$$\int_0^{x_t} k\,(\partial T/\partial y)_{y=0}\,dx = \int_0^{\infty} \rho u\,(c_p T - c_{p_\infty} T_\infty)\,dy\,, \qquad (5.65)$$

and

$$\int_0^{x_q} D\,(\partial q/\partial y)_{y=0}\,dx = \int_0^{\infty} u\,(q - q_\infty)\,dy\,. \qquad (5.66)$$

5.5 Approximate Integral Methods.

The finite difference model of the mass transfer boundary layer outlined above has as its starting point, the partial differential boundary layer equations for laminar flow over a flat plate. Suitable substitutions reduce the partial differential equations to ordinary differential form. The ordinary differential equations are expressed in finite difference form and solved numerically on a high speed digital computer.

It is possible to start at a rather higher level by selecting a functional relation which approximates the velocity distribution in the boundary layer. By using this functional approximation together with the integral equations relating the momentum, mass and energy fluxes across the boundary layer to the respective fluxes at the surface, it is possible to obtain useful estimates of the velocity, temperature and humidity variations within the boundary layer.

Rohsenow and Choi (Ref. 45) chose the simple analytical function.

$$u = ay + by^3 \quad , \tag{5.68}$$

to approximate the velocity distribution in the boundary layer. By specifying that at $y = \delta$,

$$u = U_\infty \quad \text{and} \quad \frac{du}{dy} = 0 \, , \tag{5.69}$$

the function becomes

$$f = \frac{u}{U_\infty} = \frac{3}{2}\left(\frac{y}{\delta}\right) - \frac{1}{2}\left(\frac{y}{\delta}\right)^3 , \tag{5.70}$$

where δ is the thickness of the velocity boundary layer. Equation (5.70) is used in the momentum integral equation (Ref. 46) viz.,

$$\frac{d}{dx}\int_0^\delta f(1-f)\,dy = \nu\left(\frac{\partial u}{\partial y}\right)_{y=0} \, , \tag{5.71}$$

to give the relation

$$\delta \frac{d\delta}{dx} = \frac{140}{13}\frac{\nu}{U_\infty} \quad , \tag{5.72}$$

which is integrated from O to x along the flat plate to give

$$\delta = 4.64 \sqrt{\frac{\nu x}{U_\infty}} \qquad (5.73)$$

A comparison between the velocity profile plotted from equations (5.70) and (5.73), the similar profile obtained from the finite difference solution and the measured profile on which the computed profiles are based is shown in figure (5.2). The agreement is not good. This is thought to be due to the variation of the bulk flow velocity along the plate (a favourable pressure gradient).

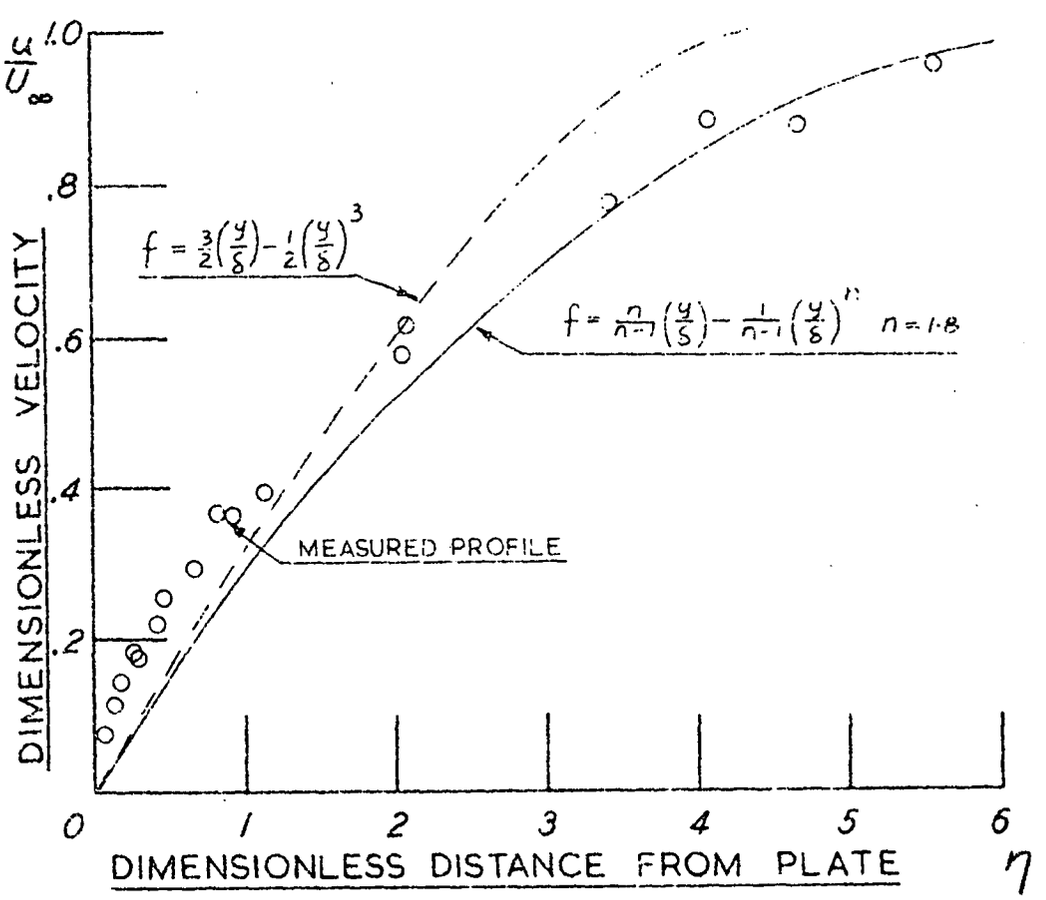

Fig. 5.2. Approximate and measured velocity profiles.

The energy integral equation (Ref. 47),

$$\frac{d}{dx}\int_0^{\delta_T} \rho c_p (T-T_\infty) f \, dy = k\left(\frac{\partial T}{\partial y}\right)_{y=0}, \qquad (5.74)$$

provides a method of estimating the thickness of the thermal

boundary layer. If the temperature distribution across the boundary layer is approximated by the expression

$$\theta = \frac{T-T_W}{T_\infty - T_W} = \frac{3}{2}\left(\frac{y}{\delta_T}\right) - \frac{1}{2}\left(\frac{y}{\delta_T}\right)^3 , \qquad (5.75)$$

where δ_T is the thickness of the thermal boundary layer, then the substitution of equations (5.70) and (5.75) into equation (5.74) gives

$$\frac{d}{dx}\left[U_\infty \delta \left(\frac{3}{20}\varsigma^2 - \frac{3}{280}\varsigma^4\right)\right] = \frac{3}{2}\frac{\alpha}{\delta_T} \qquad (5.76)$$

where $\varsigma = \frac{\delta_T}{\delta}$

The ς^4 term is neglected. By substituting equations (5.72) and (5.73) into equation (5.76) and integrating along the plate from the start of the thermal boundary layer at $x = x_o$ there results;

$$\varsigma = \sqrt[3]{\frac{13}{14\,Pr}}\sqrt[3]{1-\left(\frac{x_o}{x}\right)^{3/4}} . \qquad (5.77)$$

This enables δ_T to be found. The temperature profile thus determined from equation (5.75) is shown in figure 5.3 together with the measured and computed profiles as before.

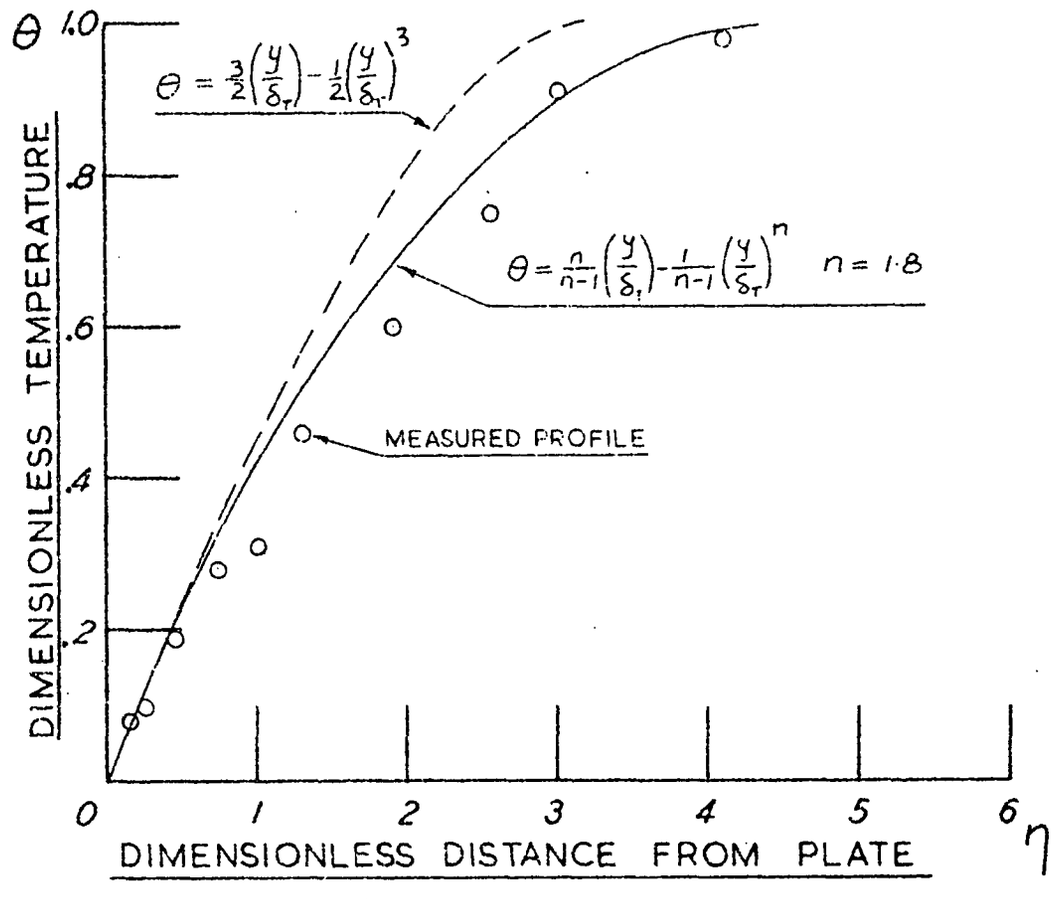

Fig. 5.3. Measured and approximate temperature profiles.

A precisely similar operation gives the thickness of the humidity boundary layer δ_M as

$$\frac{\delta_M}{\delta} = \sqrt[3]{\frac{13}{14\,Sc}}\sqrt{1-\left(\frac{x_0}{x}\right)^{3/4}} \quad . \tag{5.78}$$

The humidity profiles are shown in figure 5.4.

It can be seen from figures 5.2, 5.3 and 5.4 that the agreement between the approximate solution, the finite difference solution, and the measured profiles leaves something to be desired. The discrepancy between the approximate and finite difference solution for the temperature profile is thought to be due to the small temperature difference between the wet plate and the bulk air flow (approximately 2 degC. for these particular measurements). This leads to a relatively small heat flux through the boundary layer and an ill-conditioned solution, as small variations in the profile shape give large changes in the heat flux through the boundary layer compared with the heat flux across the surface.

The discrepancy between both theoretical solutions and the measured results is due to poor approximation to the velocity profile. There is undoubtedly a departure from the zero pressure gradient situation assumed for the finite difference solution and it can be seen that the chosen approximate velocity profile is rather far from the real profile (Fig. 5.2.).

The first step towards improving the fit of the approximate integral solution is to find a functional form of the velocity profile which gives a reasonable fit to the measured profile. Several avenues are open. The Polhausen distribution (Ref. 48) viz;

$$f = F(\eta) + \Lambda\, G(\eta),$$

where

$$F(\eta) = 2\eta - 2\eta^3 + \eta^4,$$

$$G(\eta) = \frac{1}{6}\,\eta\,(1-\eta)^3 \quad , \tag{5.79}$$

and

$$\Lambda = \frac{\delta^2}{\nu}\,\frac{d\,U_\infty}{dx} \quad ,$$

provides for a variation in free stream velocity along the plate, but proved difficult to use with the integral equations (equations 5.71 and 5.74).

Allowing the velocity gradient at the wall to vary along the plate, and relaxing the boundary condition that the slope $\frac{\partial u}{\partial y}$ is zero at $y = \delta$, leads to a velocity distribution of the form

$$f = (1-k)\left(\frac{y}{\delta}\right)^3 + k\left(\frac{y}{\delta}\right) \qquad (5.80)$$

This expression integrates to give a good fit to the temperature profile, but overshoots badly in the velocity profile and predicts a humidity profile in which the humidity increases faster than linearly with distance from the plate.

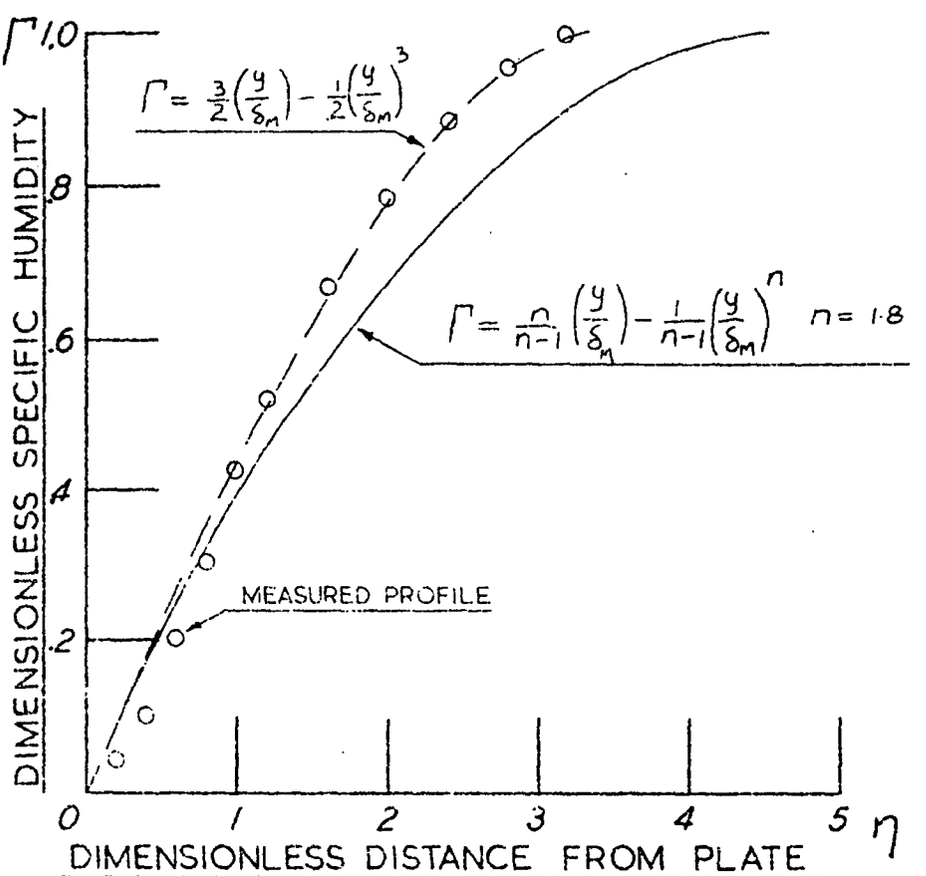

Fig. 5.4. Measured and approximate humidity profiles.

The most satisfactory functional form of the velocity distribution was found by the author to be

$$f = \left(\frac{n}{n-1}\right)\left(\frac{y}{\delta}\right) - \left(\frac{1}{n-1}\right)\left(\frac{y}{\delta}\right)^n . \qquad (5.81)$$

The substitution of equation (5.81) into the momentum integral equation (equation 5.71) and integrating along the plate as before gives an expression for the boundary layer thickness δ ;

$$\delta = \sqrt{\frac{12(n+1)(n+2)(2n+1)}{(n-1)(2n^2+5n+6)}} \sqrt{\frac{\nu x}{U_\infty}} \quad . \qquad (5.82)$$

It was possible to choose a value of the exponent n , ($n = 1{\cdot}8$), to give a close fit of the approximate distribution given by equation (5.81), to the measured velocity profile (Fig. 5.2.).

The temperature and humidity profiles are expressed as follows;

$$\theta = \frac{T-T_W}{T_\infty - T_W} = \frac{n}{n-1}\left(\frac{y}{\delta_T}\right) - \frac{1}{n-1}\left(\frac{y}{\delta_T}\right)^n , \qquad (5.83)$$

and $$\Gamma = \frac{q-q_W}{q_\infty - q_W} = \frac{n}{n-1}\frac{y}{\delta_M} - \frac{1}{n-1}\left(\frac{y}{\delta_M}\right)^n . \qquad (5.84)$$

Substituting equations (5.83) and (5.84) into the energy and humidity integral equations and performing the integrations in a similar manner to those of equations (5.72) and (5.76) gives the following expressions for the thicknesses of the thermal and humidity boundary layers.

$$\frac{\delta_T}{\delta} = \sqrt[3]{\frac{(n-1)(2n^2+5n+6)}{n(n+1)(2n+1)\,Pr}} \sqrt[3]{1-\left(\frac{x_o}{x}\right)^{3/4}} , \qquad (5.85)$$

and $$\delta_M = \delta_T \sqrt[3]{\frac{Pr}{Sc}} \quad . \qquad (5.86)$$

The temperature and humidity profiles, plotted from equations (5.83) and (5.84) with values of the boundary layer thicknesses δ_T and δ_M found from equations (5.85) and (5.86), are shown in figures 5.4 and 5.5 together with the measured profiles. The Prandtl and Schmidt Numbers Pr and Sc are evaluated at the mean of the temperatures of the wall and the bulk flow. It can be seen that the approximate solutions obtained in this manner are a good fit to the measured profiles.

It is possible to use the approximate profiles to predict the heat and mass fluxes through the plate. This could be done by using the derivatives $\left(\frac{\partial \theta}{\partial y}\right)_{y=0}$ and $\left(\frac{\partial \Gamma}{\partial y}\right)_{y=0}$ at the surface, but as the fit of the approximate method is poorest near the surface, the derivative of the profile can be in error by a factor of 2 or 3. A much better approach is to obtain the fluxes by taking the difference between fluxes obtained by integrating through the boundary layers at two stations a small distance apart. This difference will be the mean flux through the surface between the two stations. The variations in heat and mass fluxes through the surface along the plate is shown in figures 6.6 and 6.7, plotted from the finite difference solution.

A great advantage of the approximate integral technique is the ease with which an approximate solution can be fitted to experimental data. To give as good a fit with the finite difference solution, many computer calculations with different values of the station distance x and the pressure variation number m would be necessary. Although there is no provision in the approximate solution for variation of property temperatures with temperature and humidity, the process of fitting an approximate functional form to the measured velocity profile must to some extent include the effects of property variation in the solution.

It is quite likely that this, or a closely similar approximate integral technique, will apply to situations of transitional and turbulent air flow.

5.6 Conclusion.

The development and solution of the models of the mass transfer boundary layer above a flat plate enables a comparison to be made between the measurements and theory. A philosophical question then arises in that should one use the measurements to check the theory or the theory to check the measurements?

There are shortcomings in the theoretical model as well as in the measurements. The physical model is a smooth flat plate in a laminar air stream with zero pressure gradient; that is, no change in bulk air velocity along the length of the plate. In the real situation, of which measurements were made, the plate was not perfectly smooth or flat. There were probably secondary flows in the air stream as well as pressure gradients in the bulk flow.

The measurement, no matter how carefully carried out, can not be perfectly accurate. Tolerances, or margins of error must of necessity arise from causes outside the control of the experimenter. They have to be accepted and if possible, kept within reasonable limits.

There is the added difficulty that the introduction of a measuring device must alter the air flow in its neighbourhood.

It is not possible to resolve completely the dilemma posed above. The best that can be said is that when comparisons are made between theory and experiment, provided the limitations in both are realised and identified, then a reasonable agreement between the two gives confidence that the limitations may lie within acceptable limits.

CHAPTER 6

Solutions of the computer program based on the model developed in the first part of the previous chapter of the laminar boundary layer over a flat wet plate are included in this chapter. The computed boundary layer profiles show the effect of changes in ambient temperature and humidity. A comparison is made between the measured boundary layer profiles and the appropriate computer solution of the boundary layer model.

6.1 Boundary layers with common origins.

Part of the reason for computing mass transfer boundary layers is to examine the effect on the solution of the laminar boundary layer equations of including mass transfer and variable fluid properties. To this end, a series of computer runs with the computer program of figure 5.1 were made with data appropriate to a common origin for the three boundary layers; the same wall temperature; air at the wall saturated at that temperature; and with different ambient temperatures and humidities. The results are presented as figures 6.1 to 6.4.

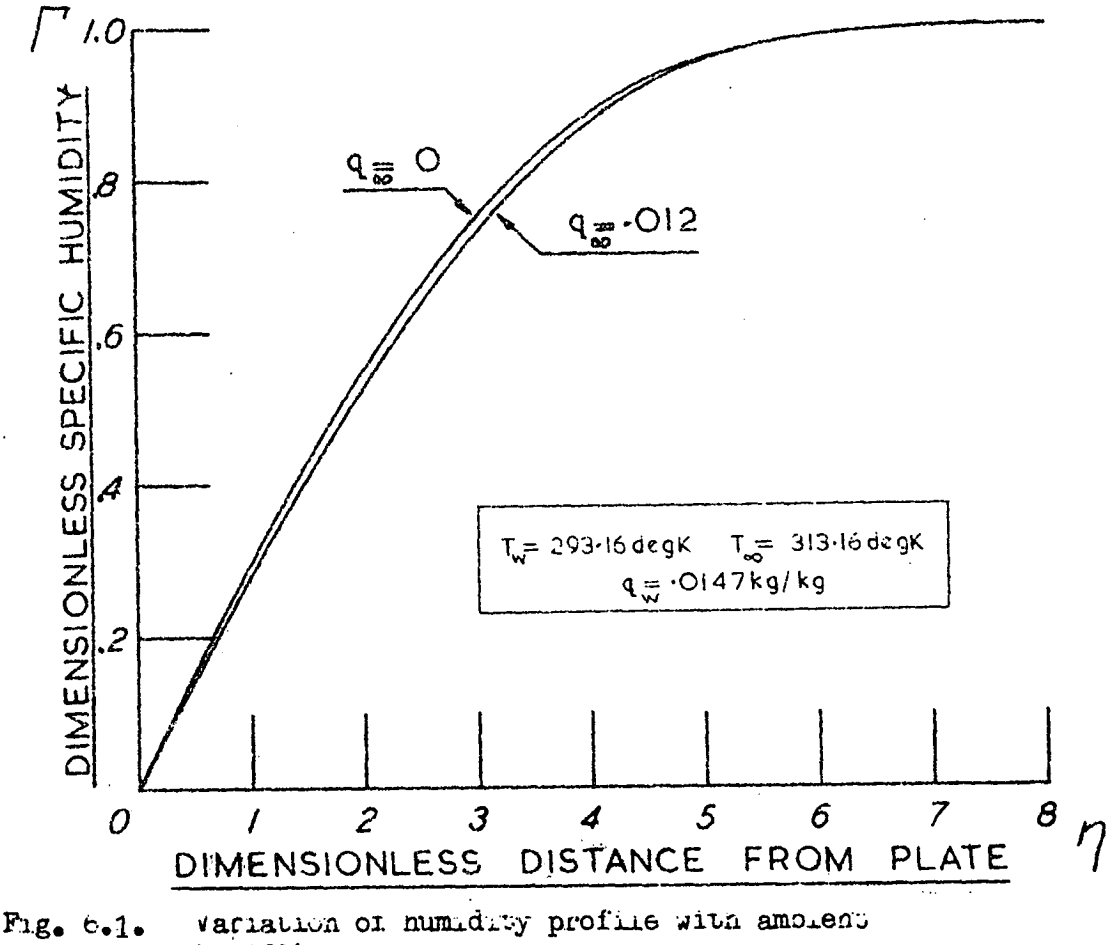

Fig. 6.1. Variation of humidity profile with ambient humidity.

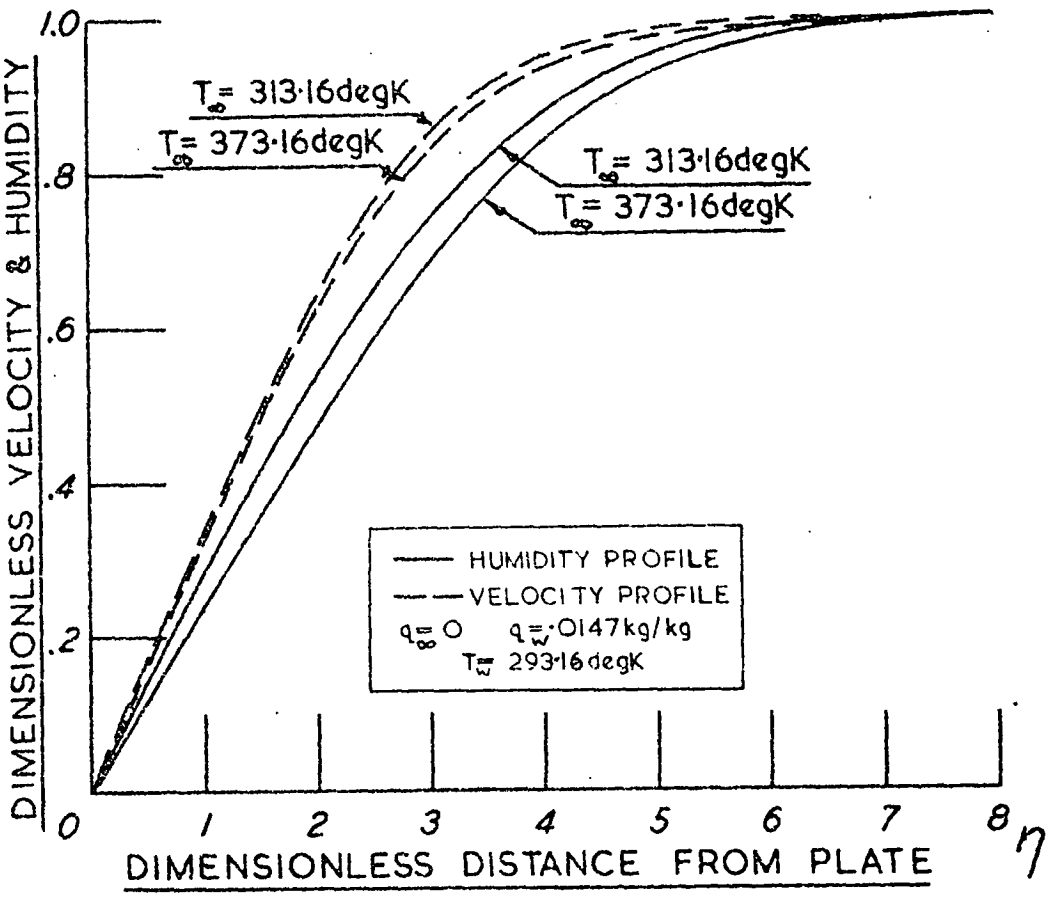

Fig. 6.2. Variation of velocity and humidity profiles with ambient temperature.

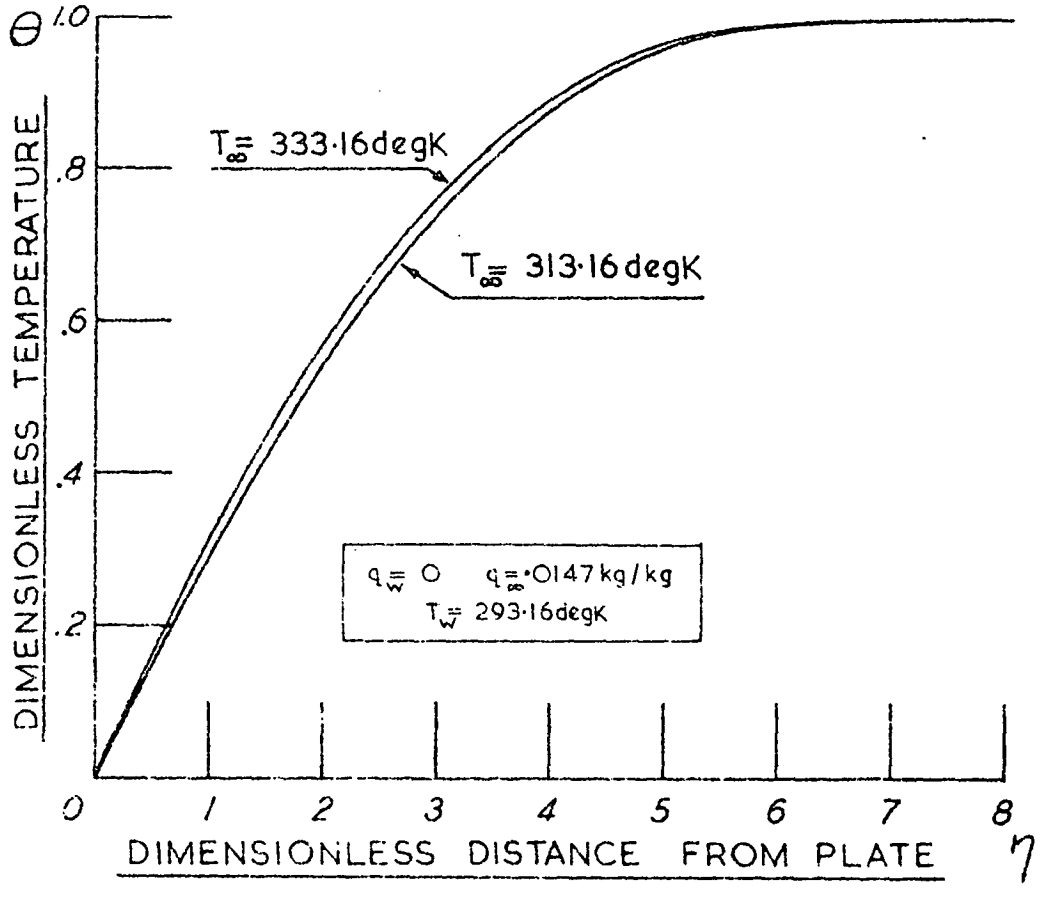

Fig. 6.3. Variation of temperature profile with ambient temperature.

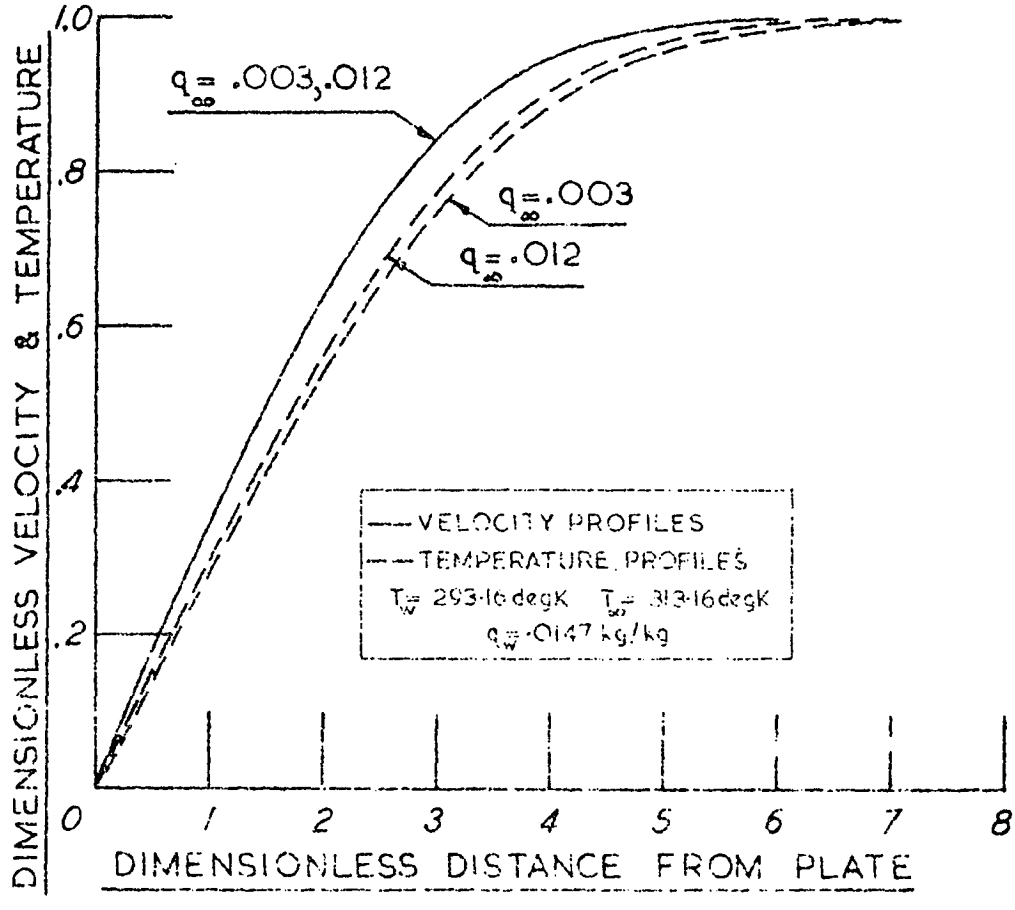

Fig. 6.4. Variation of velocity and temperature profiles with ambient humidity.

A few somewhat unexpected features emerge. The shape of the velocity boundary layer is not strongly dependent on ambient temperature or humidity. This leads to the suspicion that the large modifications to the velocity profile over a flat plate when heated (Ref. 49) arise from modifications to the pressure distribution in the bulk flow rather than from changes in fluid properties. The effect on the velocity boundary layer of a variation in the free stream pressure, obtained from a computer run with the computer program of Fig. 5.1., is shown in Fig. 6.5. This profile is in close agreement with the corresponding solution of Brown and Donoughe (Ref. 50).

Fig. 6.1 shows that the humidity profiles are largely independent of the evaporation rate (when plotted non-dimensionally), but rather more dependent on the temperature difference through the boundary layer. (Fig. 6.2.) In many practical cases the evaporation rate and temperature difference through the boundary layer are mutually dependent. An increased mass flux through the boundary layer removes more heat from the evaporating surface and lowers the surface temperature.

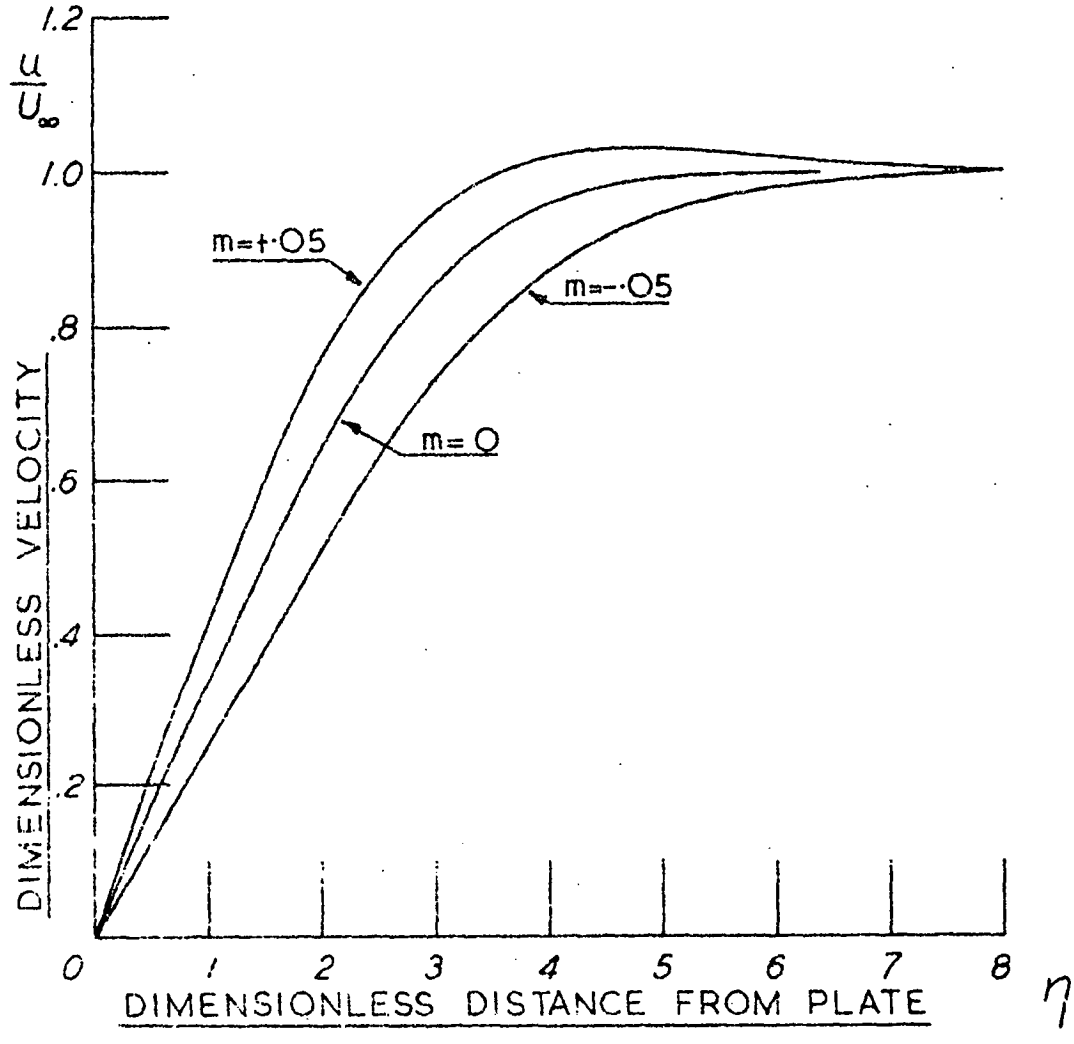

Fig.6.5. Effect of pressure gradient on velocity profile.

6.2 Boundary layers with different origins

When a velocity boundary layer starts some distance upstream of the humidity and temperature layers, the latter grows with distance along the plate inside the former. A mathematical model of this process, described in section 5.3 is used as the basis of a computer calculation of boundary layers with different origins. A series of solutions were obtained for the temperature, velocity and humidity profiles at different stations along the wet plate,

with the velocity boundary layer starting the same distance upstream of the start of the humidity and temperature layers.

From these solutions the form of the change in evaporation and heat transfer rate along the plate emerges. Fig. 6.6. shows the evaporation rate at various distances along the plate. The evaporation rate is expressed as the dimensionless derivative $\left(\frac{\partial \Gamma}{\partial \eta}\right)_{\eta=0}$. This is related to the actual evaporation rate w by the expression;

$$\left(\frac{\partial \Gamma}{\partial \eta}\right)_{\eta=0} = w \sqrt{\frac{x \vartheta_w}{U_\infty}} \frac{1}{(c_w - c_\infty) D A} . \qquad (6.1)$$

The variation of the heat flux through the plate with distance along the plate is shown in Fig. 6.7. Heat flux through the plate is given by the dimensionless derivative $\left(\frac{\partial \theta}{\partial \eta}\right)_{\eta=0}$ which is related to the actual heat flux q by the expression;

$$\left(\frac{\partial \theta}{\partial \eta}\right)_{\eta=0} = q \sqrt{\frac{x \vartheta_w}{U_\infty}} \frac{1}{k A (T_\infty - T_w)} . \qquad (6.2)$$

The evaporation rate and heat flux across the plate increases as the start of the temperature and humidity boundary layers is approached downstream. The form of the mathematical model gives rise to a singular point of infinite evaporation and heat transfer rate at the origin. The singularity was avoided in the computation by refraining from applying the boundary layer model to the region close to the start of the temperature and humidity boundary layers. It was possible to check the computed profiles by comparing the heat and mass fluxes in the boundary layer with the fluxes across the plate. The integrations through the boundary layer and across the plate according to equations (5.65) and (5.66) of section 5.3 were in good agreement. This justifies the choice of the distance parameters η_t and η_q in the mathematical model.

The distribution of the heat and mass fluxes through a typical mass transfer boundary layer are shown in Fig. 6.8.

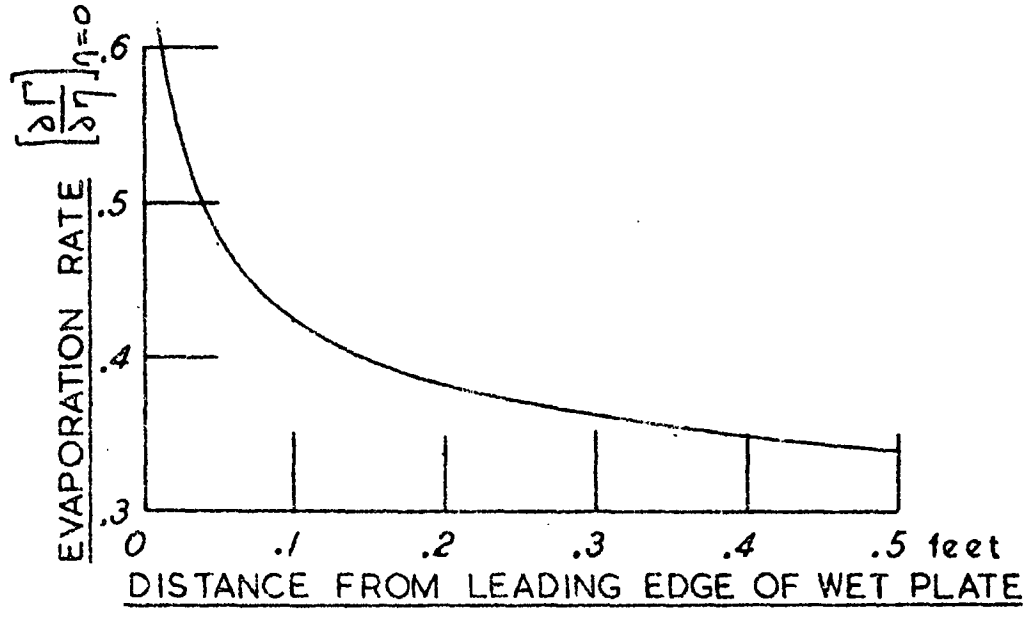

Fig. 6.6. Variation of evaporation rate along plate.

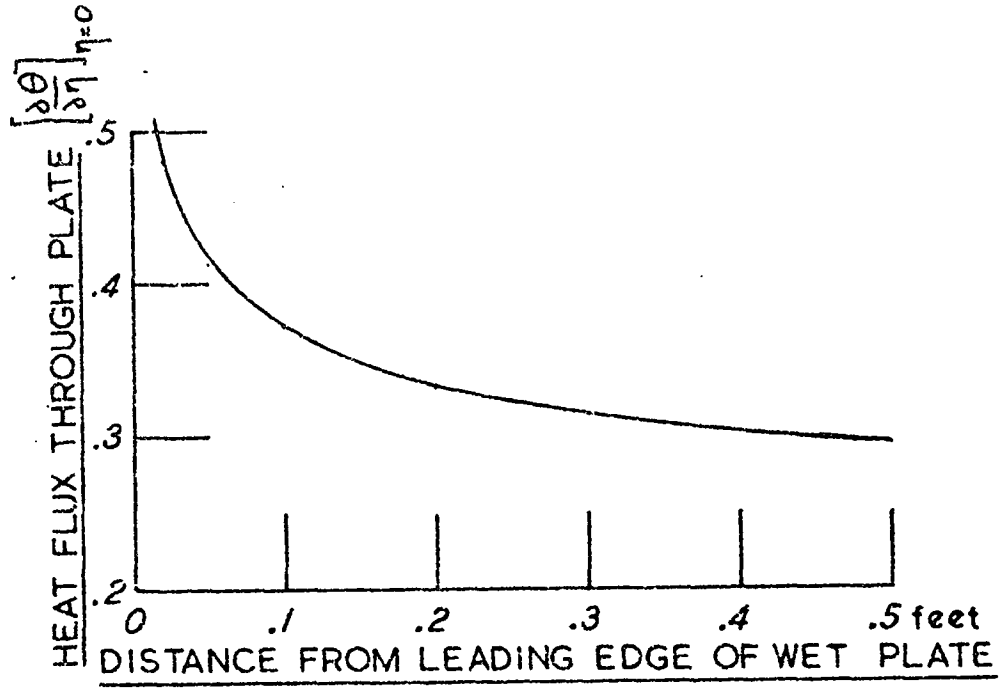

Fig. 6.7. Variation of heat flux along plate.

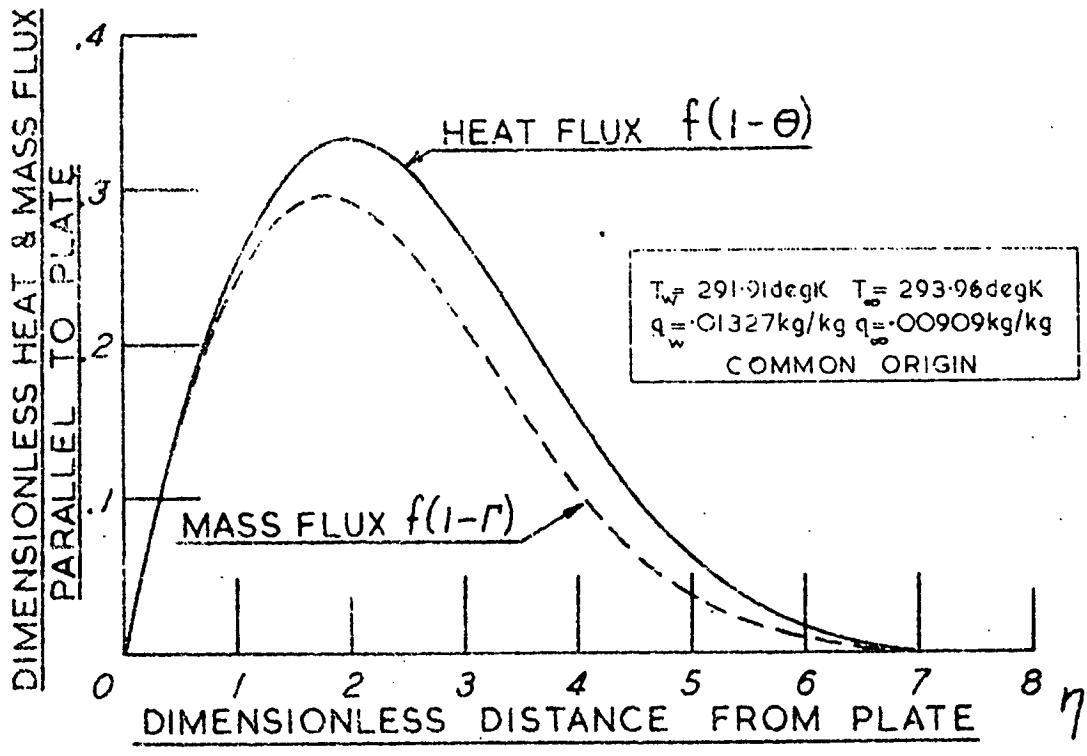

Fig. 6.8. Distribution of heat and mass flux in boundary layer.

Figure 6.9 shows humidity boundary layers at various distances from the leading edge of the wet plate, together with the velocity boundary layer at the start of the wet plate, all plotted against the dimensionless distance parameter η . It can be seen how the humidity boundary layer grows inside the velocity boundary layer. The temperature boundary layer behaves in a similar manner.

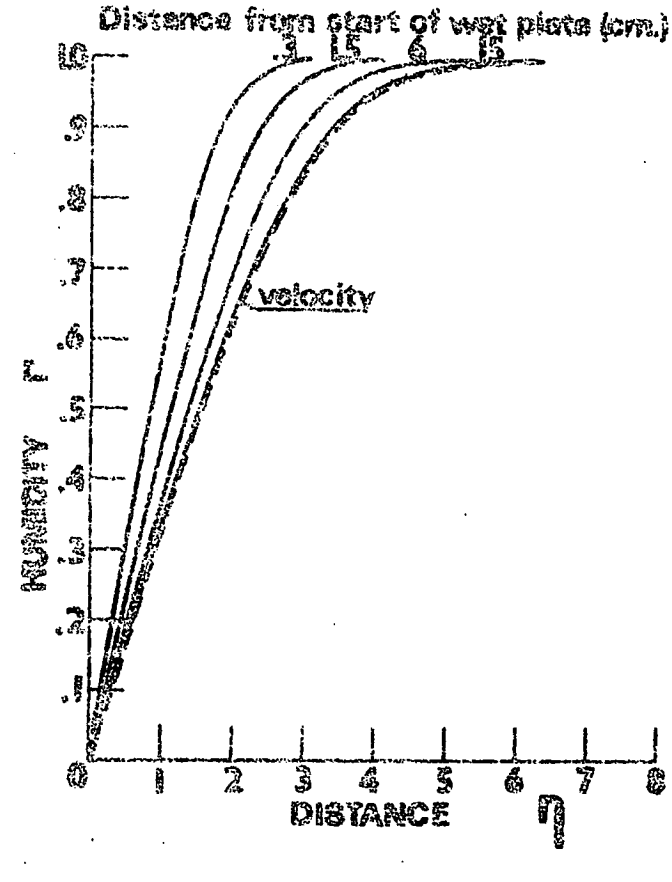

Fig. 6.9. Humidity profiles at various stations along wet plate.

6.2 Comparison with measured profiles.

Due to the uncertainty of the position of the start of the velocity boundary layer for the measured profiles, (the velocity boundary layer started at some point in the accelerating section of the wind tunnel), it was necessary, in order to compare the measured profiles with those computed, to determine the value of the ratio $\frac{\eta}{y}$ by fitting the computed velocity profile to the measured velocity profile. Figure 6.10 shows both profiles.

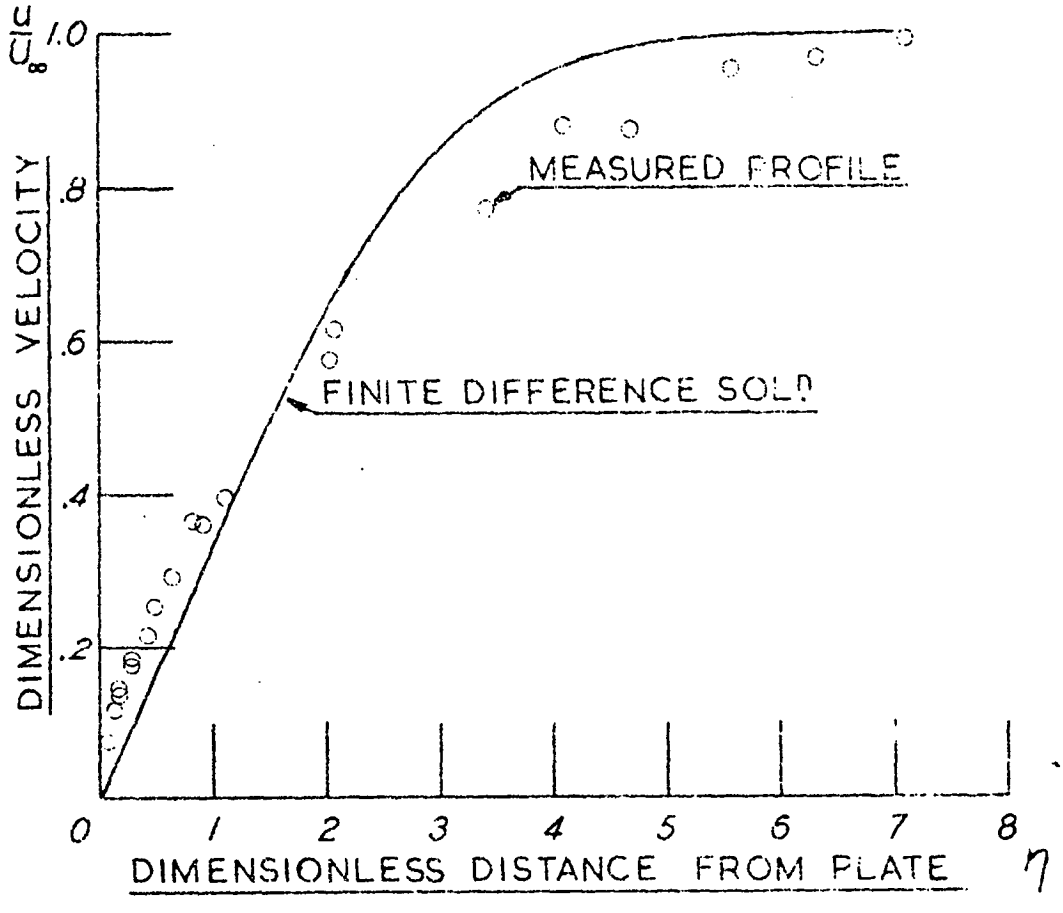

Fig.6.10. Measured and computed velocity profiles.

The quantity $\frac{\eta}{y} = \frac{1}{\sqrt{x}}\sqrt{\frac{U_\infty}{\nu w}}$, can be seen to depend on the ill-defined dimension x.

With the value of $\frac{\eta}{y}$ determined in this manner it is possible to compare the computed and measured temperature and humidity profiles (Figs. 6.11 and 6.12).

The measured profiles are those corresponding to the series of runs performed in one afternoon with near constant ambient conditions (Figs. 4.11, 4.12 and 4.13).

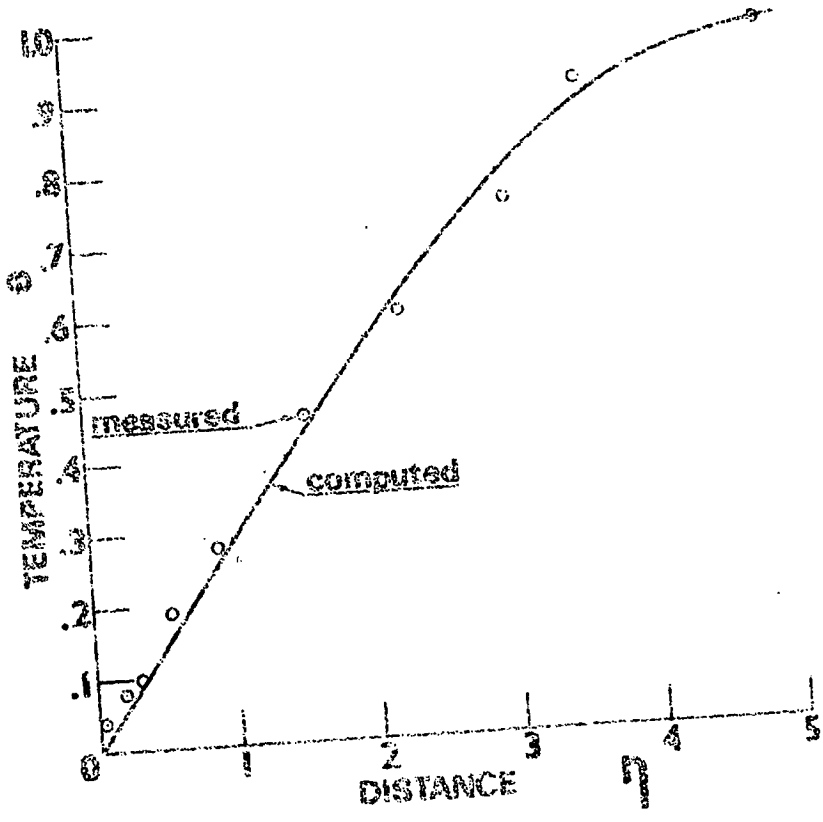

Fig. 6.11. Measured and computed temperature profiles.

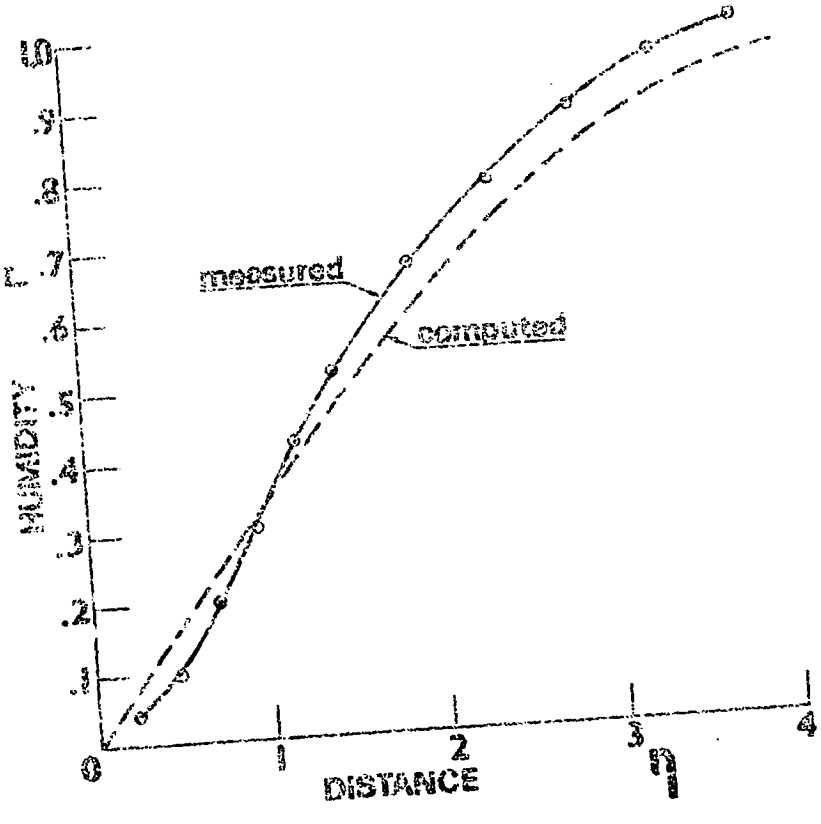

Fig. 6.12. Measured and computed humidity profiles.

It can be seen from figure 6.11 that the measured and computed temperature profiles are in close agreement. There are, however, discrepancies between the computed and measured humidity profiles (Fig. 6.12.), particularly in the region close to the evaporating surface. Similar trends in the measured humidity profile close to the evaporating surface are apparent in the other measurements (Figs. 4.8 and 4.9). These discrepancies suggest that it may be necessary to apply corrections to the measurements of humidity with the thermocouple for proximity to a solid boundary.

6.4 Wall corrections for the thermocouple psychrometer.

Figures 4.8, 4.9 and 6.12, indicate that the proximity to a solid boundary has an effect on measurements with a thermocouple psychrometer. This is no doubt due to the modifications of the velocity distribution and air flow pattern around the thermocouple psychrometer when near a solid boundary, which changes the convective heat and mass flux to and from the junction.

As yet, no details of the applicable correction can be given. It is proposed to conduct further measurements of laminar mass transfer boundary layers with carefully controlled ambient conditions with a view to obtaining the data for determining wall corrections.

Pending the further measurements, one approach is to apply a method of correction for wall proximity based on an analogy of the corrections to hot wire anemometer readings. Wills (Ref. 32) measured the rate of heat loss from a hot wire in a moving air stream at various distances from a solid boundary. The results are collated by the expression:

$$Nu\,(\theta_w/\theta_a)^{-0.17} = A + 0.56\,R_w^{0.45}\,, \qquad (6.3)$$

where Nu is the wire Nusselt number,

θ_w is the wire temperature,

θ_a is the temperature of the surrounding air,

R_w is the Reynolds number based on the wire diameter and the mean of film temperature,

and A is a constant related to the ratio of the distance from the wall and the wire diameter.

The expression for mass transfer, analogous to equation (6.3) is;

$$Sh\,(C_s/C_a)^{-0.17} = A + 0.56\,Re^{0.45} \qquad (6.4)$$

where Sh is the Sherwood number,

C_s is the absolute humidity adjacent to the psychrometer,

and C_a is the absolute humidity of the air in the neighbourhood of the psychrometer.

The application of this analogy requires geometrical similarity between the hot wire and the psychrometer junction. Furthermore, Wills has not included in his corrections, the effect of a wall temperature other than equal to the ambient temperature. Thus the analogous expression (equation 6.4) does not include a different humidity at the boundary from that of the ambient air.

Despite these difficulties, the application of corrections based on the analogous expression to Wills' data gives encouraging results.

Figure 6.13 shows the effect of applying the corrections to a measured humidity profile according to equation (6.4.) It is expected that a rather better method of correcting for wall proximity will result from the further measurements envisaged.

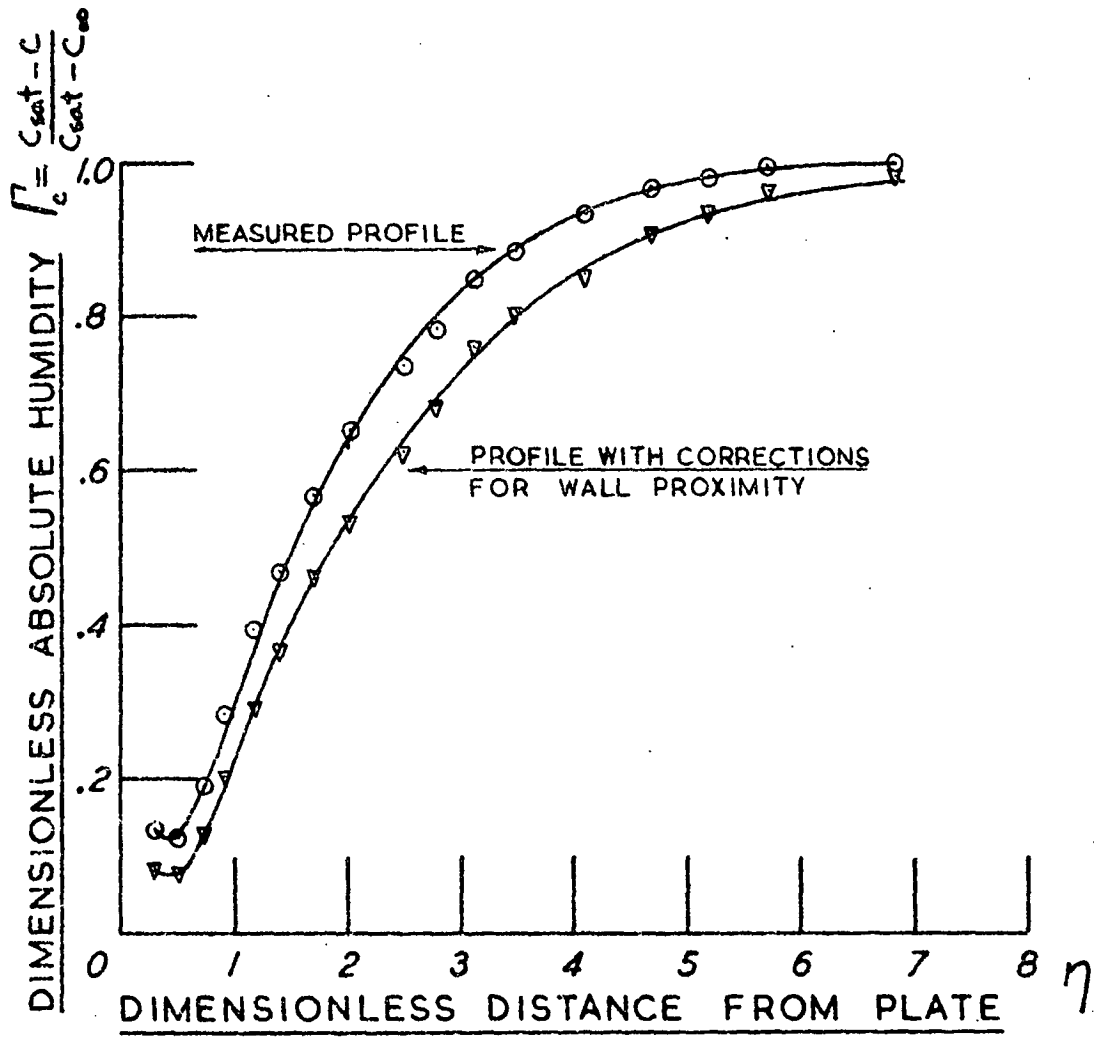

Fig. 6.13. Analogous wall corrections applied to thermocouple psychrometer measurements.

6.5 Conclusion.

Because well established techniques were used for the measurement of velocity and humidity within the mass transfer boundary layer over the flat wet plate, the close agreement between the computed and measured velocity and temperature profiles (Figs. 6.10 and 6.11) gives confidence that the approximations tc the real situation inherent in the physical and mathematical models do not lead to serious errors.

The consistency of the humidity measurements using the thermocouple psychrometer (Figs. 4.9 and 4.1) and the fair agreement between the measurements and the computed profile (Fig. 6.12) lend weight to the statements in Chapter 3 and Appendix III concerning the efficacy of the thermocouple

psychrometer. However it is apparent that the measurements with the thermocouple psychrometer are effected by the proximity to a solid boundary and further work is indicated in order to find a method of correcting for this effect.

CHAPTER 7

The intention of this chapter is to formulate a model of the evaporative process. The evidence on which this model is to be based includes the measurements of laminar mass transfer boundary layers and the corresponding theoretical model described above, numerous measurements of "free" evaporation rates by various investigators, and observations of drying processes, particularly of wet fish and wet asbestos sheets.

The discussion begins by giving an overall description of the evaporative process and then describes such simplifying assumptions as are necessary to refine the descriptive picture intc a useable model.

The evaporative process consists of the transfer of mass from one substance in the liquid phase by a phase change resulting in the removal of mass in the gaseous phase, usually as a mixture with another gas or gases. The particular example of evaporation that is the concern of this investigation is the important case of the evaporation of liquid water into a moving air stream. Various gradients and fluxes can be identified in the evaporative process. These are best identified by following an infinitesmal particle of the fluid from a starting point in the bulk of the liquid. The particle is conveyed towards the region of the phase change (or the 'phase interface' or 'surface') by convection and molecular movement within the fluid supplying matter to replace that evaporated.

It should be mentioned that we are concerned here with the steady state process. Temperature and concentration at particular points in the system are constant with time.

As the fluid particle approaches the surface its temperature falls as there is a net heat flux towards the surface from the bulk of the liquid helping to supply the energy necessary for the change of phase.

At the surface, molecules of water are continually evaporating and condensing. A net quantity of molecules escape from the region adjacent to the surface and are not recaptured. These molecules move away from the surface by diffusing towards regions of lower molar concentration. There is in addition a thermal diffusion effect due to the increase in temperature as the particle moves away from the surface. This temperature increase results from a heat flux to the surface from the air. The direction of action of thermal diffusivity is such that the component of lower molecular weight diffuses in the direction of increasing temperature, in this case, water vapour diffuses away from the surface. However, when compared with mass diffusion, thermal diffusion is sufficiently small as to be negligible in the cases examined.

Supplementing the mass diffusion from the surface is the process of convection. The joint processes of diffusion and convection operate on the water vapour as far as the edge of the boundary layer; beyond this the air properties are those of the bulk flow.

Thus five regions associated with the evaporative process can be identified. There is the bulk of the liquid remote from the phase interface; there is the region in the liquid adjacent to the interface in which the temperature may differ from that of the bulk of the liquid, and in which there is a net movement of liquid towards the interface; there is the ill-defined region in which the phase change takes place; there is the region in the air stream adjacent to the interface (known as the boundary layer) in which the air properties differ from those of the bulk air flow; and finally, there is the bulk of the gaseous phase remote from the interface. The two bulk states serve to define the start and finish of the evaporative process.

7.1 Controlling Features.

Part of the model of the evaporative process is the identification of the controlling feature or features. It can be seen experimentally that the evaporation rate from a wet surface is independent of the rate at which water is supplied to the surface, provided the supply is sufficient to keep the surface wet. This can be contrasted to the "analogous" heat transfer process in which, with steady conditions, the surface temperature regulates itself so that the heat flux from the surface exactly balances the heat flux to the surface.

As each part of the evaporative process is examined in detail, features that may contribute tc the control of the evaporation rate are considered.

7.2 Region of temperature variation in the liquid.

When steady state conditions are established, the temperature in the liquid varies linearly with the distance from the surface according to the relation

$$q = k A \frac{dT}{dy} \quad . \qquad (7.1)$$

The magnitude of the temperature change depends on the heat flux through the liquid and the thermal conductivity of the liquid. The heat flux depends on the heat paths from the surroundings tc the evaporating liquid. In cases such as fish drying or the drying of asbestos sheets (Appendices I and II) there is very little heat conducted from the surroundings to the evaporating liquid. The temperature of the evaporating liquid and indeed of the bulk of the evaporating body falls rapidly and remains at the wet bulb temperature of the surrounding air. But in situations similar to that of the wet plate in the wind tunnel used for the measurements of the mass transfer boundary layer, the plate was in good thermal contact with the wind tunnel and thus a significant amount of heat was conducted to the evaporating surface through

the liquid. In such cases the surface temperature is significantly above that of the wet bulb temperature of the air and there is a heat flux and hence a temperature variation within the liquid.

It can be seen that any heat flux to the surface by conduction through the liquid enhances the evaporation rate. The experimental evidence of Powell and Griffiths (Ref. 5) relates the evaporation rate to the difference between the partial vapour pressure at the surface and the partial pressure of the water vapour in the bulk flow, which difference increases with surface temperature. Also it can be reasoned that an increase in surface temperature leads to an increase in the mobility of the liquid molecules near the surface.

Although the heat flux by conduction to the surface influences the evaporation rate, it is not a controlling feature as evaporation is possible with no heat conducted through the liquid to the surface; in such cases the evaporation rate is still characterised by an upper limit for a particular air flow and condition.

7.3 Region of phase change.

Perhaps less is known and there is more conjecture concerning the region a few hundred molecular diameters either side of the liquid-gas interface than any other aspect of the evaporative process.

In 1915, Knudsen (Ref. 51) measured the evaporation rate of mercury by photographing droplets at various times and determining the volume graphically. Knudsen's results are presented as;

$$m = 43.75 \times 10^{-6} P \sqrt{\frac{M}{T}} \quad , \qquad (7.2)$$

where m is the evaporative mass flux (gm/cm^2 sec.),

P is the saturation vapour pressure corresponding to the temperature of the drop ($dynes/cm^2$),

M is the molecular weight of the evaporating substance,

and T is the surface temperature (deg.).

Langmuir (Ref. 52) obtained the same relationship for the evaporation of metallic tungsten. In both these experiments, the evaporation was into a high vacuum.

Alty (Ref. 53) found that the Knudsen formula (equation 7.2) applied to carbon tetrachloride but evaporation rates for water were a factor of 0.01 to 0.02 lower than predicted. In a later experiment (Ref. 54) Alty measured the evaporation of water droplets on a fine tip in a partially evacuated chamber. The surface temperature of the drop was inferred from the surface tension of the drop, found by measuring the weight of the drop. Alty's results are presented in a form similar to that of Knudsen:

$$m = 43{\cdot}75 \times 10^{-6}(P-p)f\sqrt{\frac{M}{T}} \quad , \qquad (7.3)$$

where P is the saturation partial pressure of the vapour at the surface temperature of the drop (dynes/cm^2),

p is the partial pressure of the water vapour in the partially evacuated chamber (dynes/cm^2),

and f is the evaporation fraction.

The value of f for water was found to be about 0.04. Hickman (Ref. 13) uses a similar approach when he defines an evaporation coefficient ε as the ratio of the measured evaporation rate to the rate calculated from the Knudsen formula (equation 7.2). However, Hickman maintains that the low measured evaporation coefficients arise from evaporation into a foreign gas (usually air) and evaporation into a layer of nearly saturated vapour. By evaporating into a near vacuum and continuously removing the vapour from the liquid surface, Hickman measured much higher evaporation rates than those of other experimentors. His

apparatus comprised a high velocity jet of water evaporating into a high vacuum. The vapour was collected and weighed in a remote condenser. Hickman concludes that the evaporation coefficient of water under these conditions is not less than 0.25 and probably approximates unity.

Further experiments by Alty and Mackay (Ref. 12) led to the definition of an accommodation coefficient α, as the "ratio of energy actually transferred during evaporation to the maximum possible value". With pure water at 10 degC, Alty and Mackay found $\alpha = 1.0$ and $f = 0.036$ where f is, as before, the ratio of the calculated to the actual evaporation rate.

An explanation for the low value of f is given by Fowler and Bernel (Ref. 55) in their conclusion which states, inter alia, "These results indicate that, so far as interaction with the vapour molecules is concerned, the surface behaves more like a solid than a liquid. Most of the vapour molecules incident on it are unable to penetrate into the liquid but, on the other hand, they are all able to attain the temperature equilibrium with the surface before re-evaporating into the vapour phase". This concept of a liquid acting as a solid is used by Lype (Ref. 14) in a theory of the evaporation rates of liquid based on the kinetic theory of the escape of molecules from the surface of a solid. Lype refers to water as a "psuedocrystalline liquid". With this model, Lype obtains good agreement with measurements of the rate of growth of vapour bubbles in boiling water.

Additional evidence as to the behaviour near the phase change boundary comes from work on the evaporation of water droplets. Fuchs (Ref. 29) reports the results of numerous measurements of droplet evaporation rates. Fuchs developed a theory of evaporation based on the assumption of a vapour concentration at the surface equal to the concentration of the saturated vapour at the temperature of the drop. The analysis is for drops

stationary with respect to the surrounding fluid. A correction is applied for a variation of concentration within a distance of the order of one mean free path of the molecules from the surface, analogous to the "temperature jump" and "slip velocity" predicted by the kinetic theory at a solid-gas interface. (Ref. 56). The equation for the evaporation rate in this region is

$$I = 4\pi r^2 (c_0 - c_1) \upsilon \alpha \quad , \tag{7.4}$$

where $\upsilon = \sqrt{\frac{kT}{2\pi m}}$,

k is Boltzman's constant,

m is the weight of a molecule,

c_0 is the vapour concentration at the surface,

c_1 is the concentration at a distance from the surface,

α is the accommodation coefficient ($\alpha \simeq 0.034$)

and r is the radius of the droplet.

This evaporation rate is equated to the loss of vapour into the surrounding space by diffusion according to

$$I = -4\pi \rho^2 D \frac{dc}{d\rho} \quad \text{at} \quad \rho = r + \Delta \quad , \tag{7.5}$$

where D is the mass diffusion coefficient.

Fuchs' model is in good agreement with the measured rates of evaporation of droplets.

Cary (Ref. 57) uses a method of irreversible thermodynamics to predict the mass flux between two liquid surfaces at different temperatures. Cary's conclusions are of particular interest. He states, inter alia, that "The rate of vapour diffusion into air was the rate limiting process rather than the ability of the air-water interface to supply its equilibrium value of vapour pressure".

As mentioned in Chapter 1, by using a molecular kinetic model, Berman (Ref. 11) finds the evaporation rate to be

$$3.6 \times 10^{7}\, a_f \sqrt{\frac{g M_w}{2\pi R T}}\, \Delta p \,, \qquad (7.6)$$

where a_f is a combined accommodation coefficient ($a_f = 0.04$),

g is the gravitational acceleration (m/sec^2),

R is the universal gas constant (kgf/kg-mol degK),

M_w is the molecular weight,

T is the absolute temperature (degK),

and Δp is the difference between the saturated partial pressure at the surface and the partial pressure of the vapour air mixture directly adjoining the surface.

This approach is similar to that of Fuchs.

This discussion on the behaviour in the region of the phase change close to an evaporating surface can be summarised as follows;

Although there are considerable differences between the models proposed by the various authors, then provided that the only limitation to evaporation is that the concentration of vapour adjacent to the surface must not exceed the equilibrium saturation concentration at the surface temperature, the evaporation rate $\mathcal{E}$ can be found from an expression of the type

$$\mathcal{E} = C\,(p_s - p_a)\sqrt{\frac{M}{T}} \,, \qquad (7.7)$$

where C is a constant,

p_a is the partial vapour pressure adjacent to the surface,

p_s is the saturation partial vapour pressure corresponding to the temperature of the surface.

M is the molecular weight of the evaporating substance,

and T is the absolute temperature of the surface.

The considerably body of experimental evidence described above enables a value to be put on the constant in equation (7.7). If the various data are reduced to a common form with common units, there results;

$$\left.\begin{aligned} &\text{for equation (7.3), (Alty)} && \varepsilon = 1.6\times10^{6}\ \Delta p\sqrt{\frac{M}{T}} \\ &\text{for equation (7.6), (Berman)} && \varepsilon = 1.54\times10^{6}\ \Delta p\sqrt{\frac{M}{T}} \\ &\text{and for equation (7.4), (Fuchs)} && \varepsilon = 1.59\times10^{6}\ \Delta p\sqrt{\frac{M}{T}} \end{aligned}\right\} \quad (7.8)$$

The units in each case are [kg /m² hr atm].

Thus, there is good agreement between the evaporation rate formulae of the three independent investigators. It can be seen that the evaporation within the region close to the surface is characterised by an upper limit. The maximum rate at which mass can pass through this layer is directly proportional to the saturation partial pressure at the surface, which in turn depends on the surface temperature. The maximum rate can be realised in theory and according to Hickman (Ref. 13) in practice when evaporation occurs into a high vacuum with continuous removal of the evaporated vapour from the surface.

The actual evaporation rate, subject to the upper limit mentioned above, is determined by the rate at which the vapour is removed from the region adjacent to the surface; this then is the controlling feature of the evaporation process.

7.4 The region of convective and diffusive mass transfer.

That the rate of convective and diffusive mass transfer in the boundary layer controls the whole evaporation process is illustrated by a practical example. In the drying of asbestos sheets (Appendix II) a typical set of measurements was as follows;

Air mass rate	130 kg/hr
Air dry bulb temperature	37.5 degC
Air wet bulb temperature	20.3 degC
Total evaporating area	13.0 m^2
Surface temperature	20.3 degC
Drying rate	6.45 kg/hr

From these data, the maximum possible rate of evaporation corresponding to the saturation partial pressure at the surface temperature is given by equation (7.8);

thus at $\theta_s = 20.3$ deg C , $p_s = 0.0235$ atm,

and $\varepsilon_c = 1.6 \times 10^6 p_s \sqrt{\frac{M}{T}} = 9.3 \times 10^3$ kg/m^2 hr.

The measured evaporation rate is

$$\varepsilon_m = 6.45 / 13.0 = 0.496 \text{ kg/m}^2 \text{ hr}.$$

The calculated maximum rate corresponds to evaporation into a vacuum. The calculated evaporation rate assuming that the air adjacent to the surface has the same partial pressure as the bulk air flow is given by equation (7.8);

at $\theta_D = 37.6$ deg C , $\theta_W = 20.3$ deg C , $p_a = 0.0122$ atm,

and $\varepsilon = 1.6 \times 10^6 (p_s - p_a) \sqrt{\frac{M}{T}} = 4.9 \times 10^2$ kg/hr m^2.

Thus the calculated evaporation rate is nearly 1000 times that measured.

Another way of looking at the problem is to calculate the partial pressure in the layer adjacent to the surface to give a calculated mass flux equal to that measured. Thus we require Δp so that

$$\varepsilon_m = 1.6 \times 10^6 \Delta p \sqrt{\frac{M}{T}} ,$$

which gives

$$\Delta p = 5.05 \times 10^{-6} \text{ atm}.$$

Thus the partial pressure of the water vapour near the surface is very close to the saturation partial pressure corresponding to the surface temperature.

Because of the controlling nature of the boundary layer flow, this aspect of the evaporative process has received the greatest attention in this investigation. In predicting evaporation rates, the greatest difficulty is the complexity of the boundary layer flow. In theory, the model of boundary layer flow developed in Chapter 5 can be applied to more general cases of laminar flow. The technique for doing this is to predict the variation in the pressure in the bulk flow and use the predicted pressure gradients in the pressure varying form of the mathematical model of the laminar boundary layer to compute evaporation rates at numerous stations along the evaporating body. The mass flux at each station along the evaporating body is then determined from the humidity profile by the expression

$$\varepsilon = \rho D \left(\frac{\partial q}{\partial y}\right)_{y=0} \qquad (7.9)$$

It is possible to generalise the mathematics to apply to three-dimensional shapes.

A large number of commercial mass transfer processes take place in a turbulent air stream. The formulation of a useful model is rather more difficult in this case. It is anticipated that the thermocouple psychrometer will be of great assistance in developing a model of the transitional and turbulent mass transfer boundary layer.

The most useful data at present available for transitional and turbulent evaporation is that of Powell and Griffiths (Ref. 5) who measured the evaporation rates from objects of various simple geometrical shapes in a moving air stream. The alternative is to use mass transfer coefficients derived from measured heat transfer coefficients using the analogy as described in section 1.4.1. There is some justification for this. Perry (Ref. 58) points out that small errors in the measurement of temperature have a negligible effect on the heat transfer coefficient, whereas the same errors

lead to large errors in the vapour pressure and hence in measured mass transfer coefficients.

Analogous methods can be avoided by using measurements of local concentration gradients to check measured evaporation rates. Overall evaporation rates can be measured as was done by Powell and Griffiths, and the thermocouple psychrometer can be used to measure the humidity gradient near the surface and hence the local evaporation rates.

Another promising tool for the investigation of evaporation from three dimensional bodies, developed in conjunction with Mr. J.M. Eyles in work on the drying of wet asbestos sheeting, is the use of a layer of china clay (kaolin) over a black base, sprayed with a volatile dope. Objects prepared in this manner allow a direct observation of the evaporative process as regions of slow evaporation remain transparent and remain dark while regions of higher evaporation appear white. This technique has been widely used in aerodynamics for the visualisation of boundary layer transition, (Ref. 59) but is a direct measure of the local evaporation rate.

Thus, to summarise the state of the art of predicting evaporation rates; the mathematical models of the laminar boundary layer, proposed in Chapter 5, together with measured humidity, temperature and velocity profiles can be used to predict evaporation rates in laminar flow from bodies of simple shape. Either measurements similar to those of Powell and Griffiths of evaporation rates from scale models, or the measurement of the analogous heat transfer situation can be used in transitional and turbulent flow. Local evaporation rates can be found for bodies of complex shape in laminar and turbulent flow using the china clay technique, and in laminar flow, using the thermocouple psychrometer.

CHAPTER 8

It is proposed in this conclusion to examine and criticise those aspects of the foregoing which for reasons to be discussed are not completely resolved. From this examination, areas of further work emerge.

The foundation of the whole project is the measurement of mass concentration within the boundary layer. A considerable part of this thesis deals with the development and use of the thermocouple psychrometer, and although the method has proved reasonably successful, there are three areas in which improvements can be effected.

The requirement that the thermocouple junction must be wet by Peltier cooling in a region of high humidity, and then traversed through the boundary layer, is inconvenient and limiting. It is unfortunate that limitations of the Peltier cooling of the thermocouple junction require that there be a region of high humidity for wetting the junction. If the cooling could be improved to give wetting of the junction at normal ambient humidities (perhaps with a semiconducting material such as n and p=type bismuth telluride used in Peltier "batteries",) there would be no need to traverse the thermocouple through the region.

By alternately cooling and wetting the junction, then using the junction as a psychrometer (as envisaged in the original method described in Chapter 1) the danger of the junction becoming partly dry is avoided.

The second region of uncertainty is in calibration. A calibration against a conventional wet and dry bulb psychrometer in the ambient air stream gives consistent results, but there could be measurement situations where the presence of a wet and dry bulb psychrometer is impracticable or undesirable. It is shown in Appendix III how the amount of water condensed onto the junction effects the psychrometer constant. It is possible that this could cause a change in calibration during a traverse, although this is

not indicated by successive traverses preceded by different cooling times and hence different degrees of wetting. This difficulty is obviated by the pulsed cooling described above. With a regular periodic cooling, the amount of water condensed on the junction would remain constant.

The third region yet to be fully investigated is the possible effect due to the proximity of a solid boundary. Measurements so far suggest that there is a "wall effect", but there are insufficient data to gauge the magnitude of the effect or its dependence on the various factors involved.

There is some doubt as to the most realistic manner of providing for the different origins in the theoretical models. The justification for the choice of a square root variation in the distance parameter (section 5.3) is that this gives an acceptable balance between the heat and mass fluxes through the plate and in the boundary layer. The approximate integral method leads to a cube root variation (section 5.5, equation 5.85). This, because of the poor fit of the approximate profile near the wall, does not give a good balance between the fluxes across and along the plate. The most natural method of allowing for different regions would be to solve the boundary layer equations in partial differential form by finite difference techniques, starting at the leading edge of the plate, and progressing downstream at discrete intervals, maintaining the balance between the fluxes through the plate and boundary layer. This was not pursued in view of the reasonable agreement of the measured profiles with those computed by the finite difference method, and the considerable computer time needed for the solution in partial differential form.

The setting up and measurement of the laminar mass transfer boundary layer above a flat wet plate posed some difficulties. It was necessary to let the plate into the floor of the tunnel. This meant that the heat and mass transfer boundary layers started some

distance downstream from the start of the velocity boundary layer. There was no way of controlling the temperature and humidity of the bulk air flow in the open-ended wind tunnel. Due to surface tension forces, the liquid surface adhered to the various probes when the probes were brought into contact with the surface. This made it difficult to locate the surface in such a manner as to eliminate the backlash in the traverse. It is usual to wind the probe up to the wall to make electrical contact, then wind away from the wall until contact breaks, thus locating the wall with the probe being driven in the direction of the traverse.

All of these points, with the exception of the lastmentioned, introduce departures of the real situation from the ideal or model situation of a "flat wet plate". None of these difficulties arises if it is the real situation which is of interest. The measurements apply to precisely the real situation of a "slightly rough wet plate let into the floor of an open-ended wind tunnel".

On the other hand, if the real situation is closely approximated by a model of sufficient simplicity, the comparison of the measured and predicted results gives a useful check on the experiment. Likewise, once the experimental efficacy has been established by reference to simple models, measurements in more complicated situations can help in the development of more sophisticated models. For example, one of the uses to which the thermocouple psychrometer is to be put is the measurement of mass concentrations and hence evaporation rates from arrays of bodies of simple shape. It is hoped that this will lead to better data for predicting drying rates of foodstuffs and other similar objects.

The essay on evaporation included as Chapter 7 is an attempt to rationalise the vast literature on the subject, and to formulate both a picture and a model of the process which can be used to predict evaporation rates.

Further work is envisaged on the completion of a closed circuit wind tunnel at present under construction with provision for fine control of humidity and temperature. It is proposed to set up a smooth flat wet plate and measure laminar humidity profiles in order to find the magnitude of the wall effect on the thermocouple psychrometer.

The next logical step is to extend the investigation to transitional and turbulent mass transfer boundary layers.

NOMENCLATURE

Symbol	Significance	Equation	Units
A	Area associated with heat flux.	(1.2)	m^2
A	Cross section area of thermocouple wire.	(2.1)	m^2
A	Parameter in equation for wall corrections.	(6.3)	-
$A(p)$	Function used in the solution of equation (2.17).	(2.19)	-
A_o	Psychrometer constant.	(3.1)	deg^{-1}
a	Correction factor (Berman).	(1.13)	-
a	Circumference of thermocouple wire.	(2.1)	m
a	Constant in approximate velocity profile.	(5.68)	-
$B(p)$	Function used in the solution of equation (2.17).	(2.19)	-
b	Parameter involving properties of a thermocouple wire.	(2.1)	$s^{-\frac{1}{2}}$
b	Constant in approximate velocity profile.	(5.68)	-
C	Specific heat of thermocouple wire material.	(2.1)	J/kg deg
C	Correction factor (Wexler).	(5.14)	-
C	Constant in evaporation rate equation.	(7.7)	-
$C(q), C$	Specific heat of moist air.	(5.24)	J/kg deg
C_p	Specific heat of moist air.	(5.3)	J/kg deg
C_{pa}	Specific heat of dry air.	(5.24)	J/kg deg
C_{pv}	Specific heat of water vapour.	(5.24)	J/kg deg
c_o	Vapour concentration at surface (Fuchs).	(7.4)	kg/m^3
c_1	Vapour concentration at distance from surface (Fuchs).	(7.4)	kg/m^3
c_a	Absolute humidity of air in neighbourhood of thermocouple psychrometer.	(6.4)	kg/m^3
c_s	Absolute humidity of air at the surface of a thermocouple psychrometer.	(6.4)	kg/m^3
c_w	Mass concentration.	(1.3)	kg/m^3

D	Mass diffusivity.	(1.3)	m^2/s
d	Diameter of thermocouple wire.	(2.26)	cm
d	Any property such as k, ρ, μ, etc. of moist air.	(5.11)	-
e	Partial pressure of water vapour at the 'dry bulb' temperature.	(3.1)	N/m^2
e_s^*	Partial pressure of water vapour at the temperature of adiabatic saturation.	(3.1)	N/m^2
$F(\eta)$	Function in an approximate velocity distribution (Polhausen).	(5.79)	-
f	Accomodation coefficient (Berman).	(1.13)	-
f	Surface heat transfer coefficient of wet wire.	(2.27)	W/m^2mm-Hg
f	Dimensionless velocity.	(5.8)	-
f	Evaporation fraction (Alty).	(7.3)	-
f'	Derivative of f with respect to η.	(5.40)	-
f''	Derivative of f' with respect to η.	(5.48)	-
$f(t)$	A function expressing the variation of thermocouple cooling current with time.	(2.20)	(arbitrary)
$G(\eta)$	Function in an approximate velocity distribution (Polhausen).	(5.79)	-
g	Acceleration due to gravity.	(1.13)	m/s^2
g	Dimensionless temperature.	(5.9)	-
g'	Derivative of g with respect to η.	(5.44)	-
$g(t)$	Function of time.	(2.22)	$s^{-\frac{1}{2}}$
g_{ev}	Evaporation rate (Berman).	(1.12)	kg/s
h	Surface heat transfer coefficient of thermocouple wire.	(2.1)	W/m^2dsg
h	Increment in η used in finite difference solution.	(5.62)	-
I	Current in thermocouple after increasing linearly from zero for a time T.	(2.5)	A
I	Integral function appearing in the boundary layer equations.	(5.35)	-
I	Evaporation rate (Fuchs).	(7.4)	kg/s
i	Current in thermocouple.	(2.1)	A

i	Number of distance increments on finite difference grid.	(2.14)	-
i	Number of increments of η in finite difference solution.	(5.62)	-
i_o	Current through thermocouple bridge which produces identifiable signal.	Fig.2.7.	A
j	Number of time increments in finite difference calculation.	(2.15)	-
K	Proportionality factor (Berman).	(1.13)	kg/m^2 hr atm
$K(q), K$	Variation of thermal conductivity of moist air with specific humidity.	(5.22)	-
k	Thermal conductivity.	(1.2)	W/m deg
k	Thermal conductivity of thermocouple wire material.	(2.1)	W/m deg
k	Boltzmann constant.	(7.4)	J/deg
k	Parameter in an approximate velocity distribution.	(5.80)	-
L	Latent heat of vaporisation of water.	(2.27)	J/kg
l	Parameter involving the slope of a linearly increasing current.	(2.6)	deg/s^3
M	Molecular weight of evaporating substance (Knudsen).	(7.2)	gm-mol
$M(q), M$	Variation of absolute viscosity of moist air with humidity.	(5.20)	-
M_a	Molecular weight of dry air.	(5.12)	kg-mol
M_w	Molecular weight of water vapour.	(1.13)	kg-mol
m	Exponent in expression for Falkner-Skan flow (Euler Number).	(5.51)	-
m	Evaporative mass flux (Knudsen).	(7.2)	$gm/cm^2 s$
m	Weight of a molecule of evaporating substance (Fuchs).	(7.4)	kg
Nu	Nusselt number.	(6.3)	-
n	Parameter in approximate velocity distribution.	(5.80)	-
P	Peltier coefficient of thermocouple junction.	(2.2)	V
P	Total pressure of air water-vapour mixture.	(3.1)	N/m^2
P	Saturation partial pressure of water vapour (Knudsen, Alty).	(7.2)	$dynes/cm^2$

$\rho(q), \rho$	Variation of density of moist air with humidity.	(5.18)	-
P_r	Prandtl number.	(5.77)	-
p	Static pressure.	(1.5)	N/m^2
p	Partial pressure of water vapour (Alty).	(7.3)	$dynes/cm^2$
p''	Partial pressure of water vapour in air saturated at the temperature of the water surface (Berman).	(1.12)	atm
p_a	Partial pressure of water vapour in moist air.	(2.27)	mm Hg
p_w^*	Partial pressure of water vapour in moist air immediately adjacent to the water surface (Berman).	(1.12)	atm
p_w	Partial pressure of water vapour at wet bulb temperature.	(2.27)	mm Hg
q	Heat flux.	(1.2)	W
q	Specific humidity of moist air.	(5.4)	kg/kg
R	Universal gas constant (Berman).	(1.13)	kgf/kg-mol de
R_e	Reynolds number.	(6.4)	-
R_w	Reynolds number of hot wire.	(6.3)	-
r	Resistivity of thermocouple wire material.	(2.1)	Ω-m
r	Mixing ratio of moist air.	(5.14)	-
r	Radius of water droplet (Fuchs).	(7.4)	m
S_c	Schmidt number.	(5.78)	-
Sh	Sherwood number.	(6.4)	-
T	Temperature.	(1.2)	deg
T	Absolute temperature.	(1.13)	degK
T	Time for thermocouple current to increase from zero to I.	(2.5)	s
T	"Dry bulb" temperature of moist air.	(3.1)	deg
T	Surface temperature (Knudsen).	(7.2)	degK
T_a, T_b, T_j	Temperatures of thermocouple junctions.	(3.2)	deg
T_s^*	Temperature of adiabatic saturation.	(3.1)	deg
t	Time.	(2.1)	s
U_∞	Velocity of air outside a boundary layer.	(5.8)	m/s

u	Velocity component parallel to the general direction of flow.	(1.1)	m/s
V	Velocity of air over a thermocouple.	(2.26)	cm/s
V	Potential appearing across thermocouple.	(3.2)	V
v	Velocity component normal to the general direction of flow.	(1.4)	m/s
v'	Specific volume of moist air.	(5.14)	m^3/kg
v_{air}	Velocity of dry air component in direction.	(1.9)	m/s
v_w	Velocity of component crossing a boundary.	(1.8)	m/s
w	Mass flux.	(1.3)	kg/s
x	Distance parallel to general direction of flow.	(1.4)	m
x	Distance along thermocouple wire.	(2.1)	m
x	Mole fraction of water vapour in moist air.	(5.19)	-
x_o	Distance along flat plate to start of heat and mass transfer boundary layers.	(5.77)	m
x_q	Distance along flat plate to start of mass transfer boundary layer.	(5.66)	m
x_t	Distance along flat plate to start of heat transfer boundary layer.	(5.65)	m
y	Distance in direction perpendicular to general direction of flow.	(1.1)	m
y	Distance parallel to heat and mass fluxes.	(1.3)	m

GREEK SYMBOLS

α	Thermal diffusivity.	(1.7)	m^2/s
α	Ratio of wet bulb depression to the depression of a "standard" psychrometer.	p.50	-
α	Accomodation coefficient (Alty and Mackay).	p.113	-
α_{ab}	Seebeck coefficient of thermocouple material a with respect to material b.	(3.2)	V/deg
β	Parameter expressing the size of grid in a finite difference calculation.	(2.16)	-

Γ	Dimensionless specific humidity.	(4.8)	-
Δ	Incremental droplet radius (Fuchs).	(7.4)	m
δ	Boundary layer displacement thickness.	(4.6)	m
δ_T	Temperature displacement thickness.	(4.7)	m
ε	Evaporation coefficient (Hickman).	p.112	-
ε	Evaporation rate.	(7.7)	kg/m^2hr
φ	Ratio of thermal and momentum boundary layer thicknesses.	(5.76)	-
η	Dimensionless boundary layer distance parameter.	(5.10)	-
η_q	Dimensionless distance parameter for humidity profiles.	(5.67)	-
η_t	Dimensionless distance parameter for temperature profiles.	(4.4)	-
η_v	Dimensionless distance parameter for velocity profiles.	(4.1)	-
θ	Temperature in thermocouple wire.	(2.1)	deg.
θ	Dimensionless temperature in boundary layer.	(4.3)	-
θ_a	Temperature of air in vicinity of hot wire.	(6.3)	degK
θ_J	Part of thermocouple temperature which is independent of x.	(2.10)	deg
θ_P	Part of thermocouple temperature which varies with x and t.	(2.9)	deg
θ_t	Temperature momentum thickness of a boundary layer.	(4.5)	-
θ_v	Momentum thickness of a boundary layer.	(4.1)	-
θ_w	Temperature of hot wire.	(6.3)	-
Λ	Function in an approximate velocity distribution (Polhausen).	(5.79)	-
λ	Ratio in which heat absorbed at a thermocouple junction is conducted along each wire.	(2.2)	-
μ	Absolute viscosity.	(1.1)	$N\ s/m^2$
ω	Parameter involving the Peltier coefficient.	(2.7)	deg/m s
ω	Parameter in evaporation equation (Fuchs).	(7.4)	m/s
ω_w	Kinematic viscosity of air at boundary.	(5.10)	m^2/s

ξ	Dimensionless function representing f, g or q.	(5.62)	-
ρ	Density.	(1.5)	kg/m^3
ρ	Radius of sphere slightly larger than water droplet (Fuchs).	(7.4)	m
τ	Shear stress.	(1.1)	N/m^2
ϕ	Modified temperature in thermocouple wire.	(2.24)	cm s
ϕ	Wet bulb temperature ratio.	p.64	-
$\phi(q)$	A function of temperature.	(5.11)	-
ψ	Modified temperature in thermocouple wire.	(2.25)	s^3
ψ	Boundary layer stream function.	(5.26)	-
$\psi(q)$	A function of specific humidity.	(5.11)	-

SUBSCRIPTS

a	Refers to dry air.
v	Refers to water vapour.
w	Refers to wall or boundary.
∞	Refers to bulk flow outside the boundary layer.

OPERATORS

Δ	Increment.
δ	Increment.
d	Differential operator.
∂	Partial differential operator.
p	Laplace transform operator.
$\mathcal{L}$	Laplace transform.

REFERENCES

1. P.E. Doe : A new method of measuring humidity in a small space. Int. J. Heat Mass Transfer. Vol. 10, No. 3, p. 311/319 (1967).

2. P.E. Doe : Measurement of a mass transfer boundary layer. Nature, Vol. 216, No. 5120, p.1101/1103 (1967).

3. W.M. Rohsenow and H.Y. Choi : in Heat, Mass and Momentum Transfer, Prentice-Hall, Inc., (1961) p. 384.

4. T.K. Sherwood and R.L. Pigford : in Absorption and Extraction, McGraw Hill Book Company Inc. (1952), p.63.

5. R.W. Powell and E. Griffiths : The evaporation of water from plane and cylindrical surfaces. Trans. Inst. Chem. Engrs. Vol. 13, p. 175/192 (1935).

6. R.W. Powell : Further experiments on the evaporation of water from saturated surfaces. Trans. Inst. Chem. Engrs. Vol. 18, p. 36/55 (1940).

7. M.M. El Wakil, G.E. Myers and R.J. Schilling : An interferometric study of mass transfer from a vertical plate at low Reynolds numbers. Trans. Amer. Soc. Mech. Engrs., Series C, Vol. 88, p. 399/406 (1966).

8. W.M. Rohsenow and H.Y. Choi, loc. cit., p.3.

9. ibid, p. 47.

10. P.J. Hartnett and E.R.G. Eckert : Mass transfer cooling in a laminar boundary layer with constant fluid properties. Trans. Amer. Soc. Mech. Engrs. Vol. 79, p. 247/254 (1957).

11. L.D. Berman : in Evaporative Cooling of Circulating Water, Pergamon Press (1961), p. 7.

12. T. Alty and C.A. Mackay : The accommodation coefficient and the evaporation coefficient of water. Proc. Roy. Soc. Vol. 149, Part A, p. 104/116 (1935).

13. K.C.D. Hickman : Maximum evaporation coefficient of water. Indus. & Eng. Chem. Vol. 46, No. 7, p. 1442/1446 (1954).

14. E.F. Lype : Kinetic theory of evaporation rates of liquids. Trans. Amer. Soc. Mech. Engrs. Vol. 77, No. 2, p. 211/223 (1955).

15. E.J. Minnar : in Transducer Compendium, Plenum Press, New York (1963).

16. A. Wexler : in Humidity and Moisture, Vol. 1, Principles and methods of measuring humidity in gases (R.E. Ruskin ed.), Reinhold Publishing Corp. (1965).

17. A.F. Joffe : in Semiconductor Thermoelements and Thermoelectric Cooling, Infosearch, London (1957).

18. P.H. Egli : in Thermoelectricity, Wiley, New York, (1961).

19. R.R. Heikes and R.W. Ure, Jr. : in Thermoelectricity : Science and Engineering, Interscience, New York (1961).

20. D.C. Spanner : The Peltier effect and its use in the measurement of suction pressure. J. Exp. Bot. Vol. 2, No. 5, p. 145/168 (1951).

21. J.L. Montieth and P.C. Owen : A thermocouple method for measuring relative humidity in the range 95-100%. J. Scient. Instrum. Vol. 35, No. 12, p. 443/446 (1958).

22. J. Strong : in Procedures in Experimental Physics, Prentice-Hall, New York (1945), p. 311.

23. N.A. Lange : in Handbook of Chemistry, McGraw-Hill, London, 10th edition (1961), p. 1420.

24. W.M. Rohsenow and H.Y. Choi : loc. cit., p. 452.

25. E.W. Washburn (ed.-in-chief) : in International Critical Tables of Numerical Data Physics, Chemistry and Technology, McGraw Hill, New York (1929).

26. R.G. Wylie : in Psychrometery, CSIRO, Nat. Stand. Lab. Div. Phys. Monograph No. PA-4 (1949).

27. R.W. Powell : The use of thermocouples for psychrometric purposes. Proc. Phys. Soc., Vol. 48, p. 406/414 (1936).

28. A. Wexler : in Humidity and Moisture, Reinhold Publishing Corp. (1965), Vol. 3, p. 71.

29. N.A. Fuchs : in Evaporation and Droplet Growth in Gaseous Media, Pergamon Press (1959).

30. E. Ower and R.C. Pankhurst : in The Measurement of Air Flow, Pergamon Press (1966), 4th edition, p. 305.

31. ibid. p. 304.

32. J.A.B. Wills : The correction of hot-wire readings for proximity to a solid boundary. J. Fluid Mechanics, Vol. 12, p. 388/396 (1962).

33. H. Schlichting : in Boundary Layer Theory, Pergamon Press, London (1955) p. 94.

34. A.R. Oliver : in an unpublished note, University of Tasmania (1968).

35. W.B. Brown : Exact solutions of the laminar boundary layer equations for a porous plate with variable fluid properties and a pressure gradient in the main stream. U.S. NATIONAL CONGRESS OF APPLIED MECHANICS (1951).

36. W.M. Rohsenow and H.Y. Choi : loc. cit. p. 403.

37. A. Wexler : loc. cit., Vol. 3, p. 128.

38. ibid. p. 266.

39. ibid. p. 270.

40. M. Jakob and G.A. Hawkins : in Elements of Heat Transfer, Wiley, New York (1957), 3rd edition, p. 276.

41. A. Wexler : loc. cit., Vol. 3, p. 91.

42. W.M. Rohsenow and H.Y. Choi : loc. cit., p. 30.

43. H. Schlichting : loc. cit., p. 117.

44. L. Rosenhead : in Laminar Boundary Layers, Oxford University Press (1963), p. 234.

45. W.M. Rohsenow and H.Y. Choi : loc. cit., p. 40.

46. ibid. p. 41.

47. ibid. p. 149.

48. H. Schlichting : loc. cit., p. 207.

49. U.E. Nilsson : in an unpublished honours thesis, University of Tasmania (1969).

50. W.B. Brown and P.L. Donoughe : Tables of exact laminar-boundary-layer solutions when the wall is porous and fluid properties are variable. National Advisory Committee for Aeronautics, Technical Note No. 2479 (1951).

51. M. Knudsen : Die Maximale Verdampfungsgeschwindigkeit des Quecksilbers. Ann. der Physic, Vo. 47, p. 697/708 (1915).

52. I. Langmuir : The vapour pressure of metallic tungsten. Phys. Rev., Vol. 2, p. 329/342 (1913).

53. T. Alty : The reflection of vapour molecules at a liquid surface. Proc. Roy. Soc. London, Vol. 131, Series A, P. 555/564 (1931).

54. T. Alty : The Maximum rate of evaporation of water. Phil. Mag., Vol. 15, p. 82/103 (1933).

55. J.D. Bernal and R.H. Fowler : A theory of water and ionic solution, with particular reference to hydrogen and hydroxyl ions. J. Chem. Phys. Vol 1, No. 8, p. 515/548 (1933).

56. H. Payne : Temperature jump and velocity of slip at the boundary of a gas. J. Chem. Phys. Vol. 21, No. 12, p. 2127/2131 (1953).

57. J.W. Cary : An evaporation experiment and its irreversible thermodynamics. Int. J. Heat Mass Transfer, Vol. 7, p. 531/538 (1964).

58. J.H. Perry : in Chemical Engineers Handbook, McGraw Hill (1963), 4th edition, p. 15-36.

59. R.C. Pankhurst and D.W. Holder: in Wind Tunnel Technique, Pitman, London (1952) p. 152.

APPENDIX I

The following work was carried out by the author while on study leave in Aberdeen, Scotland. The paper entitled "A mathematical model of the Torry fish drying kiln" has been published as reference 1 .

I.1 Summary

Proposed developments of the Torry fish drying kiln have led to a need for a closer understanding of commercial fish drying processes. In order to investigate the effects on fish drying of air velocity, air temperature and humidity, and fish packing density, a mathematical model of the kiln has been proposed. This model establishes partial differential equations for fish weight, air temperature and humidity. The model is applicable to the drying of other materials. A solution is obtained numerically by standard finite difference techniques.

I.2 Introduction

Fish drying in Britain underwent a change from traditional natural draft dryers to controlled condition mechanical drying following the development at the Torry Research Station, Aberdeen, of the Torry kiln (Fig. 1) around 1940 (Ref. 2). The Torry kiln in its present form comprises a closed circuit wind tunnel with provision for heating and circulating air, venting to atmosphere and the addition of smoke. The fish is hung in a more or less uniform fashion across the rectangular cross-section of the kiln.

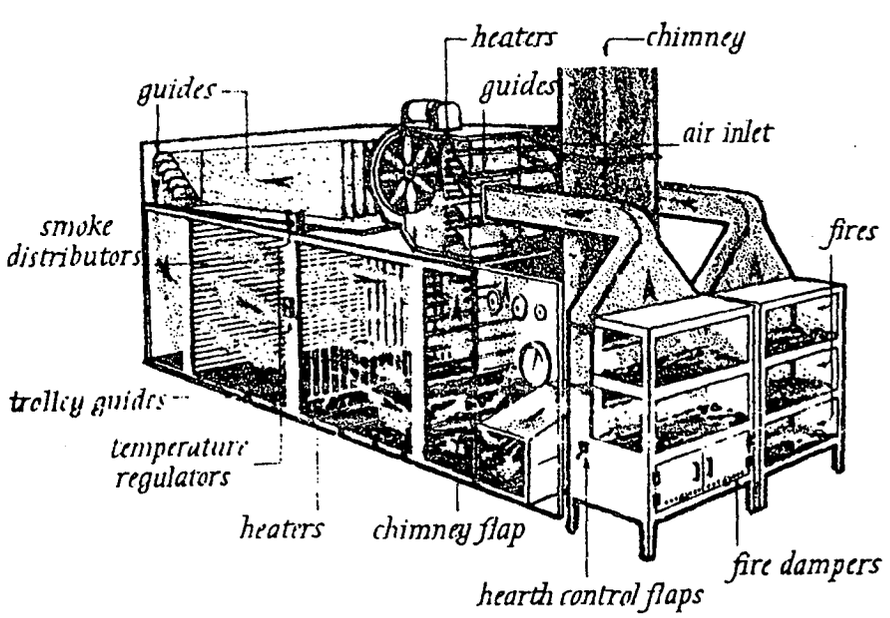

Fig. 1. Cutaway diagram of the Torry Kiln (Crown Copyright Reserved).

Recently there has been a trend towards automatic operation of Torry kilns as a means of optimising performance and economy. For this to be successful, a detailed knowledge of the effects of the various variable quantities associated with fish drying, such as air velocity, temperature and humidity, is required.

A considerable amount of investigation into the running of existing kilns has been carried out by the Research Station. This work is of necessity limited to existing operating methods and is subject to uncontrolled variations in atmospheric conditions; furthermore, it is not practicable to perform a long series of controlled experiments on a kiln producing dried fish in commercial quantities. An alternative is to make a scale model of the kiln and investigate the behaviour of the model. This has been done at Torry, but experience has shown that results of studies on models, or even small commercial kilns, do not scale up readily to the larger kilns.

This paper describes the development of a mathematical model to complement the experimental work on model and prototype kilns. The mathematics is general to the forced air drying of materials in which the internal diffusion processes can be described by Fick's law of diffusion. The model is amenable to computer solution and can predict the separate effects of the various factors on the performance of a kiln. A mathematical model also is capable of easy and rapid modification in order to simulate real behaviour. Thus typical operating data can be input to the mathematical model and the model progressively modified to fit real kiln behaviour.

I.3 Outline of the problem of air drying in a mechanical kiln

The Torry kiln is basically a closed circuit wind tunnel with a large rectangular working section into which trolleys of fish (usually fillets hung vertically) are wheeled. Air circulation is maintained by a fan and venting is provided which allows humid air to be expelled and dry air or smoke to be admitted. Air temperature is controlled by heaters, and humidity is controlled by venting, steam admission and,

in some cases, cooling. Larger kilns (750 kg nominal capacity) are provided with a reheater halfway along the working section. Operation is traditionally a batch process with nearly constant air condition maintained at the upstream end of the working section throughout the drying period. There is usually some rearrangement of the fish trolleys in the kiln during drying to compensate for the upstream fish drying more rapidly than those in moister air further along the kiln. Neglecting this rearrangement, the drying process may be described as a stream of air, passing along the kiln through the racks of fish, absorbing water vapour evaporated from the fish and thus becoming cooler and more humid.

If a particular fillet is considered, the factors affecting its rate of drying are the velocity, temperature and humidity of the air stream passing around it, its shape, surface area and moisture content. Below a certain moisture content, the processes of internal diffusion and capillary action within the fillet control the rate of migration of water to the surface of the fillet. This latter state is known as '<u>falling rate drying</u>'. Prior to this, where there is no lack of free water at the surface, the drying is known as '<u>constant rate drying</u>' (Ref. 3).

At some time during the drying, there are fish near the upstream end of the kiln drying at 'falling rate' and fish further down the kiln, less dry, drying at 'constant rate'. The mathematical model of a drying kiln must be sufficiently detailed to provide for this situation.

In all such mathematical studies, the validity of the end result is dependent on the quality of the data and the validity of the assumptions inherent in the establishment of the mathematical model. Most of the relevant information incorporated in the model has been gleaned from a study by Jason on evaporation and diffusion processes in the drying of fish muscle (Ref. 4) and is thus specifically for the air drying of fish. However, much of the mathematics in this paper is general to other types of drying;

indeed to other problems involving the one-dimensional simultaneous heat and mass transfer of water vapour evaporating into air.

I.4 The physical model

Having outlined the 'real' problem of the kiln drying of fish, the first step in obtaining a mathematical model is to make such simplifying assumptions as may be considered justified. This results in a physical model of the real problem. It is hoped that the physical model will be a sufficiently good approximation to the real situation to enable the solution of the derived mathematical model to be of use. The following is a list of simplifying assumptions which describe the physical model:-

(i) The working section of the kiln may be considered a rectangular parallelepiped.

(ii) There is no preferred direction of air flow other than longitudinally along the kiln so that the properties of air and fish are at all times constant in planes transverse to the general direction of air flow. Thus the working section is considered one dimensional.

(iii) The evaporation rate from the fillets may be calculated from data of Powell and Griffiths (Ref. 5) expressed in equation (18) below. The velocity used may be computed by dividing the air flow rate by the net cross-section of the kiln.

(iv) The change in air pressure along the kiln may be neglected.

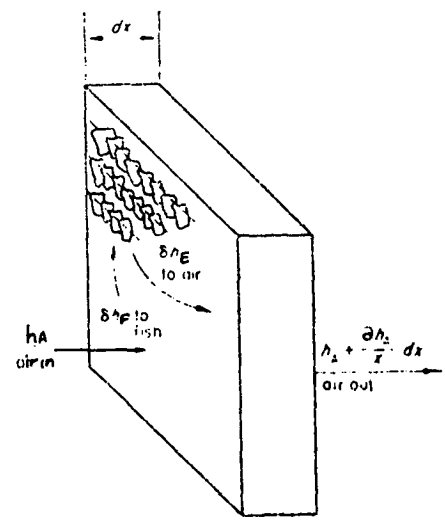

Fig. 2. Heat fluxes associated with a section of the kiln.

I.5 The Mathematical Model

I.5.1 Heat and Mass balances for constant and falling rate drying.

Figure 2 represents an incremental volume of the kiln of length dx. A heat balance over this volume must include:-

(1) The change in enthalpy of the air passing through the volume.

(2) The enthalpy of the water vapour evaporating from the fish in the volume.

(3) The enthalpy associated with any temperature change of the fish.

(4) Conduction, radiation and convection of heat through the walls of the kiln.

It is assumed that item 4 is negligible when compared with items 1, 2 and 3.

In addition to the heat balance in the volume of the kiln there must also be a mass balance which must include:-

(5) The increase in the mass of humid air in the kiln.

(6) The quantity of water evaporating from the fish.

(7) The quantity of water condensing or dripping onto the sides of the kiln.

In practice item 7 is negligible in relation to items 5 and 6. Thus, since mass is conserved, the increase in the mass of humid air is equal to the loss of mass from the fish.

Conservation of total enthalpy in the incremental volume requires that

$$\delta h_A + \delta h_F = 0 \quad , \qquad (1)$$

where δh_A is the enthalpy change of the moist air ,

δh_F is the enthalpy change of the wet fish.

(δh_A is associated with items 1 and 2 and δh_F with item 3).

The enthalpy of 1 + r units of mass of moist air may be written (Ref. 6)

$$h = h_a + r h_v \quad , \qquad (2)$$

where h_a is the enthalpy of a unit mass of dry air (specific enthalpy of dry air),

h_v is the enthalpy of a unit mass of water vapour (specific enthalpy of water vapour)

r is the mass of water vapour per unit mass of dry air (mixing ratio).

The change in enthalpy of moist air in a distance dx during the time interval dt resulting from a mass flow rate m_a of dry air is given by

$$\delta h_A = m_a \frac{\partial h}{\partial x} dx\, dt \quad . \qquad (3)$$

Putting $m_v = m_a r$, the mass flow rate of water vapour, differentiating both sides of equation (2) with respect to x and substituting in equation (3) gives

$$\delta h_A = \left(m_a \frac{\partial h_a}{\partial x} + m_v \frac{\partial h_v}{\partial x} + h_v \frac{\partial m_v}{\partial x} \right) dx\, dt, \qquad (4)$$

since $$\frac{\partial m_a}{\partial x} = 0 \quad .$$

If a 'packing density' η is defined by the expression

$$\eta = \frac{M_F}{dx} \quad , \qquad (5)$$

where M_F is the mass at time t of fish in the incremental length dx, then, since the rate of gain of mass of water vapour by the moist air is equal to the rate of loss of mass from the fish (conservation of mass)

$$\frac{\partial m_v}{\partial x} dx = -\frac{\partial M_F}{\partial t} \quad .$$

Therefore

$$\frac{\partial m_v}{\partial x} = -\frac{\partial \eta}{\partial t} \quad . \qquad (6)$$

Let the specific heats at constant pressure of dry air and water vapour be c_{pa} and c_{pv} respectively and let θ be the mean temperature in the incremental volume, then

$$\frac{\partial h_a}{\partial x} = c_{pa} \frac{\partial \theta}{\partial x} \quad ,$$

and $$\frac{\partial h_v}{\partial x} = c_{pa} \frac{\partial \theta}{\partial x} \quad . \qquad (7)$$

The specific enthalpy of water vapour may be written as

$$h_v = \int_{\theta_F}^{\theta} c_{pl}\, d\theta + L(\theta) \quad , \qquad (8)$$

where c_{pl} is the specific heat at constant pressure of liquid water and $L(\theta)$ is the latent heat of vaporisation of water at temperature θ.

By substituting in equation (4) the expressions $\frac{\partial m_v}{\partial x}$, $\frac{\partial h_a}{\partial x}$, $\frac{\partial h_v}{\partial x}$ and h_v given in equations (6), (7) and (8) and writing

$$\begin{aligned} h_F &= c_{pF}\, M_F \frac{\partial \theta_F}{\partial t}\, dt \\ &= c_{pF}\, \eta \frac{\partial \theta_F}{\partial t}\, dx\, dt, \end{aligned} \qquad (9)$$

where c_{pF} is the specific heat of fish muscle at constant pressure, equation (1) becomes

$$(m_a c_{pa} + m_v c_{pv})\frac{\partial \theta}{\partial x} - \left[\int_{\theta_F}^{\theta} c_{pl}\, d\theta + L(\theta_F)\right] \frac{\partial \eta}{\partial t} + c_{pF}\, \eta \frac{\partial \theta_F}{\partial t} = 0 \quad . \qquad (10)$$

θ carries the subscript F in the latent heat term since this relates to fish temperature.

Writing, as the mass flow rate of moist air,

$$G = m_a (r + 1) \quad , \qquad (11)$$

equation (10) becomes

$$\frac{G}{r+1}(c_{pa} + r\, c_{pv})\frac{\partial \theta}{\partial x} - \left[\int_{\theta_F}^{\theta} c_{pl}\, d\theta + L(\theta_F)\right]\frac{\partial \eta}{\partial t} + c_{pF}\, \eta \frac{\partial \theta_F}{\partial t} = 0 \quad . \qquad (12)$$

It follows from equation (11) that

$$m_v = \frac{r}{r+1} G \quad , \qquad (13)$$

which, on differentiating and substituting in equation (6), gives

$$\frac{\partial \eta}{\partial t} + \frac{G}{(r+1)^2}\frac{\partial r}{\partial x} = 0 \quad . \qquad (14)$$

I.5.2 Constant rate drying

During constant rate drying, convective mass and heat transfer determine the evaporation rate at the fish surface. Powell and Griffiths (Ref. 5) in their classical work on evaporation, measured evaporation rates from a saturated horizontal plane rectangular surface and presented the results in the expression

$$\frac{E}{P_s - p} = 1.61 \times 10^{-4} \, b \, a^{0.77} \, (1 + 0.121 \, u^{0.85}) \quad , \quad (15)$$

where E is the total rate of evaporation from a surface of length l and breadth b (g sec^{-1}),

P_s is the saturation vapour pressure at the wet bulb temperature (atm),

p is the partial pressure of water vapour (atm),

l is the length of the rectangular surface parallel to direction of air flow (cm),

b is the breadth of the rectangular surface transverse to direction of air flow (cm),

u is the air velocity (cm sec^{-1}).

Powell (Ref. 7) has shown that the presence of ridges on a cylinder can enhance evaporation rates by as much as 50 per cent, while rates of evaporation from the downstream surface of a plane rectangular plate increase as the plate is progressively inclined to the air stream, the increase being 100 per cent in extreme cases. Jason (Ref. 4), in confirming that the data of Powell and Griffiths (Ref. 5) apply to rectangular slabs of more than a certain length, demonstrated that the rate of evaporation is considerably increased locally by air turbulence generated downstream of the leading edges.

It is impossible with present knowledge to incorporate such effects analytically in the mathematical model. However, by introducing an empirical shape factor C to allow for the consequences of irregular geometry of the fillets, equation (15) may be written in the form

$$\varepsilon = k_w \, (p_s - p) \quad , \quad (16)$$

where ε is the rate of evaporation per unit area (g sec^{-1} cm^{-2}). k_w, the mass transfer coefficient for a plane rectangular surface of length L_o is multiplied by C to give a corresponding value for a fish fillet of

$$k_w = 2.415 \times 10^{-4}\, l^{-0.23}\,(1 + 0.121\, u^{0.85}) \quad . \qquad (17)$$

(A value C = 1.5, based roughly on the above considerations, appears to be reasonable when the numerical solution of the equations is compared with real behaviour as shown below).

The drying rate per unit length of the kiln may be related to the evaporation rate per unit area of fish by the expression

$$\frac{\partial \eta}{\partial t} = -\varepsilon \xi \quad , \qquad (18)$$

where ξ is the surface area of fish per unit length of the kiln.

Equations (16) and (18) give an expression for the drying rate during constant rate drying

$$\frac{\partial \eta}{\partial t} = -\xi\, k_w\, (p_s - p) \quad . \qquad (19)$$

I.5.3 Falling rate drying

During falling rate drying, the migration of water within the fish governs the drying rate. Jason (Ref. 4) has shown that, whatever the mechanism of diffusion involved, whether capillary flow, thermal diffusion, gaseous diffusion, viscous flow of water vapour, surface diffusion in a porous medium, or molecular diffusion in a solid medium the process can be adequately described by an exponential expression relating the drying rate to the drying time. In the falling rate period this behaviour may be represented by the expression

$$\frac{\eta - \eta_e}{\eta_c - \eta_e} = \exp\,[-(t - t_c)/\tau] \text{ for } t \gg t_c \quad , \qquad (20)$$

where t is the time from commencement of drying, τ is the drying time constant, and the subscripts c and e refer to values at the commencement of the falling rate period and under equilibrium conditions respectively. Jason has measured τ for fillets of various sizes and from various species over a wide range of temperature.

Differentiation of η with respect to t gives

$$\frac{\partial \eta}{\partial t} = -\frac{\eta_c - \eta_e}{\tau} \exp\left[-(t - t_c)/\tau\right] \quad . \qquad (21)$$

I.5.4 Determination of the end of constant rate drying.

Constant rate drying ends when the processes of internal diffusion of water to the surface of the fish start to control the drying. Jason (Ref. 4) has proposed a method of calculating the free water concentration at the surface of a slab of given diffusivity based on an analogous solution in the field of heat transfer (Ref. 8). The difference between the free water concentration (C_s) at the surface of time t, and the initial free water concentration (C_o) at the centre of a slab of thickness 2c is

$$C_o - C_s = \frac{\varepsilon c}{D}\left\{\frac{Dt}{c^2} + \frac{1}{3} - \frac{2}{\pi^2}\sum_{1}^{\infty}\frac{1}{n^2}\exp\left(-\frac{Dn^2\pi^2 t}{c^2}\right)\right\}, \qquad (22)$$

where ε is the flux of water at the surface. D is the effective diffusion coefficient.

Jason then proposes that, at the end of the constant rate period as soon as there is insufficient free water to saturate the air close to the surface, the concentration of water at the surface rapidly approaches a value in equilibrium with the humidity of the air stream. The equilibrium water content of fish muscle has been determined by Jason at various humidities.

If C_e is the equilibrium free water concentration, and t_c is the time at the end of constant rate drying, the evaporation rate at the end of constant rate drying, ε_c , is given by

$$\varepsilon_c = \frac{D(C_o - C_e)}{c} \Big/ \left\{\frac{Dt_c}{c^2} + \frac{1}{3} - \frac{2}{\pi^2}\sum_{1}^{\infty}\frac{1}{n^2}\exp\left(-\frac{Dn^2\pi^2 t_c}{c^2}\right)\right\}. \qquad (23)$$

At time t_c, the flux of water to the surface falls below the critical value ε_c, so that the diffusion of water to the surface can no longer support the rate of evaporation corresponding to the convective mass transfer from a free water surface as given by equation (18).

I.6 Solution of the mathematical model

The solution of the mathematical model requires the solution of the non-linear partial differential equations (12), (14), (19) and (21) so that the fish weight per unit kiln length η, air temperature, θ, and mixing ratio, r, are known for all positions x, along the kiln at any time, t.

There are necessarily initial and boundary conditions applying to the equations. The boundary conditions chosen are that the temperature and humidity of the air entering the working space of the kiln remain constant throughout the drying process. That is:-

$$\text{at } x = 0, \quad \theta = \theta_o \ , \ r = r_o \text{ for all } t \ .$$

The initial condition is that the fish is uniformly wet and the kiln is uniformly loaded at the start of drying.

That is at $t = 0$, $\eta = \eta_o$ for all x ,

where η_o is the packing density or weight of fish per unit length of kiln at the start of drying. There is, in addition, a test involving equations (18) and (23) which determines whether the fish is drying under constant or falling rate conditions.

It was found convenient in the solution to use the partial pressure of the water vapour in the moist air p instead of the mixing ratio r as a measure of humidity. These equations are related by the expression (Ref. 6)

$$r = \frac{0.622\ p}{P - p} \ , \qquad (24)$$

where P is the total pressure of the air-water vapour mixture.

With the substitution of equation (24), equation (12) becomes

$$\frac{G\ (P - p)}{(P - 0.378\ p)} \left[c_{pa} + \frac{0.622\ p}{P - p}\ c_{pv} \right] \frac{\partial \theta}{\partial x} - \frac{L(\theta_F)\partial \eta}{\partial t} + c_{pF} \eta \frac{\partial \theta_F}{\partial t} = 0 , \qquad (25)$$

it being noted that $$\int_{\theta_F}^{\theta} c_{pl}\, d\theta \ll L(\theta_F) ,$$

and equation (14) becomes

$$\frac{\partial\theta}{\partial t} + \frac{0.622\ G\ P}{(P - 0.378\ p)^2}\ \frac{\partial p}{\partial x} = 0 \quad . \qquad (26)$$

The following two simplifications apply to equation (25)

$$\frac{\partial\theta_F}{\partial t} = 0 \qquad \text{for constant rate drying ,} \qquad (27)$$

$$\theta_F = \theta \qquad \text{for falling rate drying.}$$

Equation 25, together with the initial and boundary conditions and the test for the end of constant rate drying (equations (19) and (23)), represents the mathematical model in the form chosen as the most convenient for solution.

The solution was obtained by using standard finite difference approximations to the partial derivatives (Ref. 9). The finite difference approximations were chosen so that the computation proceeded in a marching fashion.

The computer program was written in the Algol programming language and run on the Elliott 503 machine at the University of Tasmania. A flow chart of the computation is shown in figure 3.

I.7 Convergence of the solution

The author knows of no way to predict the convergence of this solution analytically. That the solution is basically stable is demonstrated by the results obtained. The convergence was assessed by producing a number of solutions with the same data except that progressively smaller time and distance increments were used in the finite difference approximations.

I.8 Effects not included in the model

The evaporation rate during constant rate drying is calculated from the results of Powell and Griffiths (Ref. 5) for a flat wet plate. Although no attempt has been made to correct the

mathematical model for the effect of proximity of the fish fillets to each other, edge and shape effects and the disordered air flow conditions undoubtedly existing in the kiln, an empirical shape factor C has been introduced, as noted above, to allow for these factors. Although it is admitted that C is chosen to represent typical values encountered when turbulent flow is deliberately introduced, it will be seen below that the results are in reasonable agreement with the only available experimental data.

The assumptions involved in the change to falling rate drying and the application of equation (2), impose a discontinuity on the surface temperature of the fish at times $t - t_c$. In reality there are temperature gradients along particular fillets, with parts of the same fillet drying in the two regimes. The disordered flow conditions in the kiln and lack of detailed knolwedge of fish temperature precludes any attempt to include these effects in the model.

The effect of shrinkage is also neglected; but as shrinkage is only significant during the latter stages of falling rate drying, and as drying in this period is computed from measured time constants which must include any effects due to skrinkage, the omission of shrinkage from the model appears justified.

I.9 Results

Computer runs to date have been confined to a study of the drying of haddock fillets (Gadus aeglefinus) of a type known as 'golden cutlets'. A close study of the drying in commercial quantities of this fish has been made by Mr. R.M. Storey of the Torry Research Station, who has kindly given permission for his data to be used in this paper. The data used in the computer runs pertaining to the 750 kg Torry kiln and 'golden cutlets' are given in the table.

Figures 4 and 5 represent the computer solution with a time increment of 450 seconds and a distance increment of 15 cm.

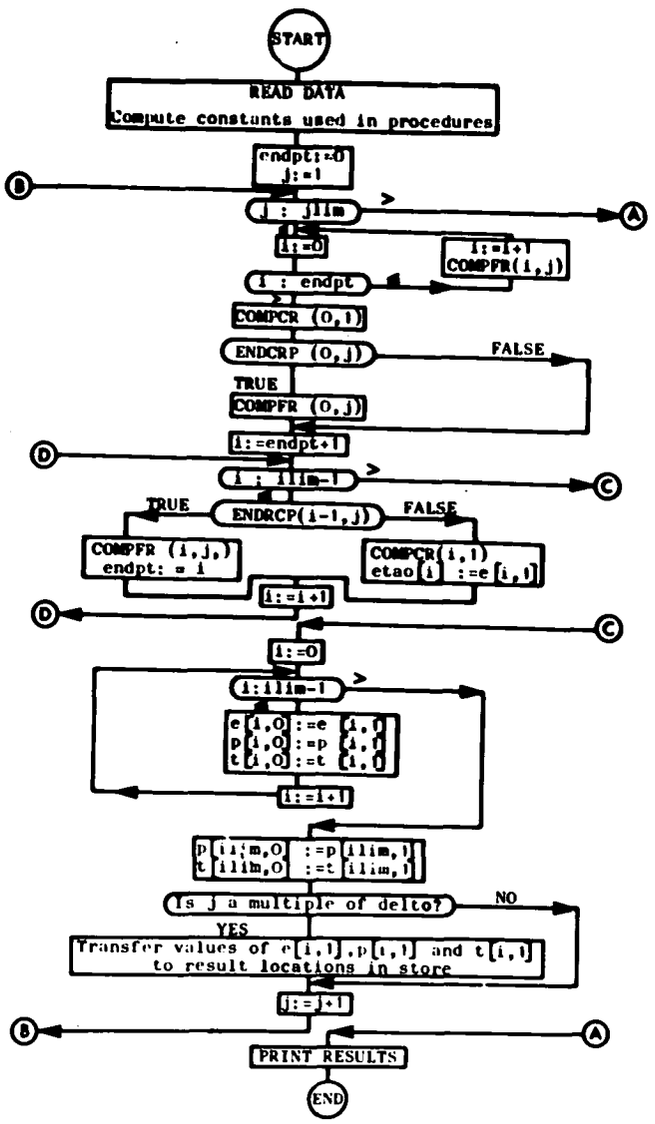

LIST OF IDENTIFIERS AND PROCEDURES

IDENTIFIERS: INTEGER

i	Counter for distance increments
j	Counter for time increments
ilim	Number of distance increments
jlim	Number of time increments
endpt	Counter to mark end of constant rate drying
delto	Number of time increments between results printout

ARRAY

e[i,j]	Value of fish weight/unit kiln length,η,after j time increments and i distance increments
p[i,j]	Value of partial pressure of water vapour at [i,j]
t[i,j]	Value of air temperature at [i,j]
etao[i]	Value of η at end of constant rate period at [i]

PROCEDURES:

COMPCR (i,j)Computes values of e[i,j] p[i+1,j] and t[i+1,j] during constant rate period from values previously computed.

COMPFR (i,j)Computes similar values during falling rate period.

TYPE BOOLEAN

ENDCRP (i,j) Has the value TRUE if the constant rate period is finished, otherwise is FALSE.

Fig. 3. Flow chart of computer program.

Several somewhat unexpected features emerge from these results. The rate obtaining in the so-called 'constant rate period' is only constant at the upstream end of the kiln (Fig.4(a).) Due to the varying condition of the air further down the kiln following the change to falling rate drying at the upstream end of the kiln, the fish further down the kiln dries rather faster than at constant rate, although 'constant rate' or more strictly 'convection governing' conditions apply. Another feature which is somewhat puzzling at first view is the change in temperatures and humidities at all stations along the kiln at the same time (about 6 hours) (Figs.4(a),4(b)) regardless of the progressive onset of 'falling rate' drying as indicated in figure 4(a). This is explained by the fact that the temperature and humidity at each station remain constant with time only so long as all the fish in the kiln is drying at constant rate. This occurs while the station at the upstream end of the kiln dries at constant rate. After this (i.e. after 6 hours in figures 4 and 5) the air reaching stations further along the kiln is rather dryer than previously (indicated by a decrease in vapour pressure in figure 4(c) and an increase in temperature in figure 4(b)) and so, while these stations are still drying under 'convection governing' conditions, the air properties are changing.

I.10 Comparison with real behaviour

R.M. Storey (Ref. 10) in his work on the drying of 'golden cublets' presents two graphs. One is of the effect of drying rate of variations in mean wet bulb depression (Fig. 6) and the other gives the effect of changes in kiln loading (Fig. 7). Figures 6 and 7 also show similar curves obtained from the computer solution using the data given in the table, together with the appropriate values of upstream humidity and initial loading.

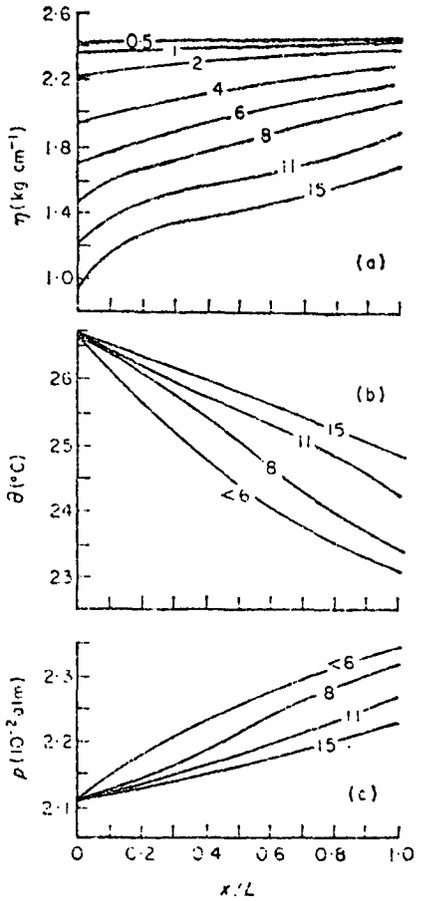

Fig. 4. Variation with time t at various distances x/L along kiln of : (a) fish weight per unit kiln length η , (b) dry bulb temperature θ , (c) partial pressure of water vapour p . Numerals on curves indicate values of x/L.

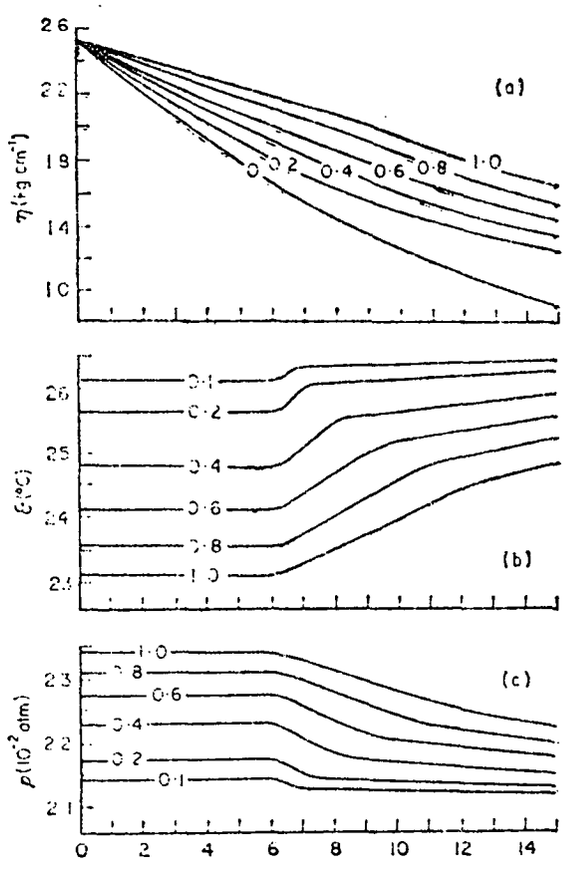

Fig. 5. Variation with distance x/L along kiln at various times t of: (a) fish weight per unit length η , (b) dry bulb temperature θ , and (c) partial pressure p of water vapour. Numerals on curves indicate values of t (hr).

Figures 8 and 9 show the effect on the drying rate of variations in air temperature and fish thickness. The drying rate is expressed as a percentage of moisture lost per hour and is computed on the basis of a mean 13 per cent reduction in fish weight over the entire kiln, this being roughly the normal weight loss in the drying of 'golden cutlets'.

I.11 Further development of the model

There are several extensions to the physical and mathematical models which would make the predicted characteristics more realistic. The effects of reheating midway along the kiln, as is practised in larger kilns, and of changing the order of the loaded trolleys within the kiln during drying, could be included. The model could be readily extended to fatty fish by the inclusion of a fat content term in the diffusivity, D, (Ref. 11). A more complete simulation could be achieved by including the effects of varying upstream conditions during the drying cycle.

All these improvements will probably be necessary before achieving the eventual aim of this study, the selection of optimum operating conditions for automatic control of fish drying kilns.

The facility for varying the temperature and humidity of the air in a kiln throughout the drying cycle has been developed at the Torry Research Station. The immediate application of this model is in the selection of a control program for economical automatic operation of the Torry kiln for particular drying processes.

I.12 Conclusion

The reasonable agreement between the actual and computed behaviour of the drying situation examined, gives encouragement that the model will produce a reasonable prediction of many drying processes with similar geometry to that selected for the model.

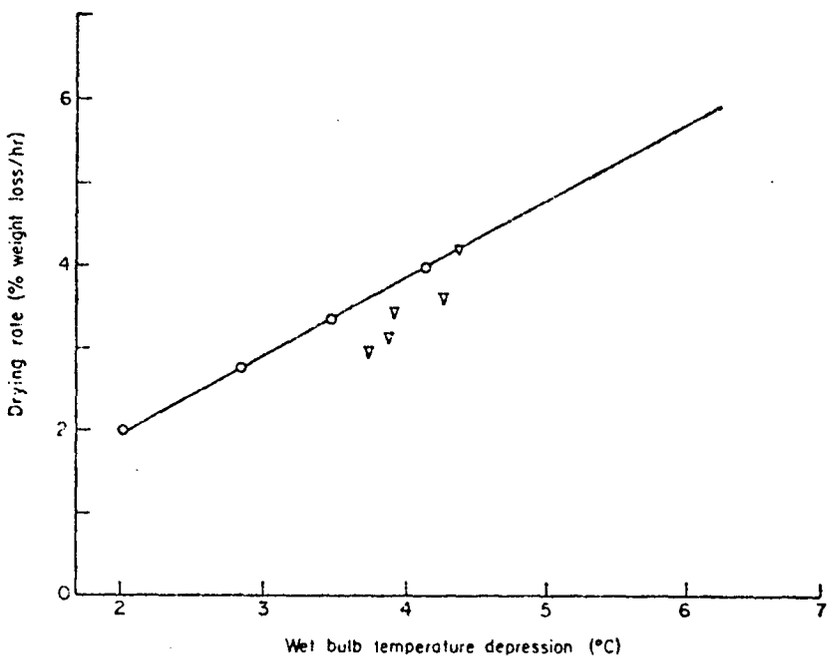

Fig. 6. Variation of drying rate with wet bulb depression.
o , computed; ▽ , measured.

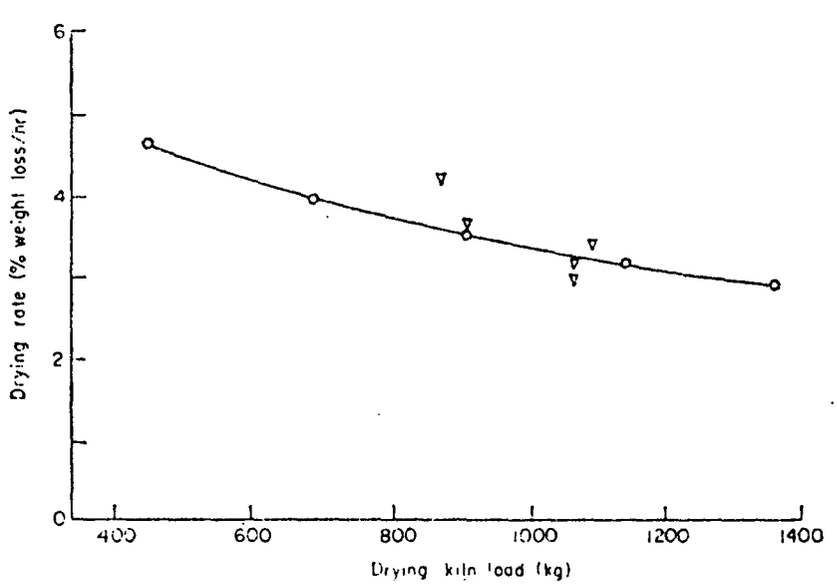

Fig. 7. Variation of drying rate with kiln loading.
Key as Fig. 6.

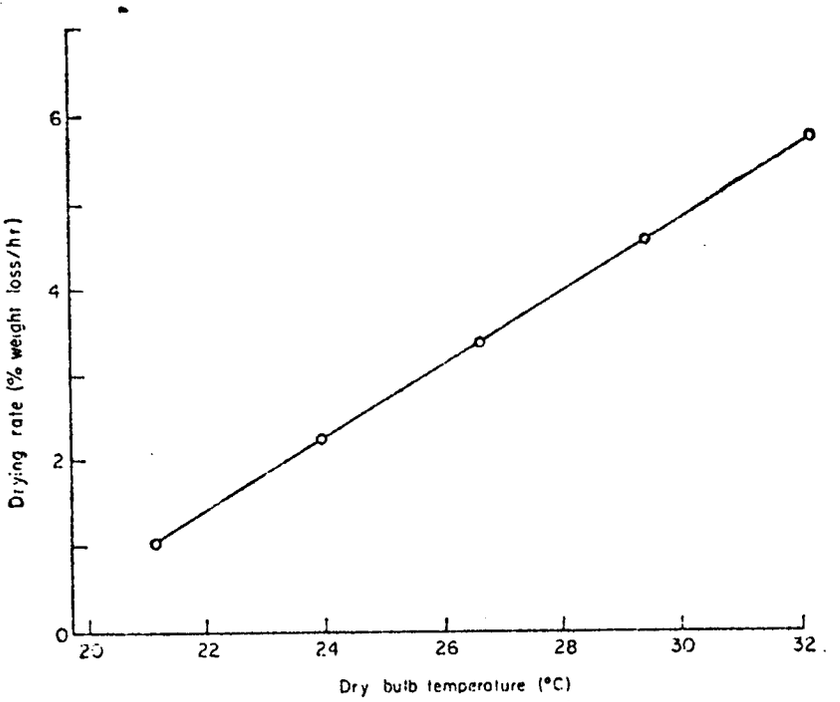

Fig. 8. Variation of drying rate with air temperature.

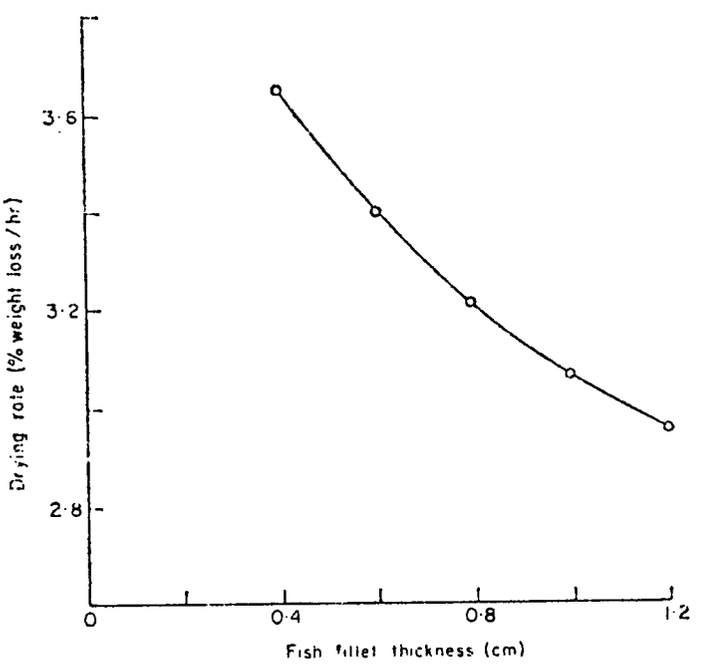

Fig. 9. Variation of drying rate with fish fillet thickness.

I.13 Acknowledgements

The work formed part of the programme of the Torry Research Station, Aberdeen, (Ministry of Technology) where it was carried out while the author was a visiting Research Fellow on study leave from the University of Tasmania. The author wishes to thank, for their assistance, Dr. A.C. Jason, Mr. H.R. Sanders, Dr. A. Aitken and Mr. R.M. Storey of the Torry Research Station.

NOMENCLATURE FOR APPENDIX I

Symbol	Significance	Equation	Units
b	Breadth of rectangular surface transverse to direction of air flow	15	cm
C	Shape factor	17	-
C_e	Equilibrium free water concentration	23	g cm^{-3}
C_o	Initial free water concentration	22	g cm^{-3}
C_s	Free water concentration at surface of fillet	22	g cm^{-3}
c	Half thickness of fillet	22	cm
c_{pa}	Specific heat of dry air at constant pressure	7	cal g^{-1} C^{-1}
c_{pF}	Specific heat of fish muscle at constant pressure	9	cal g^{-1} C^{-1}
c_{pv}	Specific heat of water vapour at constant pressure	7	cal g^{-1} C^{-1}
c_{pl}	Specific heat of liquid water	8	cal g^{-1} C^{-1}
D	Effective diffusion coefficient of water in fish muscle	22	cm^2 sec^{-1}
E	Total rate of evaporation from a surface of length l and breadth b	15	g sec^{-1}
G	Mass flow rate of moist air	11	g sec^{-1}
h	Enthalpy of 1 + r units of mass moist air	2	cal g^{-1}
h_a	Specific enthalpy of dry air	2	cal g^{-1}
h_g	Specific enthalpy of water vapour	2	cal g^{-1}
h_A	Enthalpy of moist air	1	cal
h_F	Enthalpy of fish muscle	1	cal
k_w	Overall mass transfer coefficient for surface of length l	16	g sec^{-1} cm^{-2} at
$L(\theta)$	Latent heat of vaporisation of water at temperature	8	cal g^{-1}
l	Length of rectangular surface parallel to the direction of air flow	15	cm
M_f	Mass of fish muscle in length dx	5	g
m_a	Mass flow rate of dry air	3	g sec^{-1}
m_v	Mass flow rate of water vapour	4	g sec^{-1}

n	Integer	22	-
P	Pressure of moist air	24	atm
p	Partial pressure of water vapour	15	atm
p_s	Saturation partial pressure of water vapour	15	atm
r	Mixing ratio of moist air, i.e. mass of water vapour per unit mass of dry air	2	-
r_o	Mixing ratio of moist air entering working space	-	-
t	Time	3	sec
t_c	Time of commencement of falling rate period	20	sec
u	Air velocity	15	cm sec^{-1}
x	Distance along kiln	3	c

GREEK SYMBOLS

Symbol	Significance	Equation	Units
$\mathcal{E}$	Evaporation flux	15	g sec^{-1} cm^{-2}
$\mathcal{E}_c$	Evaporation flux at end of constant rate period	23	g sec^{-1} cm^{-2}
η	'Packing density' - mass of fish per unit kiln length	5	g cm^{-1}
η_c	'Packing density' - at start of falling rate period	20	g cm^{-1}
η_e	'Packing density' under equilibrium conditions	20	g cm^{-1}
η_o	'Packing density' at start of drying	-	g cm^{-1}
θ	Air temperature	7	^oC
θ_F	Fish temperature	9	^oC
θ_o	Dry bulb temperature of air entering kiln	-	^oC
ξ	Surface area of fish per unit length of kiln	18	cm
τ	Drying time constant	20	sec

OPERATORS

δ	Increment
∂	Partial differential
d	Increment

TABLE

DATA

DRYING KILN

Length	- 4.00 m
Cross section area (unloaded)	- 3.07 m^2
Cross section area (loaded)	- 2.22 m^2
Normal load of wet fish	- 1000 kg
Air flow rate	- 5.33 m^3 sec^{-1}
Mean velocity	- 2.49 m sec^{-1}
Typical condition of air at up-stream end of kiln working section	- 60% R.H. at 27.2°C

FISH ("Golden Cutlets")

Mean weight	- 0.27 kg
Approximate size : length	- 0.23 m
thickness	- 0.063 m
width	- 0.12 m
Mass diffusivity of water in fish	- 3.25 x 10^{-10} m^2 sec^{-1} at 30°C
Approximate drying time constant	- 5.4 x 10^4 sec

Equilibrium moisture content of fish

at 10% R.H.	-	4.5 kg H_2O/100 kg bone dry solid
20% R.H.	-	7.2 kg H_2O/100 kg bone dry solid
30% R.H.	-	8.8 kg H_2O/100 kg bone dry solid
40% R.H.	-	11.7 kg H_2O/100 kg bone dry solid
50% R.H.	-	14.0 kg H_2O/100 kg bone dry solid
60% R.H.	-	17.2 kg H_2O/100 kg bone dry solid
70% R.H.	-	22.0 kg H_2O/100 kg bone dry solid
80% R.H.	-	31.0 kg H_2O/100 kg bone dry solid

REFERENCES - APPENDIX I

1. P.E. Doe : A mathematical model of the Torry fish drying kiln. J. Food Technology (in press December 1969).

2. G.H.O. Burgess, C.L. Cutting, J.A. Lovern and J.J. Waterman : in Fish Handling and Processing, H.M.S.O., Edinburgh, (1965), p. 74.

3. ibid. p. 126.

4. A.C. Jason : A study of evaporation and diffusion processes in the drying of fish muscle, in Fundamental Aspects of the Dehydration of Foodstuffs, Society of Chemical Industry, London (1958), p. 103.

5. R.W. Powell and E. Griffiths : The evaporation of water from plane and cylindrical surfaces. Trans. Inst. Chem. Engrs. Vol. 13, p. 175/192 (1935).

6. A. Wexler : in Humidity and Moisture, Vol. 3, Reinhold, New York, (1965) p. 83.

7. R.W. Powell : Further experiments on the evaporation of water from saturated surfaces. Trans. Inst. Chem. Engrs. Vol. 18, p. 36/55 (1940).

8. H.S. Carslaw and J.C. Jaeger : in Conduction of Heat in Solids, Oxford University Press, (1947) p. 163.

9. H.W. Carslaw and J.C. Gaeger : in Conduction of Heat in Solids, Oxford University Press, (1959) p. 466.

10. R.M. Storey : Record Memorandum No. 432, Torry Research Station, Aberdeen.

APPENDIX II

II Drying of wet asbestos sheeting.

This is a summary of work carried out by Mr. J.M. Eyles as part of the requirements for an honours degree in engineering at the University of Tasmania. The work was carried out at the suggestion of the author and under his supervision. No attempt will be made to delineate the regions of responsibility for the work except to point out that all the experimentation and measurement was performed by Mr. Eyles. In this summary the connection with previous work on fish drying, as well as the boundary layer measurements, is discussed.

II.1 Purpose of the experiment.

The work on fish drying (Appendix I) showed that Powell and Griffiths' data (Ref. 1) on the evaporation from rectangular surfaces, are not a good fit to the drying of fish fillets. There are complications of shape, the effect of the leading edge of the fish fillet causing a disturbance to the airflow around the fillet, and the effect of having several fillets in close proximity. In order to investigate the two last mentioned effects, it was proposed to study the drying of rectangular plates cut from asbestos fibre sheeting.

The considerations leading to the choice of asbestos fibre for the drying study were first, the ability of the sheeting to absorb a considerable quantity of water (about four times the dry weight) and secondly, because the water is held rather loosely in the asbestos fibre matrix and is not to a noticeable degree absorbed into the fibres, there is little resistance to the flow of water to the surface, thus giving a considerable drying time at constant rate. As mentioned in Appendix I it is the constant rate drying period that is effected by the air flow and humidity. Once the internal diffusion processes start to govern the flow of water to the surface, the air flow and humidity have no influence on the drying. Thus, apart from the shape factor, during constant rate

drying the wet asbestos dries in the same manner as wet fish, or any other wet substance subject to similar patterns of air flow.

II.2 Apparatus.

The experimental work was carried out in a rectangular section of a wind tunnel (cross section 2 ft. x 1 ft.), supplied from an air conditioning plant. The plates of asbestos sheeting were rectangular, 10½" x 6" x 3/16" and loosely mounted in light aluminium racks, 16 plates to a rack so that the plates were uniformly spaced over the cross section of the wind tunnel. Four such frames were swung from beams and spring balances as shown in figure II.1. The suspension system made it possible to weigh the racks whilst in the tunnel.

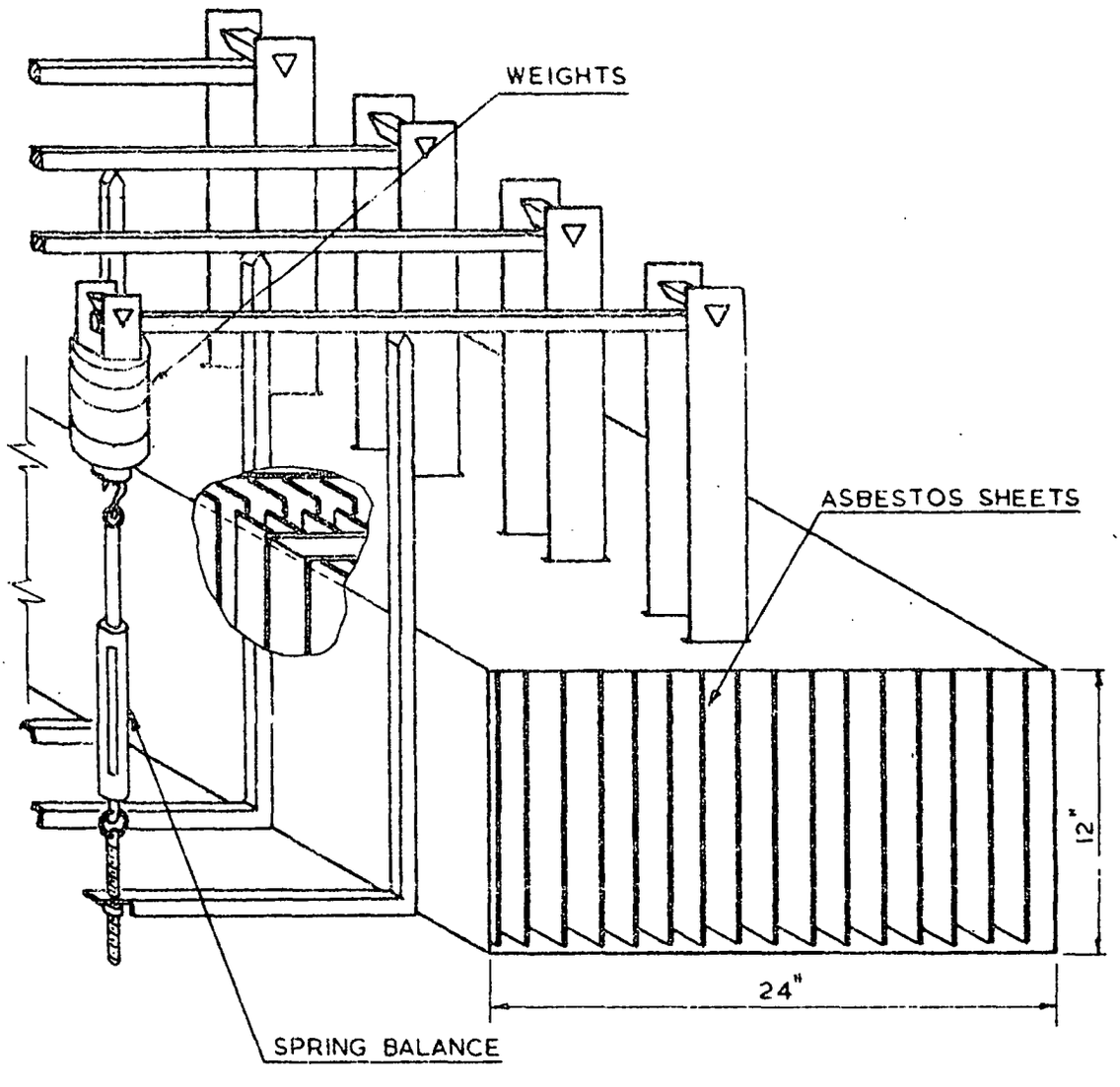

Fig. II.1. Arrangement of racks of asbestos sheeting in air conditioning tunnel.

Air flow was measured by a calibrated bell mouth at the entrance to the air conditioning plant. Velocity gradients and boundary layers were measured with a hot wire anemometer and the same probe was used as a resistance thermometer to measure local temperatures. Humidity of the bulk air flow was measured with a fully ventilated wet and dry bulb psychrometer, and local humidities were found with a wet thermocouple psychrometer. Thermocouples let into the asbestos sheet gave a measure of the plate temperature during drying.

II.3 Measurement of drying rates.

In the first set of measurements, the racks of asbestos sheeting were placed one behind the other in the wind tunnel. Drying rates were recorded for each rack. The results are here presented as a plot of the drying rate against the difference between the saturation partial vapour pressure at the surface temperature and the partial vapour pressure in the bulk flow. (Figure II.2.) A typical drying curve of rack weight against time is shown in Figure II.3.

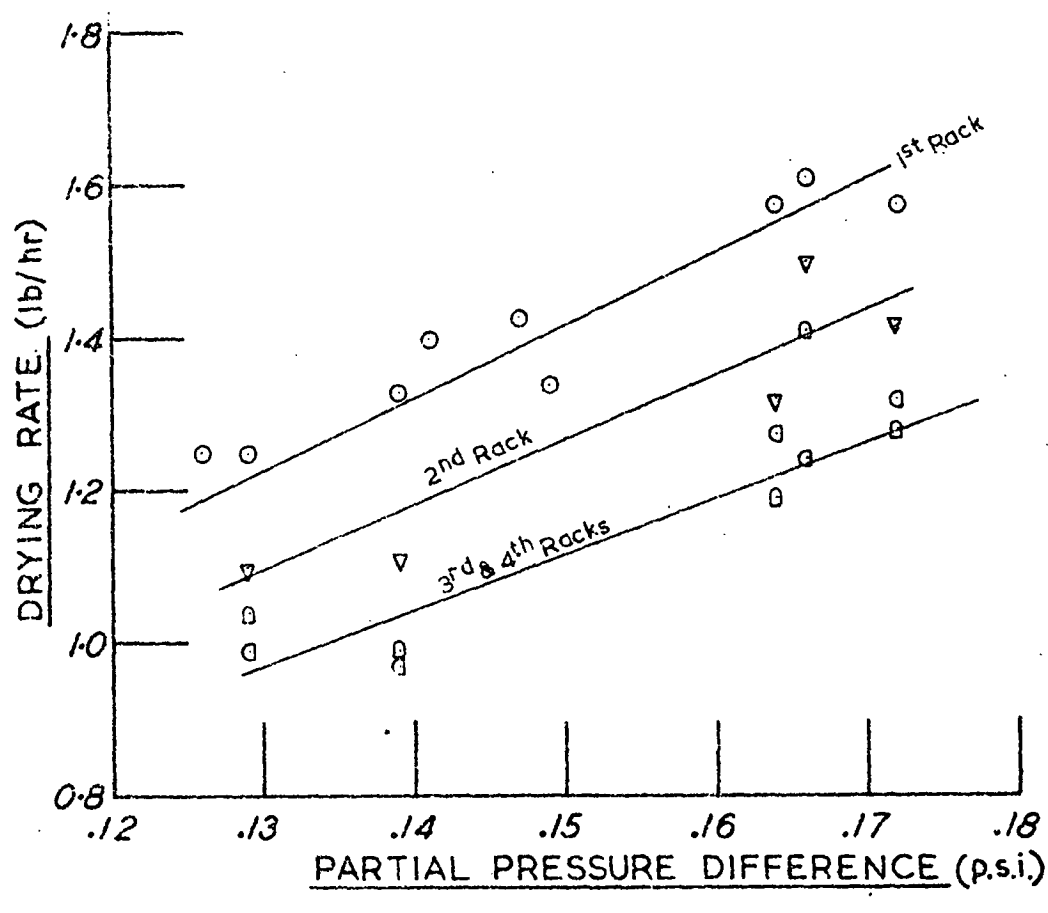

Fig. II.2. Variation of drying rate with air humidity.

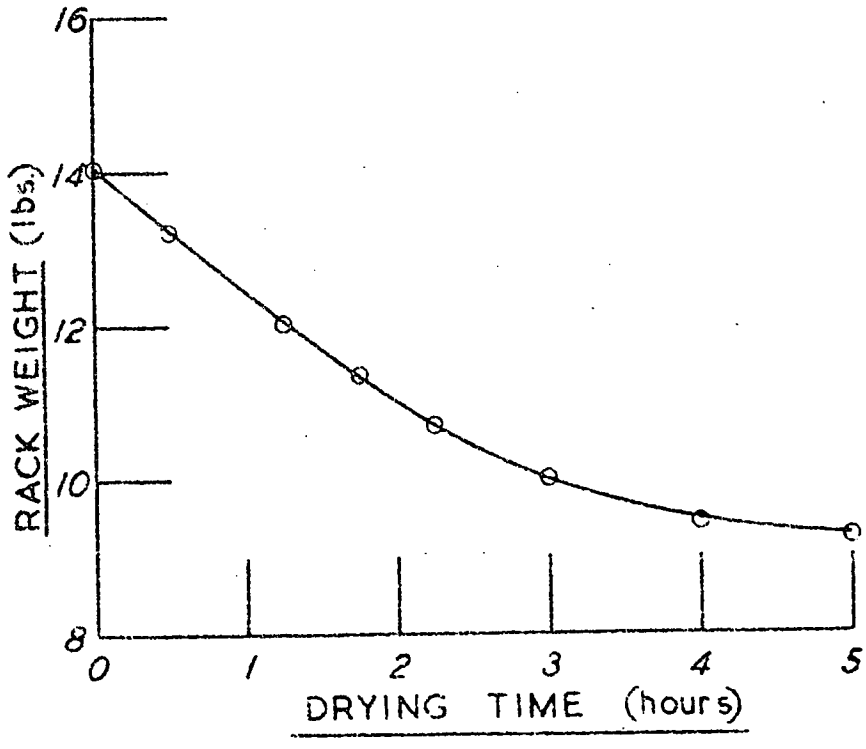

Fig. II.3. Typical drying curve.

Features that emerged from this preliminary study were the relatively high drying rate of the upstream rack and the confused situation downstream where racks were observed to dry faster than those further upstream in presumably less humid air.

A further series of experiments with metal fairings attached to the leading edges of the plates in the upstream rack gave drying rates closer to those of the downstream racks and closer to those predicated from Powell and Griffiths' data (Ref. 1.). This showed that the shape of the leading edge has a considerable effect on the drying rate.

The non-uniformity of drying rates of successive racks was found to be due to a slight misalignment of the sheets. The asbestos had a tendency to buckle out of its plane when wet. This had the effect of moving the buckled plates into the drier air outside the wakes of the sheets upstream, and thus increasing the drying rates of the buckled sheets. This wake effect was investigated in some detail, both by measuring the detail of the flow within the

wake of drying plate and by staggering the plates in successive racks so as to place them outside the wakes. It is possible, by staggering the racks to obtain an increase of 15% in the drying rate over that with the sheets in successive racks in line.

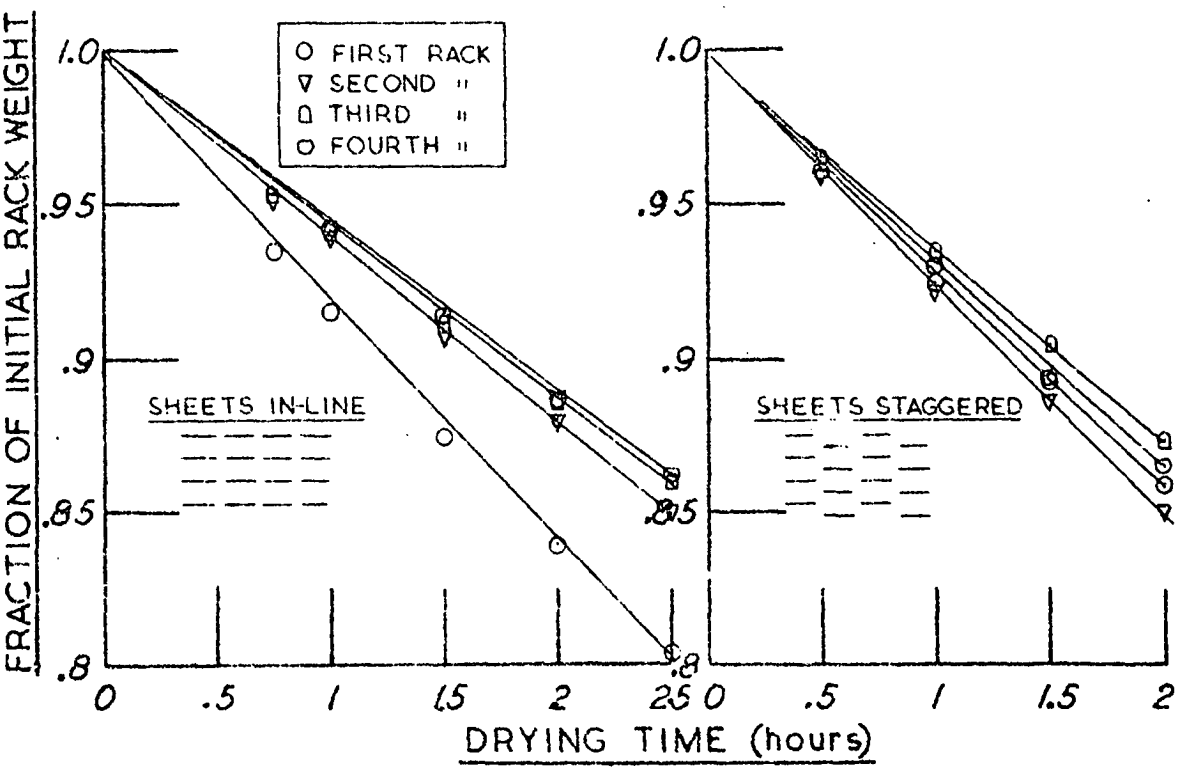

Fig. II.4. Effect of staggering sheets.

II.4 Plate temperature variation.

Eight copper constantan thermocouples imbedded in a plate in the region within one inch from the leading edge were used to measure the plate temperature during drying. Figure II.5 shows the variation of plate temperature during a typical drying run. It can be seen that the plate temperature rises to close to the wet bulb temperature of the bulk air flow shortly after the run is commenced. (The plates were immersed in water at a temperature lower than the wet bulb temperature of the surrounding air prior to the run). The plate temperature remains close to the wet bulb temperature until about 3.5 hours of drying, then increases rapidly. This increase corresponds to the change from constant to falling rate drying. The increase in temperature starts when the diffusion processes in the asbestos control the flow to the surface and the surface becomes dry.

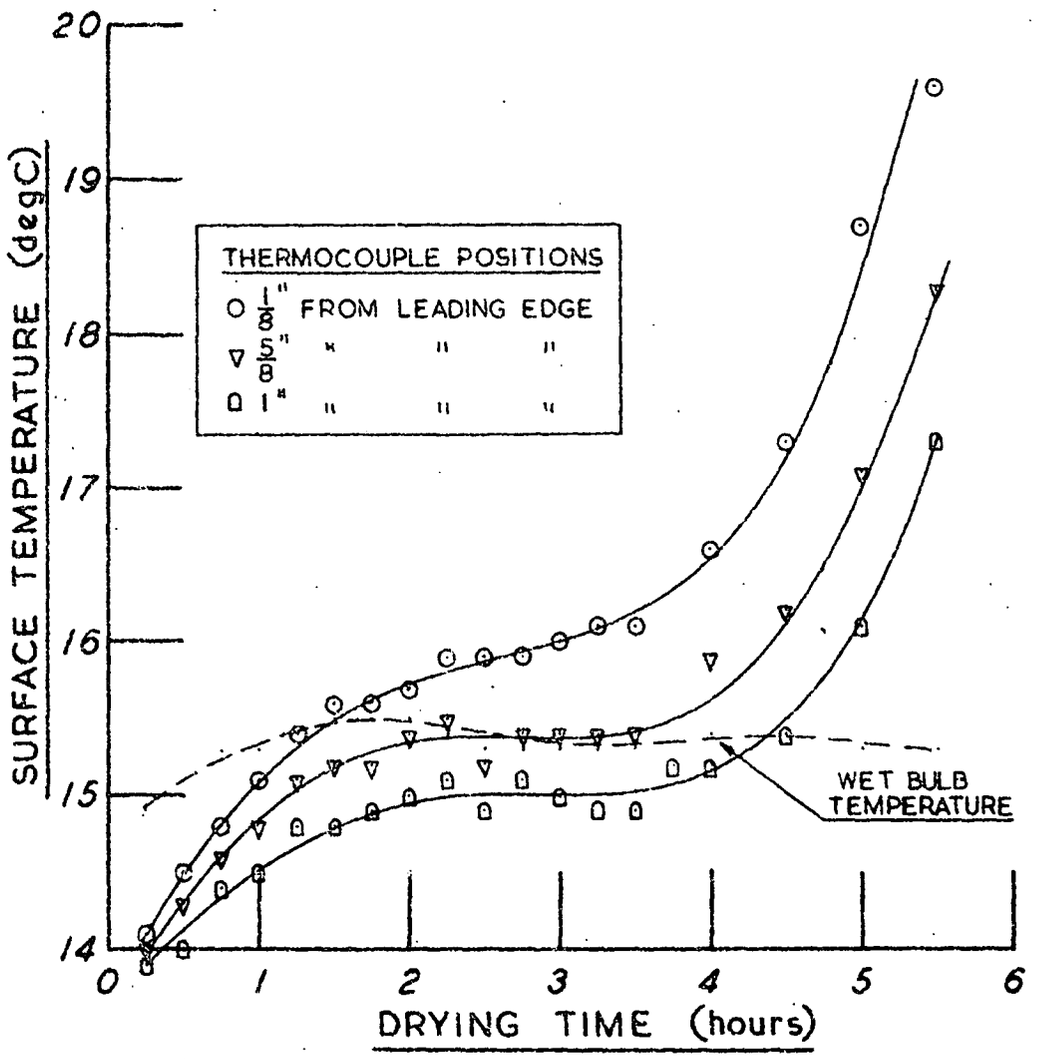

Fig. II.5. Variation of plate temperature during drying.

II.5 Velocity and temperature distributions.

Velocity and temperature distributions were measured both in the region between two plates and in the wake downstream of the plates. A .0003" tungsten hot wire anemometer was used tc measure local velocity. The same wire was used as a resistance thermometer to measure local temperature. Velocity and temperature profiles across the wake about one plate thickness downstream of the trailing edge of a plate are shown in Figs. II.6 and II.7. It can be seen that the effect of the presence of a plate is limited to a wake region larger in size than the plate thickness by the width of the boundary layers on each side of the plate.

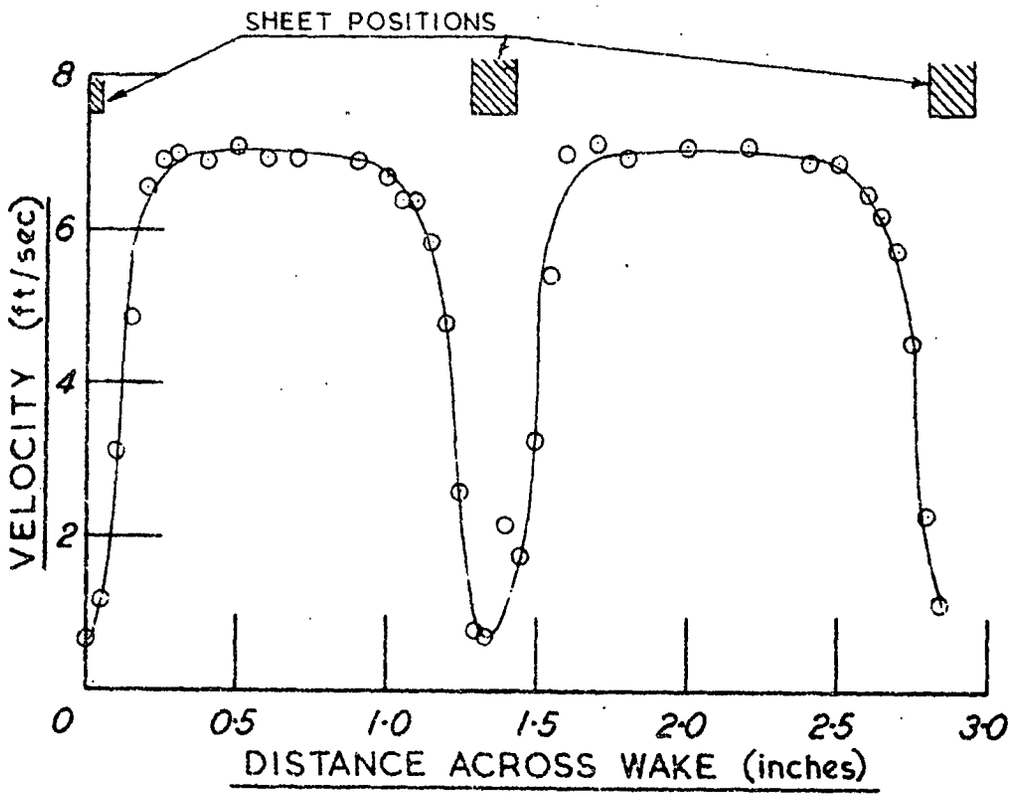

II.6. Velocity across wake.

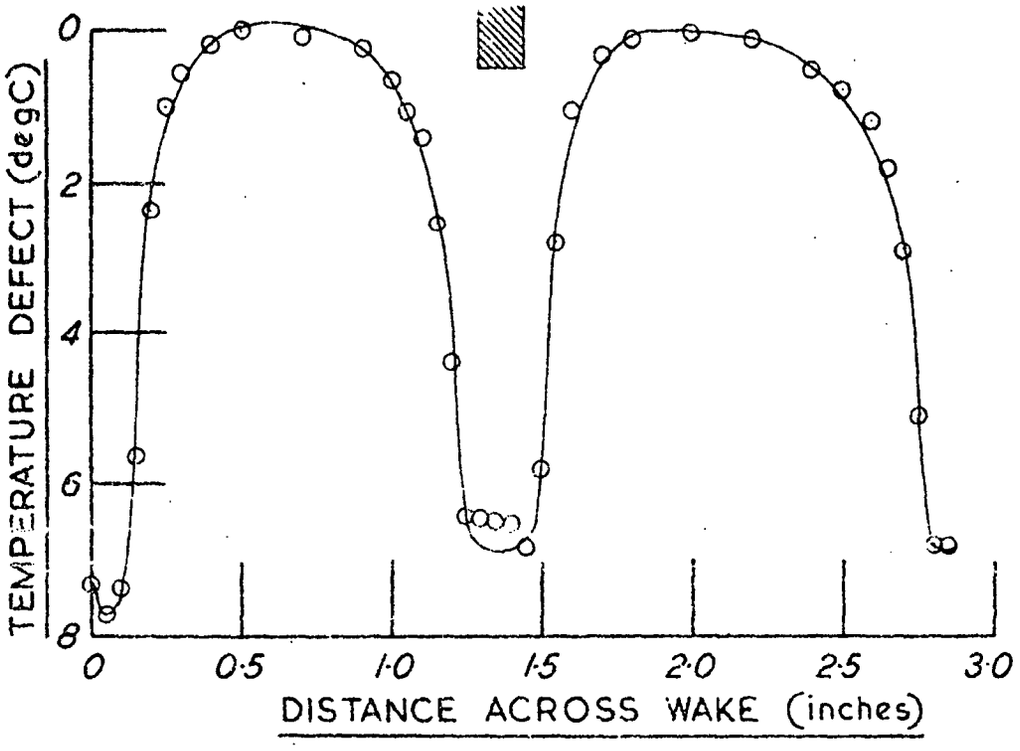

II.7. Variation of temperature across the wake.

The velocity and temperature distributions, together with the wet bulb temperature distribution, were integrated across the wake to find the mass flux in the wake. The difference between the mass flux across the wake and the mass flux in the air upstream of the plates, was in reasonable agreement with the drying rate found from the change in weight of the racks.

The velocity and temperature profiles in the boundary layers at various distances from the leading edge of a plate are shown in figures II.8 and II.9. It is apparent that there is a considerable disturbance to the flow within about three plate thicknesses from the leading edge. Smoke was injected near a large plate with air velocity at the same Reynolds number, and showed a separation bubble in this region.

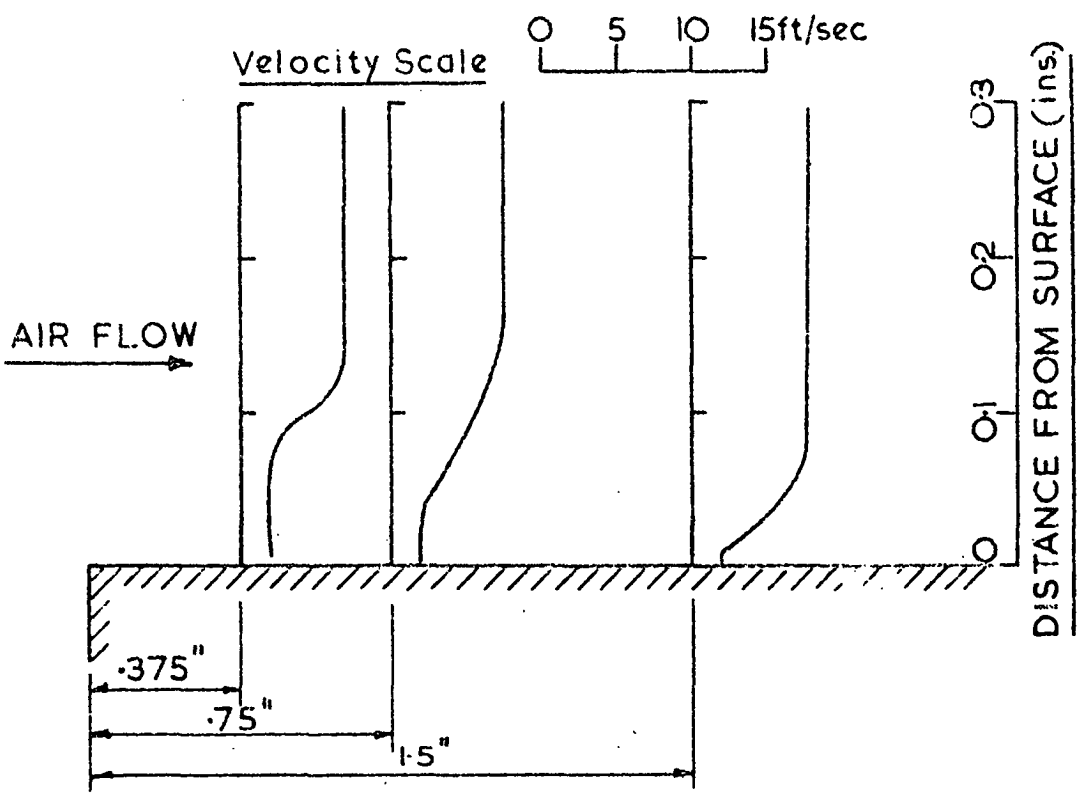

Fig. II.8. Velocity profiles along plate.

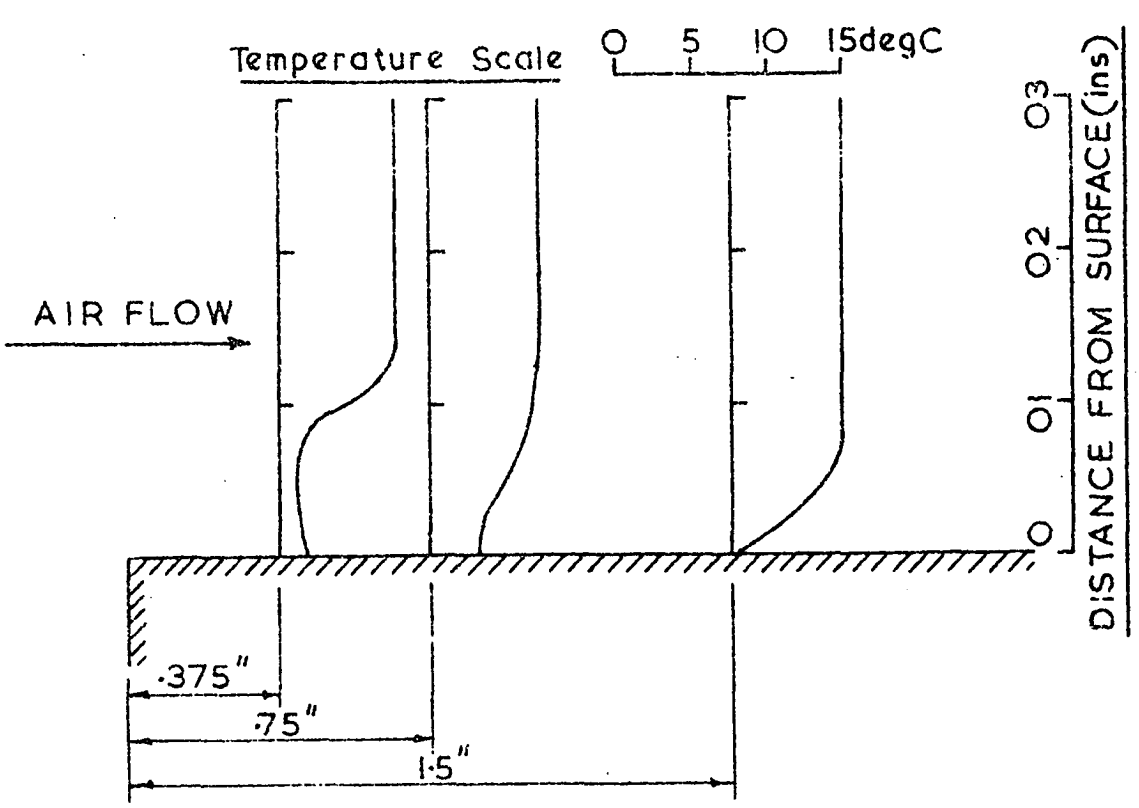

Fig. II.9. Temperature profiles along plate.

Aerodynamicists have used a "china clay" technique for many years to provide visual evidence of regions of boundary layer transition and separation (Ref. 2). The technique is to coat the object to be tested with a black paint, then with china clay (kaolin). The china clay appears transparent when a suitable liquid (such as methyl salicilate) of approximately the same refractive index is sprayed onto it allowing the black color to show through. As the liquid evaporates the china clay becomes opaque and white patches appear. The speed at which the colour change takes place is a measure of the evaporation rate of the dope. It is thus obvious (although it does not seem to have been widely used for this purpose) that this technique directly measures mass transfer but with the different liquid.

A series of photographs of a wooden plate treated with china clay and placed in a wind tunnel with air flow at the same Reynolds number as in the asbestos sheet drying experiments showed that there are considerable variations in the local mass transfer rate in the separation region. Figure II.10 shows Mr. Eyles' estimate of the variation in local mass transfer rate with distance along the plate, obtained from measurements of the intensity of the colour change of the treated plate. The absissa of Fig. II.10 is the ratio of the evaporation rate at the particular distance from the loading edge to the evaporation rate 15 plate thicknesses downstream from the leading edge.

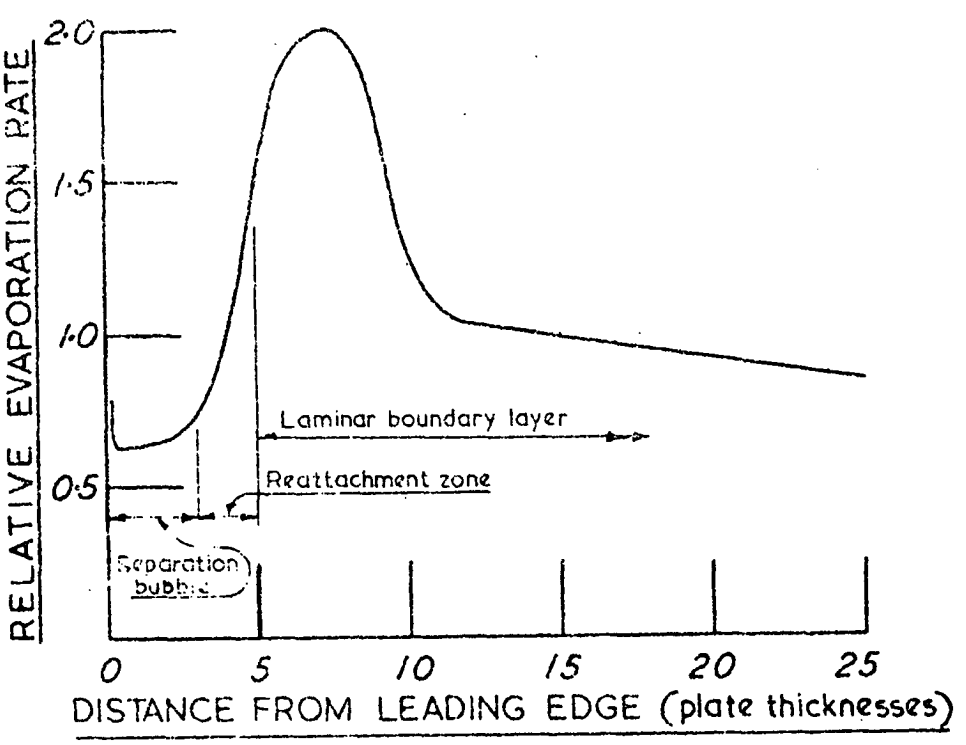

Fig. II.10. Variation in local evaporation rate along plate.

Downstream of the separation region, the flow is nearly laminar as evidenced by the closeness of the measured boundary layer velocity profiles to the familiar Blasius solution (Ref. 3).

II.6 Wet bulb temperature distribution.

A wet bulb thermocouple was made by wrapping cotton around a copper constantan thermocouple of wires .010" diameter. The cotton wick was kept moist by continuing the cotton into a reservoir in the thermocouple support. Due to the relative roughness of the asbestos sheeting it was not considered necessary to make use of the extreme spatial discrimination of the thermocouple psychrometer described in Chapter 3. Measurements of the wet bulb temperature within the boundary layer, wake, separating region and bulk air flow at various stations showed that nowhere in these regions does the measured wet bulb temperature differ by more than 0.1 degC from the wet bulb temperature of the air entering the tunnel. Due corrections were made to the readings of the wet thermocouple for measurements in slow moving air within the boundary layers using the data of Wylie (Ref. 4).

The constancy of the wet bulb temperature is in marked contrast to the measurements with the thermocouple psychrometer above a flat plate described in Chapter 4. The reason for this is the adiabatic nature of the drying of the asbestos sheeting. After the first few minutes of drying practically no heat is conducted from the surroundings to the asbestos plate. All the heat required for the phase change is convected to the surface from the air stream. The asbestos plate, the air within the boundary layer and the bulk of the air flow all have the same temperature of adiabatic saturation since the conditions of the experiment closely correspond to saturation of the air stream at constant enthalpy (Ref. 5). The temperature of adiabatic saturation can be shown to be very close to the indicated wet bulb temperature of a fully ventilated psychrometer (Ref. 6.).

This aspect of drying can lead to a much simplified model of the drying process, provided the drying material is thermally insulated from its surroundings and is therefore at a temperature close to that of the wet bulb temperature during the constant rate drying period. The model of the drying of wet fish described in Appendix I exhibits this property of constant wet bulb temperature, as could be expected as there is no provision in the model for heat conduction to the wet fish. It would simplify the calculation of the drying rate of wet fish, during the constant rate period, to use the property of constant wet bulb temperature in the model together with the heat balance instead of using both the heat and mass balances as in the present model.

II.7 Summary.

Measurements of the constant rate drying of wet asbestos plates in a controlled humidity wind tunnel have shown that the shape of the leading edge of the wet body has a marked effect on the drying rate. There is also a reduction in evaporation if a plate is in the wake of a plate further upstream. A detailed investigation of the flow near a square leading edge of a wet plate has shown that there are variations in the local evaporation rate in this region due to separation of the air flow. The china clay technique of aerodynamics has proven a useful tool for the investigation of local variations in the evaporation rate. Despite the complicated flow around arrays of bluff wet plates, the wet bulb temperature was found to be constant throughout the drying space. This feature is due to the lack of heat reaching the wet plates other than that convected to the plates from the air stream. A model based on constant wet bulb temperature would simplify the calculation of drying rates in similar situations.

II.8 Acknowledgement.

As mentioned in the introduction to this appendix, the experimental part of this project was carried out by Mr. J.M. Eyles for his Honours Degree in Engineering at this University. Because of the close connection of this project with other topics of this thesis, the increased understanding of drying processes that has resulted from this study, and the need for a permanent record of this work, it has been included here. I would like to thank Mr. Eyles for his permission to include this report.

REFERENCES - APPENDIX II

1. R.W. Powell and E. Griffiths : The evaporation of water from plane and cylindrical surfaces. Trans. Inst. Chem. Engrs., Vol. 18, p. 36/55 (1940).

2. R.C. Pankhurst and D.W. Holder : in Wind Tunnel Technique, Pitman, London (1952), p. 152.

3. H. Schlichting : in Boundary Layer Theory, Pergamon, London (1955), p. 102.

4. R.G. Wylie : In Psychrometry, CSIRO, Nat. Stand. Lab. Div. Phys. Monograph No. PA-4 (1949).

5. A. Wexler : in Humidity and Moisture, Reinhold Publishing Corp., (1965), Vol. 3, p. 71.

6. ibid., p. 85.

APPENDIX III

III.1 Two models of the thermocouple psychrometer.

Two models of the thermocouple psychrometer are here included to give weight to the arguments concerning the efficacy of the psychrometer given in Chapter 2. The reason for using two models is to span the real geometry of the thermocouple junction. The junction comprises two wires of different diameters joined by an irregular blob of silver conducting paint. When cooled, the junction and parts of the wires are wet by condensation of moisture from the surrounding air.

One model is that of two wires butt welded together and wet for a certain distance from the junction. The other model is of a spherical water droplet supported on two dry wires. The geometry of the real thermocouple psychrometer lies somewhere between these two models and is approximated by both.

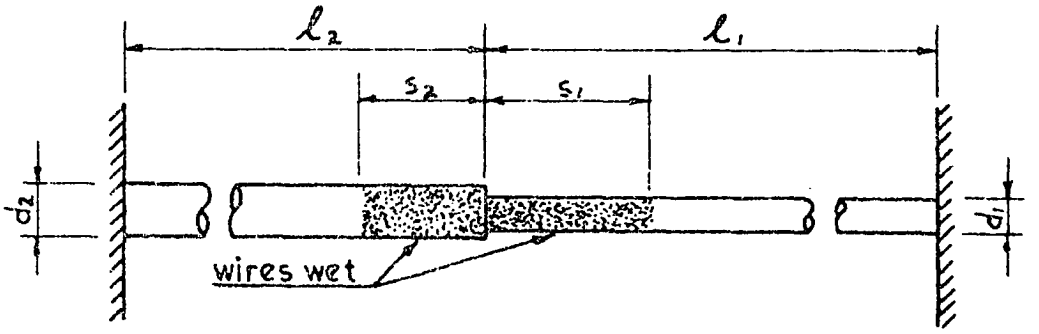

Fig. III.1. Model of two wires butting.

III.2 Model of two wet wires butting.

The model is shown in Figure III.1. Two wires, one of bismuth and the other of bismuth-tin alloy (lengths ℓ_1, and ℓ_2 respectively) are butted together at one end while the other ends are joined to two heat sinks, corresponding in the real situation to the supporting wires. The wires are both wet distances s_1 and s_2 from the junction. These distances are determined by the intensity of the Peltier cooling and the state of the surrounding air prior to the operation of the wet junction as a psychrometer.

It is here assumed that the wires are wet uniformly to a distance from the junction at which the temperature of the wire reached the dewpoint of the surrounding air during cooling.

During the Peltier cooling of the junction, the steady state temperature of one of the thermocouple wires at a distance x from the junction is given by (Ref. 1);

$$\theta = \frac{\lambda_1 P i\, e^{-\alpha x}}{\sqrt{k_w A h a}} - \frac{i^2 \rho}{h a A} \quad , \qquad (1.)$$

where ρ is the resistivity of the wire,

P is the Peltier coefficient of the junction,

i is the current,

k_w is the thermal conductivity of the wire,

A is the cross sectional area of the wire,

a is the circumference of the wire,

h is the surface heat transfer coefficient of the wire,

λ_1 is the proportion of heat conducted to the junction along that wire, $\lambda_1 + \lambda_2 = 1$,

and α is given by $\alpha = \sqrt{\frac{ha}{k_w A}}$.

The heat conducted to the junction from a particular wire is

$$q_1 = k_w A \left(\frac{d\theta}{dx}\right)_{x=0} = -\lambda_1 P i \, . \qquad (2.)$$

Thus the total heat conducted to the junction is

$$q = q_1 + q_2 = -(\lambda_1 + \lambda_2) P i = -P i \, . \qquad (3.)$$

Thus the boundary condition that the heat absorbed at the junction through Peltier cooling should be Pi is satisfied by equation (3.). The temperature of the junction is found from equation (1.) with $x = 0$ to be

$$\theta = \frac{\lambda_1 P i}{\sqrt{k_{w_1} A_1 h_1 a_1}} - \frac{i^2 \rho_1}{h_1 a_1 A_1} = \frac{\lambda_2 P i}{\sqrt{k_{w_2} A_2 h_2 a_2}} - \frac{i^2 \rho_2}{h_2 a_2 A_2} \quad , \qquad (4.)$$

which, with $\lambda_1 + \lambda_2 = 1$ becomes,

$$\lambda_1\left[\frac{1}{\sqrt{k_{w_1}A_1h_1a_1}} + \frac{1}{\sqrt{k_{w_2}A_2h_2a_2}}\right] = \frac{1}{\sqrt{k_{w_2}A_2h_2a_2}} + \frac{1}{P}\left[\frac{P_1}{a_1A_1h_1} - \frac{P_2}{a_2A_2h_2}\right] \quad (5.)$$

Thus λ_1 and λ_2 can be determined. s_1 and s_2 are found by putting $\theta = \theta_d$, the dewpoint temperature, in equation (1.) and solving for x. At the end of the cooling period, the situation of the junction and wires are as shown in Figure III.1. with the wires wet for distances s_1 and s_2 from the junction. It is convenient to assume that all the wet parts of the wires are at the temperature θ_J. In reality there will be a temperature rise from the junction to the point at which the wire is dry, but provided the heat flux along the wire is small when compared with the evaporative and convective heat fluxes (as is shown below to be the case for s_1 and s_2 sufficiently large), the temperature rise is negligible.

The differential equation for the heat fluxes associated with a wire convecting heat to is surroundings is

$$\frac{d^2\theta}{dx^2} - b^2\theta = 0 \quad , \quad \text{where} \quad b = \sqrt{\frac{ha}{kA}} \quad (6.)$$

With the boundary conditions $\theta = \theta_J$ at $x = s$,

and $\theta = 0$ at $x = \ell$, (7.)

The solution to equation (6) is

$$\theta = \frac{\theta_J}{e^{2b\ell - bs} - e^{bs}}\left(e^{2b\ell - bx} - e^{bx}\right) \quad . \quad (8.)$$

The heat conducted in the wire at $x = s$ is given by

$$q_1 = k_w A\left(\frac{d\theta}{dx}\right)_{x=s} = -k_w A b \theta_J\left(\frac{1+e^{2bs-2b\ell}}{1-e^{2bs-2b\ell}}\right) \approx -k_w A b \theta_J \text{ , for } \ell > 7s. \quad (9.)$$

The heat convected to the wire between $x = 0$ and $x = s$ is given by

$$q_2 = h a \theta_J s \quad . \quad (10.)$$

The heat lost through evaporation from the wet wire is

$$q_3 = L a s h_M \Delta C \qquad (11.)$$

A heat balance over the wet sections of both wires from $x = s_1$ to $x = s_2$ gives

$$(h_1 a_1 s_1 + h_2 a_2 s_2)\,\theta_J = L \Delta C (h_{m_1} a_1 s_1 + h_{m_2} a_2 s_2) - \theta_J (k_{w_1} A_1 b_1 + k_{w_2} A_2 b_2). \qquad (12.)$$

Equation (12.) is a relation between the wet bulb depression temperature θ_J of the junction, the absolute humidity ΔC of the surrounding air, and s_1 and s_2 the lengths of wet wire. Thus for particular values of s_1 and s_2, equation (12.) can be used to give values of the psychrometer constant A.

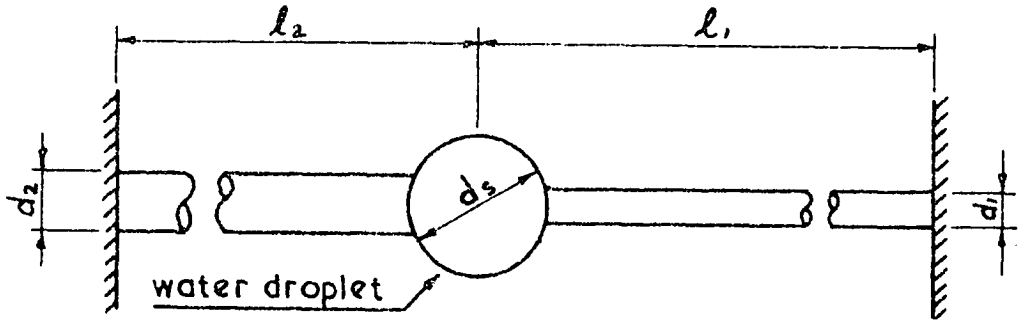

Fig. III.2. Model of spherical water droplet.

III.3 Model of a spherical water droplet at the junction.

The model comprises two wires, one of bismuth and the other of bismuth-tin alloy. One end of each wire is joined to a relatively stout support which acts as a heat sink at the temperature of the surroundings while the other two ends are joined to form the thermocouple junction. The junction supports a water droplet of approximately the size of the blob of silver conducting paint forming the real junction. The model is shown in Figure III.2. The variation of wire temperature with distance from the junction x is found from the differential equation for heat transfer from a wire (equation 6) with the boundary conditions $\theta = 0$ at $x = 0$ and $\theta = \theta_J$ at $x = l$. The solution is;

$$\theta = \theta_J \left(\frac{e^{-bx} - e^{bx}}{e^{-bl} - e^{bl}} \right), \qquad (13.)$$

where $b = \sqrt{\frac{ha}{kA}}$.

The rate of evaporation of a spherical droplet in a moving air stream has been measured by Frossling (Ref. 2) and can be expressed non-dimensionally by

$$Sh = 2\left(1 + 0.276\, Re^{\frac{1}{2}} Sc^{\frac{1}{3}}\right) \quad . \qquad (14.)$$

The rate of heat transfer from an isolated sphere has been determined by several investigators. According to reference 3, the expression

$$Nu = \left(0.97 + 0.68\, Re^{\frac{1}{2}}\right) Pr^{0.3} , \qquad (15.)$$

applies to forced convection to or from spheres in the range of Reynolds numbers $1 < Re < 10^3$. Reference 4 gives the following relation for low Reynolds numbers $Re < 20$;

$$Nu = 2.0 + 0.33\, Re^{\frac{1}{2}} \quad . \qquad (16.)$$

The heat conducted to the junction from the thermocouple wires can be found by differentiating equation (13). Thus

$$q_w = -kA\left(\frac{d\theta}{dx}\right)_{x=e} = kAb\theta_J\left(\frac{e^{be} - e^{-be}}{e^{be} - e^{-be}}\right) \approx kAb\theta_J . \qquad (17.)$$

The heat convected to the cold junction from the moving air stream is $q_s = h_s A_s \theta_J$, where A_s is the surface area of the sphere.

The heat required to evaporate the water vapour from the sphere is

$$q_e = h_{ms} L A_s \Delta C \qquad (18.)$$

Thus a heat balance for the sphere can be written as

$$q_e = q_{w_1} + q_{w_2} + q_s \quad , \qquad (19.)$$

or $$h_{ms} L A \Delta C = \theta_J\left(k_1 A_1 b_1 + k_2 A_2 b_2 + h_s A_s\right) . \qquad (20.)$$

Equation (20.) is used to determine the relation between θ_J and ΔC for several values of the droplet diameter d_s, and thus to determine the variation of the psychrometer constant with the droplet diameter.

III.4 Calculations.

Data applicable to both models.

Wire material	bismuth	bismuth-tin
Wire diameter	2.0×10^{-5} m	4.0×10^{-5} m
Thermal conductivity	8.4 W/m deg.	5.0 W/m deg.
Length	2.0×10^{-3} m	2.0×10^{-3} m
Air velocity	1.5 m/s	
Air temperature	20 deg.	

Data applicable to the model of two wires butting;

Wire resistivity	1.065×10^{-6} m	2.70×10^{-6} m
Peltier coefficient at 0°C	- 20.3 mV	+ 9.3 mV
Cooling current	2.9 mA	

III.4.1 Model of two wires butting.

The convective heat transfer from a wire to air for the range of Reynolds numbers 0.1 to 1000 can be found from the dimensionless equation (Ref. 5);

$$Nu = 0.32 + 0.43\, Re^{0.52} \qquad (21.)$$

The more general expression containing the Prandtl number is

$$Nu = 0.32 + 0.482\, Pr^{0.33}\, Re^{0.52} \qquad (22.)$$

The Reynolds numbers for the bismuth wire and the bismuth-tin wire are 2.0 and 4.0 respectively.

The mass transfer coefficient h_m is found from the expression analogous to equation (22.) viz.,

$$\frac{h_m d}{D} = Sh = 0.32 + 0.482 S_c^{0.33} Re^{0.52} . \quad (23.)$$

From the expressions for N_u and S_h, together with the values of the wire Reynolds numbers, the Prandtl and Schmidt numbers and the thermal conductivity and mass diffusivity of air, there results;

	for the bismuth wire.	for the bismuth-tin wire.
Nusselt number	$N_u = 0.936$	1.205
heat transfer coefficient	$h = 1.2 \times 10^3$ W/m²deg	7.73×10^2 W/m²deg
Sherwood number	$Sh = 0.904$	1.155
mass transfer coefficient	$h_m = 1.13$ m²/s	1.44 m²/s

The fractions of heat λ_1, and λ_2 conducted to the thermocouple junction from each wire during Peltier cooling are found by substituting the appropriate values into equations (5.) and (3.). There results $\lambda_1 = 0.381$ and $\lambda_2 = 0.619$. The lengths of wetted wire are found from equation (1.) with $\theta = \theta_d$, the dewpoint temperature of the surrounding air. Typically, with the junction close to an evaporation surface during cooling, the dewpoint depression θ_d is 0.5 degC. In this case, substituting into equation (1.) the values of the variables for each wire gives $s_1 = 1.96 \times 10^{-4}$ m and $s_2 = 3.1 \times 10^{-4}$ m.

Equation (12) shows that the operation of the thermocouple junction as a psychrometer depends on the lengths of the wet wires. By varying the cooling current or the distance from the evaporating surface to the region in which the cooling and wetting operation is performed, it is possible to produce different amounts of wetting. For this reason, the value of the ratio θ_J/DC, obtained from equation (12.), is calculated for various values of the length of the wetted wire s, taken as equal for both wires.

The psychrometer constant A is given by

$$A = \frac{\Delta p}{P\theta_J} = \frac{\Delta c}{\theta_J}\left(\frac{\Delta p}{P \Delta x}\right) \quad . \qquad (24.)$$

The value of the ratio $\left(\frac{\Delta p}{P \Delta x}\right)$ varies with temperature and humidity, but typically at around 21 degC dry bulb and 13 degC wet bulb, the ratio has the value $1.24\ m^3/kg$. The values of the psychrometer constant A for various values of s, the length of wetted wire, for this particular wire size and ambient temperature etc. are shown in figure III.3.

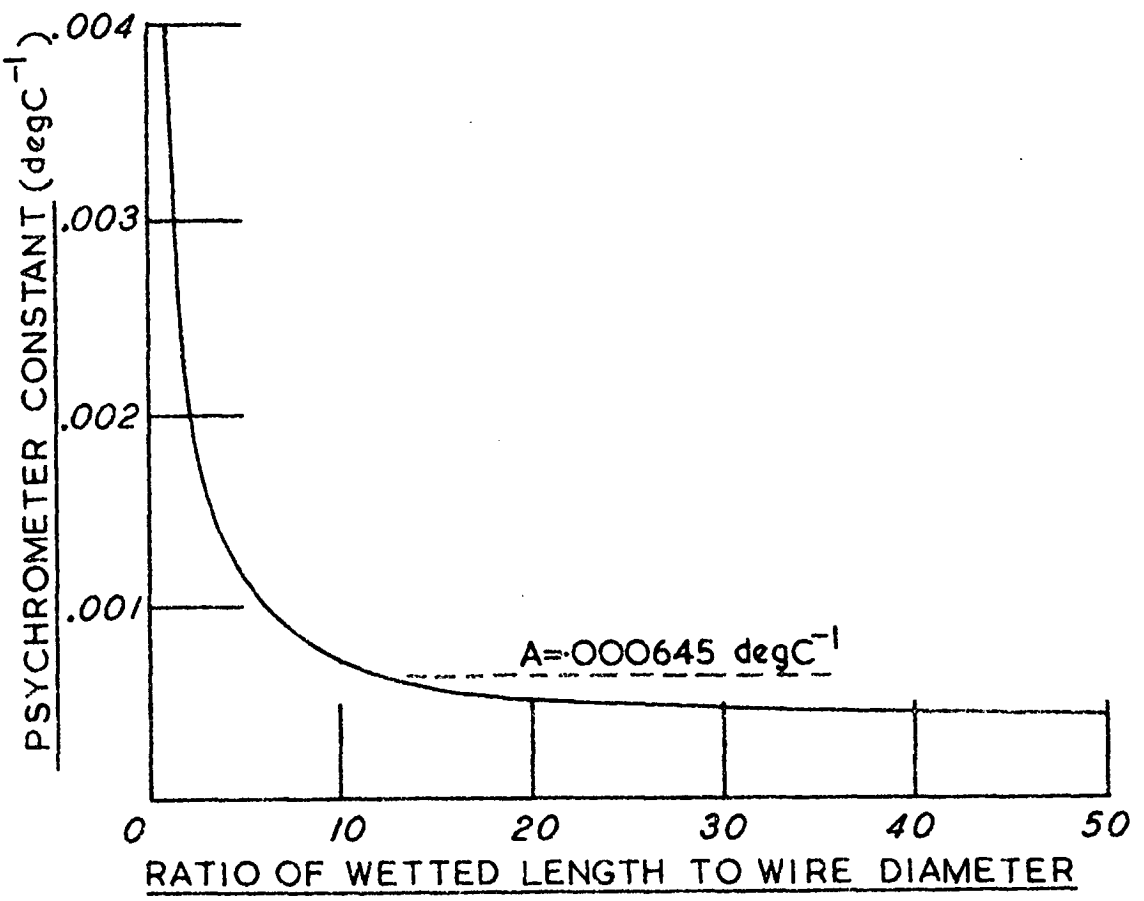

Fig. III.3. Effect of the length of wet wire.

III.4.2 Model of a water droplet at the junction.

With a droplet diameter of $7.0 \times 10^{-5} m$, the droplet Reynolds number is $Re = 7.0$. The Sherwood number is given by equation (14.) and is found to be $Sh = 3.23$, giving a value of the mass transfer coefficient $h_m = 1.15\ m/s$. The Nusselt number N_u calculated from equation (15.) is $N_u = 2.5$, while that calculated from equation (16.)

is $N_u = 2.87$. Using the average of the two values of the Nusselt number, the heat transfer coefficient is found to be $h_s = 9.18 \times 10^2$ W/m²deg. These values, when substituted into equation (20.) give a value of the ratio

$$\frac{\theta_I}{\Delta c} = 8.19 \times 10^2 \text{ deg m/kg}.$$

The choice of droplet size used in the calculations above is quite arbitrary. The calculation was repeated with other values of droplet diameter and the results presented as figure III.4.

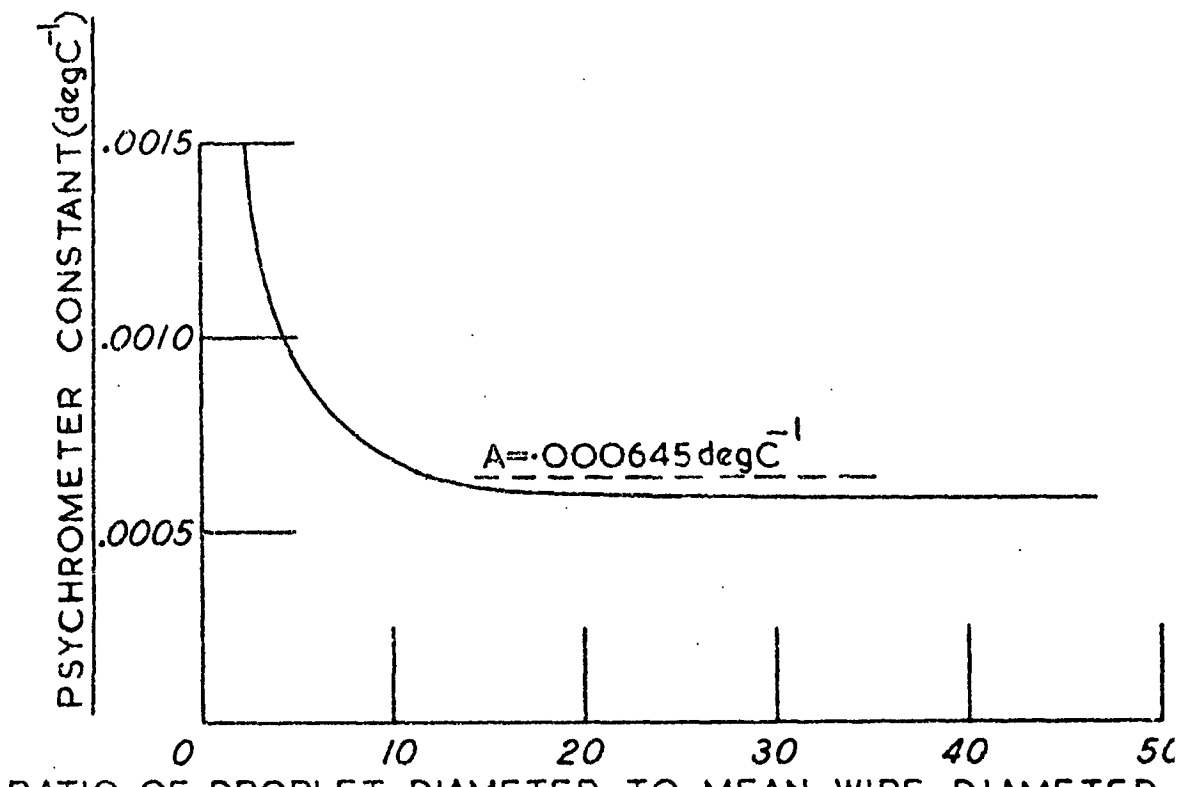

Fig. III.4. Effect of droplet size.

III.5 Conclusions.

By selecting two models of the thermocouple psychrometer and the calculation of psychrometer constants for the models it is possible to demonstrate that the amount of water condensed onto the thermocouple has a marked effect on the subsequent operation of the thermocouple as a psychrometer.

Figure III.3 shows that, for the model of two wires butting, satisfactory operation as a thermocouple psychrometer occurs if a length of wire of around ten diameters of the small wire from the junction is wet. Figure III.4 shows that a similar effect is obtained if a water droplet of about 3×10^{-4} m diameter, or about 15 times the diameter of the smaller wire, surrounds the junction.

It is felt that the real psychrometer, being wet about 10 to 20 diameters from the junction and having a droplet diameter of around 3 or 4 diameters, will fall onto the flat part of figures III.3 and III.4, and thus is not strongly dependent on droplet size or length of wet wire.

Another feature of the exercise is the closeness of the calculated psychrometer constants (about .00045 $degC^{-1}$ in figure III.3 and .00059 $degC^{-1}$ in figure III.4) to the observed constant for a fully ventilated thermometer psychrometer (.000645 $degC^{-1}$). This agreement is quite good when the accuracy of the data used in the calculations and the simplifications in the models are taken into consideration.

REFERENCES - APPENDIX III

1. D.C. Spanner : The Peltier effect and its use in the measurement of suction pressure. Journal of Experimental Botany, Vol. 2, No. 5, p. 145/8 168 (1951).

2. N.A. Fuchs : in Evaporation and Droplet Growth in Gaseous Media, Pergamon Press, (1959), p. 44.

3. W.M. Rohsenow and H.Y. Choi : in Heat, Mass and Momentum Transfer, Prentice-Hall, (1961), p. 202.

4. S.T. Hsu : in Engineering Heat Transfer, Van Nostrand, (1963), p. 335.

5. W.H. McAdams : in Heat Transmission, McGraw Hill (1942), p. 220.

NOMENCLATURE - APPENDIX III

Symbol	Significance	Equation	Units
A	Cross section area of thermocouple wire.	1	m^2
A	Psychrometer constant.	24	deg^{-1}
A_s	Surface area of water droplet on thermocouple junction.	20	m^2
a	Circumference of thermocouple wire.	1	m
b	Parameter involving the Nusselt number of the thermocouple wire.	6	m^{-1}
ΔC	Difference between the absolute humidities of the air around the thermocouple and the air at the surface of the thermocouple.	12	kg/m^3
d_s	Diameter of water droplet on thermocouple junction.	p.176	m
h	Surface heat transfer coefficient of thermocouple wire.	1	W/m^2deg
h_m	Mass transfer coefficient of wet thermocouple wire.	11	m/s
h_{ms}	Mass transfer coefficient of water droplet.	18	m/s
h_s	Surface heat transfer coefficient of water droplet on thermocouple junction.	20	W/m^2deg
i	Current in thermocouple.	1	A
k	Thermal conductivity of air close to thermocouple.	6	W/m.deg
k_w	Thermal conductivity of thermocouple wire material.	1	W/m.deg
L	Latent heat of vaporisation of water.	11	J/kg
l	Length of thermocouple wire.	1	m
P	Peltier coefficient of thermocouple junction.	1	V
P	Total pressure of air-water vapour mixture.	24	N/m^2
P_r	Prandtl Number.	22	-
Δp	Difference between the partial pressures of water vapour in the air around the thermocouple and the air at the surface of the thermocouple.	24	N/m^2

q_f	Heat flux along thermocouple wires.	2	W
q_e	Heat flux associated with evaporation from water droplet.	18	W
q_s	Heat convected to water droplet.	19	W
q_w	Heat flux along thermocouple wires.	17	W
R_e	Reynolds Number.	14	-
S_c	Schmidt Number.	14	-
S_h	Sherwood Number.	14	-
s	Length of wet part of thermocouple wire.	9	m
x	Distance along thermocouple wire.	1	m

GREEK SYMBOLS

α	Parameter involving the heat transfer coefficient and thermal conductivity of a thermocouple wire.	1	m^{-1}
θ	Temperature difference between thermocouple wire and surrounding air.	1	deg
θ_d	Dewpoint temperature.	p.175	deg
θ_J	Temperature difference between thermocouple junction and surrounding air.	7	deg
λ	Proportion of heat conducted along an individual thermocouple wire to junction.	1	-
ρ	Resistivity of thermocouple wire material.	1	Ω m